NUI MAYNOOTH

Ollscoil na hÉireann Má Nuad

Modelling Controlled Arrays of Wave Energy Converters

A thesis presented to the National University of Maynooth Ireland

by

Philip Balitsky

for the degree of Masters of Engineering Science by Research

June 2013

Department of Electronic Engineering
Faculty of Science and Engineering

Supervisor: Prof. John Ringwood
Head of Department: Dr. Ronan Farrell

Abstract

Given the great potential resource, the utilization of wave energy for electricity production can make a significant contribution to the renewable energy portfolio of coastal nations such as Ireland and the UK. There are, however, many challenges that must be overcome in order for wave energy to be commercially viable. One of the key objectives of the wave energy industry today is to produce commercially viable wave farms by placing multiple wave energy converters (WECs) together in an array. In this thesis, the WEC array problem is investigated from two different points of view: control and layout of individual WECs in an array.

WEC arrays are modelled using hydrodynamic coefficients from the Boundary Element Method code WAMIT ® in the frequency domain, and a discretized time-domain controller is then applied to calculate motion and energy of the system. A new application of an energy equivalent linearization procedure is developed to model viscous forces for a heaving cylinder. Three control methods are subsequently applied to arrays of two and three WECs in various sea states and the resulting power output of the array is investigated. Results are presented which show the benefit of using adaptive control for arrays of WECs over a simple fixed damping schemes.

Additionally, the layout of a controlled array of multiple WECs is investigated given the objective of power maximization. It is shown that as the number of devices in closely-spaced arrays increases, a control scheme that is able to utilize radiation properties of devices can offset the net loss of power effected by shadowing. Furthermore, the relationship between the

inter-device spacing and wave angle of incidence is derived for a two-body array and shown to hold for multi-body arrays. A recommendation on the optimal spacing and number of devices given a specific WEC geometry is made for a controlled array.

Acknowledgements

First, I would like to thank my supervisor, Professor John Ringwood, whose help made this work possible and whose guidance helped me become a better student and engineer. I would like to thank Mr. Giorgio Bacelli for this contributions to the work presented in this thesis, and for his advice on matters theoretical and personal.

Thanks to all the members of the Centre for Ocean Energy at NUI Maynooth, who have in two short years fostered a great platform for ocean energy research through their hard work and dedication, in particular Dr. Francesco Fusco, Dr. Ronan Costello, Dr. Josh Davidson, and Mr. Boris Teillant. Many thanks to Dr. Jan Westphalen, who, despite his short time here, has been generous in his help and knowledge. It has been my pleasure to have been part of the group. Many thanks to all the staff at the Department of Electronic Engineering at NUIM, who have created a great environment for work and study.

I would like thank my family, my parents Dr. Ian Balitsky and Ms. Elena Balitsky, and my brother Andrew, for their love and support from across the pond. Finally, I offer my sincere gratitude and thanks to my grandmother, Dr. Evgenia Balitskaia, whose path I have followed, and whose dedication to my thesis at times surpassed my own!

Contents

List of Symbols

α	fluid displacement amplitude
β	wave incidence angle
β_s	frequency parameter (Stoke's parameter)
$\dot{z}_a$	maximum heave velocity amplitude
η	wave surface elevation
$\hat{\phi}_D$	time-independent complex diffracted wave velocity potential
$\hat{\phi}_I$	time-independent complex incident wave velocity potential
$\hat{\phi}_R$	time-independent complex radiated wave velocity potential
$\hat{F}_{ex}^j$	complex excitation force in mode j
$\hat{F}_{rad}^j$	complex radiation force in mode j
κ	wavenumber
$\bar{\mathbf{E}}_k$	excitation force components as measured by the estimator on device k
$\mathbf{A}$	added mass matrix
$\mathbf{B}$	added damping matrix
$\mathbf{B}_v$	linearized viscosity coefficient
$\mathbf{C}$	hydrostatic stiffness matrix
$\mathbf{E}$	matrix of excitation force components
$\mathbf{F}$	generalized force vector
$\mathbf{F}_{ex}(t)$	excitation force
$\mathbf{f}_{ex}(t)$	excitation force impulse response function

$\mathbf{F}_{hyd}$	vector of hydrodynamic forces
$\mathbf{F}_{pto}(t)$	vector of power take-off forces
$\mathbf{G_s}$	matrix of discretized motion components for a single body
$\mathbf{G}$	matrix of discretized motion components for an array
$\mathbf{K}(t)$	radiation force impulse response
$\mathbf{M}$	mass matrix
$\mathbf{n}$	vector of normal velocity components on a body
$\mathbf{r}$	generalized position vector
$\mathcal{A}$	cross-sectional area of body perpendicular to the motion
$\mathcal{A}(\theta)$	angular variation of the radially spreading wave
$\mathrm{D_{ij}}$	matrix of hydrodynamic coefficients for mode i,j
$\mathrm{P^k}$	coefficients of PTO force for body k
$\mathrm{X^k}$	coefficients of motion for body k
μ	dynamic viscosity of water
ω	angular wave frequency
$\overline{P}_{ex}$	average excitation power
$\overline{P}_{rad}$	average radiated power
ϕ	total velocity potential of the fluid
ϕ_D	diffracted wave velocity potential
ϕ_I	incident wave velocity potential
ϕ_j	potential per unit displacement amplitude
ϕ_R	radiated wave velocity potential
ρ	density of seawater
$\Xi(\omega)$	Fourier transform of the wave elevation
ξ_j	amplitude of motion in mode j
A	wave amplitude
a	magnitude of cylinder device spacing [m]

C_D viscous drag coefficient in water

D cylinder diameter

GC global control

h water depth

H_s significant wave height

IC independent control

j index of modes of motion

k index of bodies

p pressure

$p_0(t)$ pressure at the air-water interface

P_{av} average power absorbed by an array of WECs

PT passive tuning to a single frequency

q array interaction factor

$S(\omega)$ non-directional wave spectrum

$S(\omega, \theta)$ directional wave spectrum

T_e wave energy period

T_p peak period

W total energy converted by a WEC array

w_o fundamental discretization frequency

S_b Submerged body surfaces

Abbreviations

BEM Boundary Element Method - a numerical computational method of solving linear partial differential equations which have been formulated in boundary integral form.

CFD Computational Fluid Dynamics - a branch of fluid dynamics which involves numerical methods to solve equations of fluid motion

PTO power take-off unit of a wave energy converter

WEC wave energy converter

Chapter 1

Introduction

With the looming threat of global climate change brought on by our ever-increasing burning of fossil fuels, the search for alternative clean energy sources is fast becoming one of the primary policy objectives of the century. Despite the ever-increasing proportion of renewable energies in the world electricity generating mix, it is still low, accounting for only around 20 % of the world generating capacity as of 2011 [1]. Wave and Tidal, often termed ocean energy, though currently providing only .01% of the renewable energy generating capacity, has the potential to provide a significant share in the future [1]. The total world extractable wave energy resource is estimated at 2.11 TW [2], which is approximately equal to the 2.28 TW of average electrical power produced in the world today [3]. Although extracting all of the energy reserves is not practical or realistic, wave energy can still play a significant role in the future energy mix, with the UK Carbon Trust predicting up to 180 GW of wave energy installed capacity in the world by 2050. If we look at a map of the world wave energy resource in fig 1.1, we see that areas like the west coast of North America, Europe, and South America as well as the south and west coasts of Australia are in particularly

favourable locations for wave energy extraction. According to the UN, 44 % of the world's population currently resides within 150 km of the coastline and this number is only projected to increase in the future [4]. Therefore it is natural that wave energy should play a significant role in the world energy mix.

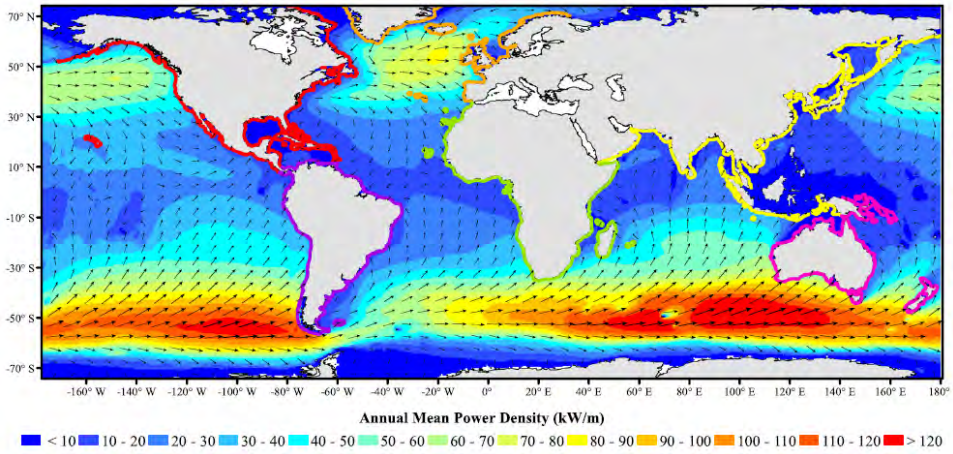

Figure 1.1: Annual mean wave power density (colour) and annual mean best direction (→) [2]

In spite of the huge potential, current world wave installed capacity is less than 5 MW [5], the majority of which is produced on a pre-commercial basis, meaning that it still costs more to produce a megawatt of wave energy than the market can offer for it. While the reasons for this are many and most are outside the scope of this thesis, the primary ones should be acknowledged. Firstly, all wave energy technology is immature. Unlike more established renewable sources like wind and solar, for which the extraction and generation technologies are well established, the wave energy industry presents a large number of vastly different technologies from which a clear leader has yet to emerge. Secondly, the harsh salt water environment and susceptibility to extreme weather conditions greatly increases the operating and maintenance costs of wave energy compared to other sources. Thirdly,

wave energy as a resource is intermittent, meaning that it greatly varies on both a short-term (second-by second) and long-term (daily and monthly variability) basis. This often necessitates having extra generating capacity for a majority of the WEC's (Wave Energy Converter) operation, which is often prohibitively costly. One solution that reduces output energy is to introduce automatic control to optimize the energy capture. As identified by numerous think tanks, including the UK Carbon Trust [6], CSIRO in Australia [7], and Ireland [8], the only way for wave energy to advance and reach its potential is by aggressive cost reduction. It is generally acknowledged that the only way to make deployment of WECs economically feasible is to place devices together in wave farms or arrays, which not only will enable cost saving via shared infrastructure but also enable wave energy projects to produce enough power to compare to other renewable energy plants. However, the placement of WECs in arrays itself presents a set of challenges, especially with regard to modelling the interaction. Both the layout of the devices in the array and an automatic control scheme will affect the power production in a WEC array and, by extension, its cost-effectiveness, and will be dual foci of this thesis.

1.1 Motivation

Even though several array demonstration projects are currently in the development stage, (for some notable projects see [1] [2] [3] [4]), there are still few studies which model realistic operating WEC scenarios, moreover, these studies have yet to reach a definitive conclusion

[1] http://www.aegirwave.com/
[2] http://www.aquamarinepower.com/projects/north-west-lewis/
[3] http://www.westwave.ie/
[4] http://www.el.angstrom.uu.se/forskningsprojekt/WavePower/Lysekilsprojektet_E.html

regarding the optimal placement of the devices in an array from the point of view of power capture. Moreover, none of these studies modelled active control strategies which were found to significantly increase power capture in single devices (see for example [9, 10, 11]). This is due, in a large part, to the difficulty of accurately modelling hydrodynamic interactions within the array. The number of modelling parameters increases geometrically with increasing device number. Therefore, to make the equations simple enough for a realistic computational time, the majority of studies on WEC arrays the hydrodynamics are modelled in the frequency domain assuming linear wave theory. While active control can be modelled within the framework of linear theory, a time-domain approach is required to accurately model it. Hence, until recently, it was computationally prohibitive to model realistic control for an array of WECs. It is the aim of this thesis to look at array layout of devices that are actively controlled to determine the layout maximizing the power capture given a set of devices and input sea states. Additionally, the difference between different array control schemes is examined.

1.2 Contribution of Thesis

The main contribution made by this thesis are:

1. A comprehensive review of the state of the art on the topic of layout and control of WEC arrays.

2. A comparison of two active control strategies for a WEC array to a passively tuned one .

3. The layout of an actively controlled array of WECs is examined and conclusions are made regarding the optimal spacing between devices as well as the positioning of the array to the prevailing wave direction.

The following publications have resulted from contributions of this thesis:

- Westphalen, J., Bacelli, G, Balitsky, P, and Ringwood, J. V. "Control strategies for arrays of wave energy devices.," in *Proceedings of the 9th European Wave and Tidal Energy Conference, Southampton, UK*, 2011.

- Bacelli, G., Balitsky, P., and Ringwood, J. V. "Coordinated control of arrays of wave energy devices - benefits over independent control," *IEEE Transactions on Sustainable Energy*, 2013, in press.

1.3 Layout of Thesis

The remainder of the thesis is structured as follows:

Chapter 2 is a comprehensive state-of-the-art review on modelling and control of WEC arrays. The theory behind wave energy conversion is presented in Chapter 3 covering the assumptions made in this thesis regarding the hydrodynamics of the system. The general results regarding array power capture are presented as well as a brief look at control theory as it applies to arrays. Chapter 4 looks at the viscous damping term in the WEC equation of motion as well as looking at the derivation of the linear damping term. In addition, results are presented presenting the effectiveness of the viscous damping term in accurately modelling the motion of a reactively controlled WEC array. Chapter 5 compares the control strategies for an array of devices. Two reactive array control strategies are compared to each other as well as to a passively tuned array.

Chapter 2

A Review of Modelling and Control of WEC Arrays

2.1 Introduction

As the first pre-commercial arrays are getting ready to be deployed and several commercial array projects are in the development stages, the topic of WEC arrays is getting due attention from numerous research groups in the UK and Europe. However, even though many aspects of the complicated problem of quantifying the power capture in an array of WECs have recently been looked at there are still many urgent questions that need to be answered. One of the most pressing, and least studied because of modelling difficulties, is automatic control of an array, because it has been shown for single devices that control greatly improves power production for a minimal additional capital cost [9, 10, 12, 11, 13]. In this chapter, an extensive review of the state of the art on array modelling and array control is presented, with a focus on the evolution of modelling as computer technologies have improved. Section 2.2 presents a brief historical overview, section 2.3

focuses on analytic approximations of WEC array hydrodynamics, section 2.4 looks at numerical methods, section 2.5 looks at studies exploring the effect of array layout on power production, and, finally, section 2.6 reviews dynamic control in the context of arrays.

2.2 Brief Historical Overview

The need to place WECs in arrays arises because of the inherent size of most wave energy conversion technologies. The majority of current and historically proposed devices are rated at less than 1 MW, with most in the 200-750 kW range. This is mainly due to the exponentially increasing capital costs of materials and deployment in the sea, as well as the costs of deployment and maintenance. Compared with other renewable technologies like wind, where some offshore models are rated up to 7 MW, individual WECs are small. Therefore, in order to be competitive with other renewable energy resources such as offshore wind, as well as with conventional power, commercial wave energy projects will need a power output of at least 10 MW, with a potential goal of hundreds of MW per project.

This need to deploy WECs in arrays was acknowledged within the first few years of extensive research into wave energy that coincided with the oil crisis in the early 1970s. In 1977 Budal [14] published the first investigation into the theory of power absorbtion of arrays of WECs. Budal was also the first to introduce the array interaction factor q as a benchmark measurement for array power capture. In simple terms, q is the ratio between the power produced by an array to the power produced by the same number of devices in isolation or:

$$q = \frac{\text{Power converted by array}}{\text{Power converted by same number isolated devices}} \tag{2.1}$$

Budal, however, made the restrictive assumption that all devices must oscillate with equal amplitudes. This assumption was proven inadequate by Falnes in 1980 [15]. Evans [16] independently arrived at the same results in 1979. A few years later both Falnes and Budal [17] and [18] showed that an array configuration can significantly increase power capture over that of isolated devices. A few commercial array projects were proposed by Budal and Falnes in Norway [17] and Salter in 1983 [19]. However, because of the oil glut of the 1980s and a strong push for nuclear power in the UK at the same time, these projects were cancelled and funding for research into arrays and into wave energy in general was severely curtailed. The majority of research carried out in the next decade and a half on arrays of floating bodies was carried out on structures other than WECs, still, some of the research was applied to the problem of WEC arrays, for example [20, 21, 22]. By the early 2000s, with increasing oil prices and the threat of climate change renewing an interest in all forms of alternative energy, wave energy conversion, and by extension WEC array research was back on the funding agenda of government agencies around the world. Coupled with a rapid increase in computing power that enabled complicated hydrodynamics to be accurately resolved, a large amount of research began to be published in the topic, especially toward the start of the new decade. For example, the number of papers submitted to the bi-annual European Wave and Tidal Energy conference, the pre-eminent forum in the field has almost doubled from 2005 to 2009 [23]. Currently, with the identification of WEC array research as a key topic in marine energy, several international efforts have been created to spearhead the consolidation and sharing of research such

as WECAN, SOWFIA [1], MARINET [2] and PerAWaT [3]. However there is an urgent need for experimental array data, especially that from sea trials, because many of the issues that commercial WEC arrays will have to face cannot be precisely replicated in the laboratory.

2.3 Semi-analytical methods for approximation of hydrodynamic forces

The full problem of calculating the power absorbtion of an array of WECs requires not only the complete knowledge of the hydrodynamics of each individual body, but also the scattering and radiation effects between all bodies in the array. Therefore, except for a few special cases, the equations cannot be fully solved analytically without making assumptions about the hydrodynamics of the problem. Even with the ready availability of powerful computers, the problem is only tractable for arrays with few bodies. As the number of bodies increases the equations become fundamentally more difficult to solve, thus necessitating analytical simplifications even when utilizing numerical methods for their solution[24]. Described below are the four main analytical approximations that have been historically used to solve the WEC array problem.

2.3.1 The Point Absorber Method

The first analytical method to be introduced, in the first published paper on array interaction by Budal in 1977 [14], is the *point-absorber approximation*. Its main assumption is that the scattered waves are negligible, which

[1] www.sowfia.eu
[2] http://www.fp7-marinet.eu/
[3] www.eti.co.uk/technologyprogrammes/marine

occurs when the wavelength is much greater than the device dimensions. This assumption was used to test the basic framework of the theory in the first wave of papers on the subject in the late 1970s and early 1980s, mainly for simplified examples of linear arrays of cylindrical WECs. The approximation is capable of calculating the optimal power absorbtion of an array regardless of individual WEC geometry, but is not capable of resolving the device motions, leading to solutions with unrealistic device displacements, as shown in [18]. To tackle this problem, an analytical method of placing restrictions on body motion was developed by Evans in 1981 [25] and extended by Pizer in 1993 [26]. However, this formulation requires knowledge of the hydrodynamic properties of the bodies, which cannot be calculated analytically except for a few special cases. Still, as a number of devices under development today fit the criteria for the validity of the point-absorber approxiamtion, it is a useful tool for WEC array analysis. The approximation has been recently used to optimize array geometry in the work of Fitzgerald and Thomas [27], and to optimize the positions of devices in an array with irregular waves by Folley and Whittaker [28]. In a study on array layout configuration, Ricci *et al.* [29] compared the point-absorber approximation with a numerical method, getting favourable agreement for a range of sea states.

2.3.2 The Plane Wave Method

Introduced by Simon in 1982 [30] and expanded by McIver and Evans in 1984 [31], the *plane-wave method* assumes that the diverging wave scattered from a cylinder is replaced by a plane wave of appropriate amplitude in the vicinity of another cylinder. In contrast to the point absorber approximation the plane-wave method assumes wide spacing between the array elements,

that is of the order of several wavelengths. Also, unlike the point-absorber method, the plane-wave approximation takes scattering into effect.

2.3.3 The Multiple Scattering Method

The *multiple-scattering method* is another semi-analytical procedure first used to calculate the scattering and radiation of surface waves on floating structures by Okhsu [32]. The method considers interaction as a series of scattering events for which the amplitude of the scattered wave decreases with each iteration, enabling a truncation to be made at a desired accuracy. Using this method, Mavrakos and Koumoustakos [21] solved the scattering problem, and Mavrakos [33] solved the radiation problem. The multiple-scattering method were applied in the context of WEC arrays by McIver *et al.* [34] and Mavrakos and McIver [35]; both groups compared the multiple-scattering method to the plane-wave and point-absorber approximations. A big benefit of the multiple-scattering method is that it enables a considerable reduction of both computing time and storage requirements, due to the fact that the formulation enables the successive satisfaction of the imposed boundary conditions on each body of the arrangement [33]. This method is, in principle, accurate to an arbitrary degree of precision, depending on where the series representation of the scattering is truncated. Nonetheless, the multiple-scattering method has an important drawback in the need for single-body hydrodynamic characteristics that can only be calculated for a simplified system without resorting to a numerical method, because the hydrodynamic response coefficients of each individual body must be known.

The point-absorber, plane-wave and multiple scattering methods were compared in a seminal paper by Mavrakos and McIver in 1997 for a linear array of 5 vertical cylinders [35]. As expected, they found that the

point absorber approximation brakes down for large values of κa where κ is the wavenumber and a is the cylinder spacing. By contrast, they observed that the plane-wave approximation, in addition to the wide-spacing regime, also works for closely spaced configurations that, in fact, violate the original assumptions behind the theory, calculating the hydrodynamic forces for $\kappa a = 0.4$ to within 5% of the more accurate multiple scattering method. Mavrakos and McIver [35] conclude that for most circumstances of practical interest the hydrodynamic forces can be calculated using the plane-wave approximation cautioning, however, that the errors might be amplified for a greater number of cylinders than the five considered in their study.

2.3.4 The Direct Matrix Method

A procedure similar to the multiple-scattering method, sometimes called the *direct matrix method*, was presented by Kagemoto and Yue in 1986 [20]. This is an exact algebraic method within the framework of linear theory, subject to truncation of an infinite series. The interaction of the bodies is accounted for by taking the scattered wave of each body to be the incident wave upon all other bodies, in addition to the ambient incident waves [20]. Doing this substitution for all members in an array, Kagemoto and Yue were able to solve for the coefficients of the scattered wave fields of all bodies simultaneously. They extended the approach to radiation in 1990 [36]. A solution for a truncated cylinder, one of the most common WEC shapes, was provided by Yilmaz and Incecik in 1998 [37] and this result, along with a model for the power take off (PTO), was used in a series of recent papers by Child and Venugopal [38, 39, 40, 41] where they analyse the influence of PTO damping, separation distance, angle of wave incidence, array device number and layout on power output. Although the direct matrix method

is versatile, only requiring that the vertical projections of the bodies do not overlap, it has a drawback in the need for solutions to the diffraction transfer matrix of the particular body considered, necessitating resorting to a numerical method for all but the simplest body shapes.

2.4 Numerical Methods

2.4.1 Boundary Element Methods

While numerical methods have been used in marine hydrodynamics since the earliest days of computers, only recently have advances in computer technology made possible the direct numerical simulations of arrays of WECs. Currently the *Boundary Element Method* ,or BEM, is the most widely used numerical approach. This computational procedure solves linear partial differential equations which have been formulated in boundary integral form. The application of the boundary element method to the problem essentially requires a mesh of the boundary of the domain only, and the determination of the boundary condition on the surface. For a comprehensive overview of the BEM method and its applications see [42]. A number of commercial software packages exist for applying BEMs to wave-structure interactions like WAMIT ®[4], developed at the Massachusetts Institute of Technology, ANSYS Aqwa ®[5] and 3DynaFS-BEM ®[6]. A number of software packages have also been developed by research institutions, particularly AQUADYN and AQUAPLUS at École Centrale de Nantes in France.

BEM methods have recently been utilized in a large number of studies pertaining to arrays of WECs, especially in studies investigating array lay-

[4] www.wamit.com
[5] http://ansys.com/Products/Other%2BProducts/ANSYS%2BAQWA
[6] www.dynaflow–inc.com/Products/Software/2_y3DynaFS/3DynaFS–BEM.htm

outs, including those by Justino and Clément [43], Babarit [13], Borgarino et al [44, 45] and Cruz *et al.*[46]. De Backer *et al.* [47] used the BEM code WAMIT to investigate different control schemes for a fixed structure array, and Taghipour *et al.* [48] used WAMIT to test the response of a floating array of 21 elements in irregular waves. Although BEM methods are computationally intensive for large arrays (of more than 10 elements), several research groups are investigating this issue. Borgarino *et al.* [49] recently presented a Fast Multipole Algorithm that shows improvement in computing time for large arrays.

2.4.2 Time Domain Methods

The studies mentioned in section 2.4.1 all calculate the motions of the devices in the frequency domain (see equation (3.3)). While these results are useful in modelling steady state motion, they are unable to resolve transient phenomena, as well as the implementation of real-time control [50]. Therefore, a time-domain formulation is employed in which equation (3.38) is employed to calculate the motion. In addition to resolving transient phenomena, the time-domain formulation enables the modelling of non-linear forces such as viscous damping, PTO forces, as well as mooring. The hydrodynamics coefficients are usually calculated in the frequency domain using frequency-domain BEM codes and then transformed into time domain responses via the inverse Fourier Transform. The main drawback of this approach is the increased computing time, especially in calculating the radiation kernel $\mathbf{K}(t)$ in (3.38). Several investigations tackled the problem by using system identification to replace the convolution by a linear system of equations. System identification is the approach taken by Taghiopour *et al.* [48] to approximate $\mathbf{K}(t)$ for a platform of closely spaced devices. A non-

linear extension to the time-domain formulation was presented by Mérigaud *et al.* [51] who used a non-linear term to represent the Froude-Krylov and diffraction force in (3.22) (for explanation see 3.1.1). They note that the increase in computational time is well justified by the improved calculation of motion for large sea states which, in turn, enables a more accurate estimate of power production [51].

2.4.3 Spectral Models

Spectral wave models are a group of phase-averaged wave propagation models which have been recently used to study WEC arrays. The basis of spectral models is the conservation of energy; thus all wave interaction effects in an array must be formulated so that a net loss or gain of energy is represented. The most popular model from this class is the SWAN model, used extensively to model near shore waves. Spectral models are able to represent energy dissipation and generation processes such as bottom effects and radiation, they are not able to model phase-dependent processes like scattering. Their biggest advantage is the computational efficiency when compared with potential flow methods, their usefulness in modelling very large WEC arrays (hundreds of elements), and the coupling of array effects into models that represent coastal processes [52]. Spectral models have recently been used to model the effects of interactions in arrays of WECs for a linear array of devices [53], as well as staggered configurations [54]. Folley and Whittaker [52] discuss the limitations of spectral models with regard to modelling array interaction, but also make the conclusion that beyond a certain distance from an array of devices, a spectral model can accurately model the change in energy predicted by theory.

2.4.4 CFD Methods

Computational Fluid Dynamics (CFD) is used to describe software that solves the Navier-Stokes equations over a complete fluid domain. The Navier-Stokes equations are the most fundamental equations of fluid dynamics, having non-linear as well as rotational terms. Therefore codes solving these equations are the most computationally intensive to run. The trade-off for this complexity is the ability to resolve non-linear effects such as viscosity, drag, non-linear PTO forces and mooring forces. Although computing hardware and software has only recently become powerful enough to tackle a complicated problem such as arrays, several studies have recently emerged which used CFD to simulate multiple devices in a wave tank. For example, Agamloh *et al.* [55] presented results from a two-device WEC array in a numerical test tank. Bhinder *et al.* [56] recently used CFD to determine the viscous drag coefficients for heaving and surging devices, results which can be directly applicable to the array problem. Even though there have been few investigations into WEC arrays using CFD, this is a very active area of research at the moment, spearheaded by a number of international task forces [52].

2.4.5 Experimental Methods

One of the biggest issues facing the wave energy industry today is the lack of widely-available experimental data. This dearth of data is especially acute in the case of WEC array experimental data, largely because most array configurations are too large to adequately test in a laboratory settings at full scale. As of late 2012, the only WEC array project in the water with multiple devices is the Lysekill project run by the University of Uppsala in Sweden (see [57] for recent progress). The situation should change in the

near future as several array projects are in the development stages. There is, however, a small set of experimental studies available using fixed-structure arrays, that is where the individual WECs are rigidly fixed to a frame. For example, the research group at Manchester University in the UK has conducted a number of experiments with a 1/7 scale prototype, comparing numerical results to experimental ones [58, 59].

2.4.6 Non-hydrodynamic issues

Even though the focus of this thesis and review is the hydrodynamic interactions in an array of WEC, in an eventual commercial array project, there will be other considerations which may be of equal if not higher importance to the project's eventual success. Therefore, we shall briefly describe them here, without going into extended discussion. Since the aim of WEC array projects is to provide electrical power to the grid, the issue of electrical connections and grid compatibility is of chief importance. To this end, several studies have looked into integration of WEC arrays into the electrical grid. Tedeschi *et al.* [60] investigated different scenarios of a hypothetical 20MW power plant from the point of view of the electrical supply variability. Molinas *et al.* [61] looked at the effect of WECs in an array on smoothing the power output to the grid. O'Sullivan *et al.* [62] and Sharkey *et al.* [63] both looked at a hypothetical WEC array off the west coast of Ireland (possible site of the WestWave project see 1.1 for detail). The two studies looked at the costs of the grid connections, with the latter study comparing different array layouts for associated electrical infrastructure costs. Moorings is another issue that will have to be dealt with in an array project. For example, Vicente *et al.* [64] studied the dynamics of a floating circular array of heaving WECs with slack-moored connections using a time-domain formula-

tion. Likewise, Ricci *et al.* [65] proposes a mooring system for a small (2-10 body) array of heaving point absorbers that is an economic improvement over individual moorings. Finally, one of the first studies to look at WEC arrays from a purely economic perspective was recently completed by Beels *et al.* [66], in which the authors evaluated the costs of three hypothetical WEC arrays consisting of overtopping devices. In addition to technical issues, there are social and environmental concerns of wave energy utilization that apply specifically to the case of arrays, for example the issue of ocean territory management, fishing right-of-ways, visual impacts, and the effect of WEC arrays on the nearshore sediment transport. None of these aspects can be completely ignored and any WEC array project will have to conduct analysis or collect applicable data before the project is finalized.

2.5 Array configuration and optimization

For a given WEC array project, the most important variable to determine is the eventual power output. Because of hydrodynamic interactions between array members, one of the key factors influencing the output is the array layout or configuration. The positioning of individual elements in an array has been acknowledged by many authors to have a significant effect on power production. In the 1980s and early 1990s, Falnes [15], Falnes and Budal [17], and Thomas and Evans [18] all showed the geometric layout to have a significant impact on the q-factor, acknowledging that the layout created phase differences in the radiated waves that lead to this phenomena. However, their studies were limited to equally spaced linear arrays of heaving point absorbers in regular waves, which limited their applicability to only a few select cases.

2.5.1 Array layout configuration studies

With improvements in modelling techniques, more recent investigations have considered different WEC shapes, modes of motions, irregular array geometries and finally true optimizations with an algorithm selecting from a range of possibilities. In the first category, that is selective optimization, McIver [22] compared a linear array of five heaving cylinders, with equal and unequal spacing, noting that the latter offers performance benefits by smoothing out big differences in power output. Ricci *et al.* [67] investigated three different configurations of heaving cylinders for regular and irregular seas, acknowledging the role of layout, but concluding that without a directional spectra for the exciting waves, their results have a limited application. Ricci *et al.* [29] followed up the previous investigation with a study of the performance of two 5-WEC arrays of heaving cylinders in a spectral wave climate from the Portuguese west coast. Ricci *et al.* establish the sensitivity of the configurations to wave spreading as well as concluding that the effects on array performance with inter-device spacing d larger than 4 device diameters can be neglected. A more recent study by Wolgamot *et al.* [68] also considers a three-member array, but with four different configurations. As well as looking at axis-symmetric heaving devices, they also looked at surge and sway motion as well as arbitrarily shaped bodies. Wolgamot *et al.* determine that matching the width of a peak in the q curve vs. the incident wave direction β to the range of expected incident wave directions would be a valuable consideration for a new array, at the same time acknowledging that the results need to be shown for cases other than the regular sea that they considered. Babarit [13] studied the influence of the array inter-device spacing on the power output of a two body array of heaving cylinders and surging barges. Investigating a range of distances from 110 m up to 20 km, for a number

wave incidence angles β, he concluded that, at close distances, interaction is significant for both types of devices and for all angles of incidence. However, at long distances, up to 2 km, only the array of surging devices aligned parallel to the incident waves exhibit significant modification of power output, with the other cases all converging within 1% of $q = 1$ at a 500 m distance. Babarit also derives an important general results that shows that, in a regular monochromatic wave, for a two-body array, the influence of interaction on the power output decays as a function of the square root of the distance d between the devices [13]. Borgarino *et al.* [45], extended the approach of [13] to two dimensions and multiple bodies, first by jointly varying the distance d between devices in an array, in what they term square-based arrays, and then letting both the x and y separating distance vary independently. For arrays of 9, 16, and 25 WECs, Borgarino *et al.* find a general area of constructive interference that is a function of both the x and y separating distance, with a similar shape for the heaving cylinder and surging barge array. Because the dependence of q is not the same as x and y change, as shown in figure 2.1 for the case of the 10-cylinder array, they note a benefit to letting both x and y separation distances vary independently.

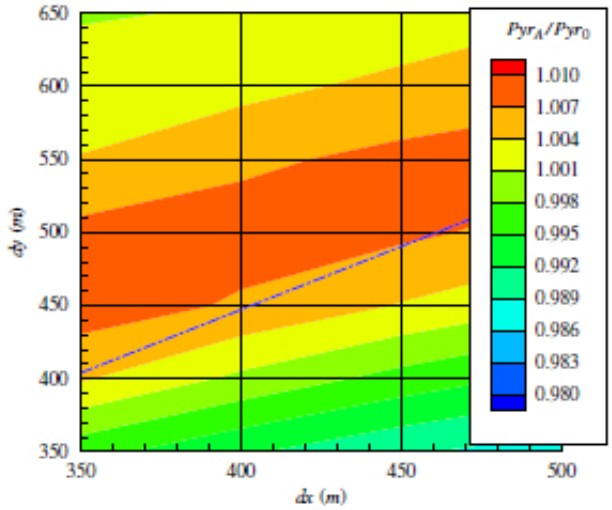

Figure 2.1: Ratio of yearly power output of an array P_{yr_A} to the yearly power produced by the same number of isolated device P_{yr_0} for an array of 10 heaving cylinders. For details see [45]

Borgarino *et al.* further investigated the masking effects in an array by first looking at a 20 body densely-packed cluster of devices, then by splitting the cluster into 2 clusters of ten devices in the same locations as the 20 body cluster, separated by increasing distances. They investigated the power output of one 10-body cluster placed in various locations behind a fixed cluster, looking at a range of sea states. Borgarino *et al.* conclude that there is a net benefit in splitting each cluster into 2 parts because, as the number of rows (devices one behind anther) increases in densely placed arrays, the overall performance of the array suffers. In addition, the authors noted a significant reduction in the wave energy immediately behind a dense cluster, indicating that separated clusters should preferably not be placed in row aligned with the wave direction, but preferably off axis. They note, however, that the masking effect diminishes when directional spreading is included in the incident wave forcing.

2.5.2 Array layout optimization studies

One of the first studies to conduct an optimization of array layout, based on the objective of maximizing power production was in 2007 by Fitzgerald and Thomas [27]. The authors applied a sequential quadratic programming algorithm to arrays of three and five point absorbers in regular incident waves, with a fixed wave number. They found a substantial increase in the q-factor for some array geometries. Indeed, by varying the angle of wave incidence, for optimal symmetric and non-symmetric layouts, they obtained a q_{max} of 2.777 and 2.746, respectively. From figure 2.2, where the q-factor is plotted for a range of incident wave directions for three array configurations (marked S for symmetrical and N for non-symmetrical) one can observe a very large peak for a specific incidence angle β around 1.5π and values of q close to unity away from that peak.

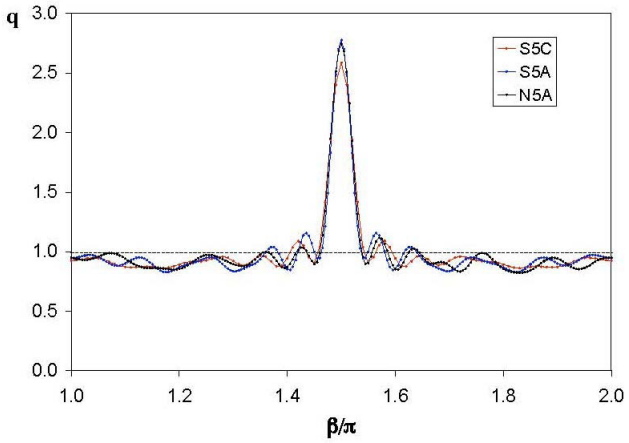

Figure 2.2: The variation in q-factor with incidence angle β for 3 array configurations (two symmetric and one non-symmetric) [27]

The increases are impressive, showing an almost three-fold improvement in device power output compared to an identical number of independent de-

vices, though the authors qualify that these increases, based on unrestricted device motions and regular seas, would be much less dramatic if more realistic operating assumptions were made. Nonetheless, the study offers valuable insight into the possibilities of using optimization and a grid-free layout for arrays of WECs. The authors also present an important consistency condition, stating that in varying the angle of incidence of the incoming waves β to the array axis, a net benefit at one angle will be offset by a decrease in performance in another:

$$\frac{1}{2\pi}\int_0^{2\pi} q(\beta)d\beta = 1. \tag{2.2}$$

In effect, this states an intuitive results that an array cannot be simultaneously maximized to all incident wave directions. Since all wave climates have a predominant direction from which the majority of the incident energy arrives, this results points to the benefits of aligning an array to the wave direction to maximize constructive interference.

The recent work by Child and Venugopal [40] tackles the same optimization problem by using two different algorithms. Using a semi-analytic procedure to calculate the array hydrodynamics, first presented in their earlier work [38], the authors optimize the array geometry for an array of five truncated cylinders oscillating in heave for regular waves, using two different methods: the first they term the Parabolic Intersection (PI) method, the second is a Genetic Algorithm (GA), a well-known heuristic algorithm. The PI method, devised by the authors for the study, utilizes the parabolic interference pattern surrounding each device in the array to place the subsequent array members. The GA is an established method that has been previously used in array applications such the design of acoustic lenses, electromagnetic

antennae and communication transmitter networks [40]. The investigation [40], however, is the first to apply GA to geometrical optimization of arrays of WECs. Here, the authors set q as the fitness function, maximizing it for two cases, the first using reactive tuning (see section 2.6), the second with real damping, then minimizing q for a reactively tuned device array. The q-factors from resulting layouts for the three experiments are shown in figure 2.3, plotted vs. non-dimensionalized wave number κa in the left column and wave incidence angle β on the right. Note that the $\overline{q}$-factor used by the authors is the same as that defined in equation 2.1.

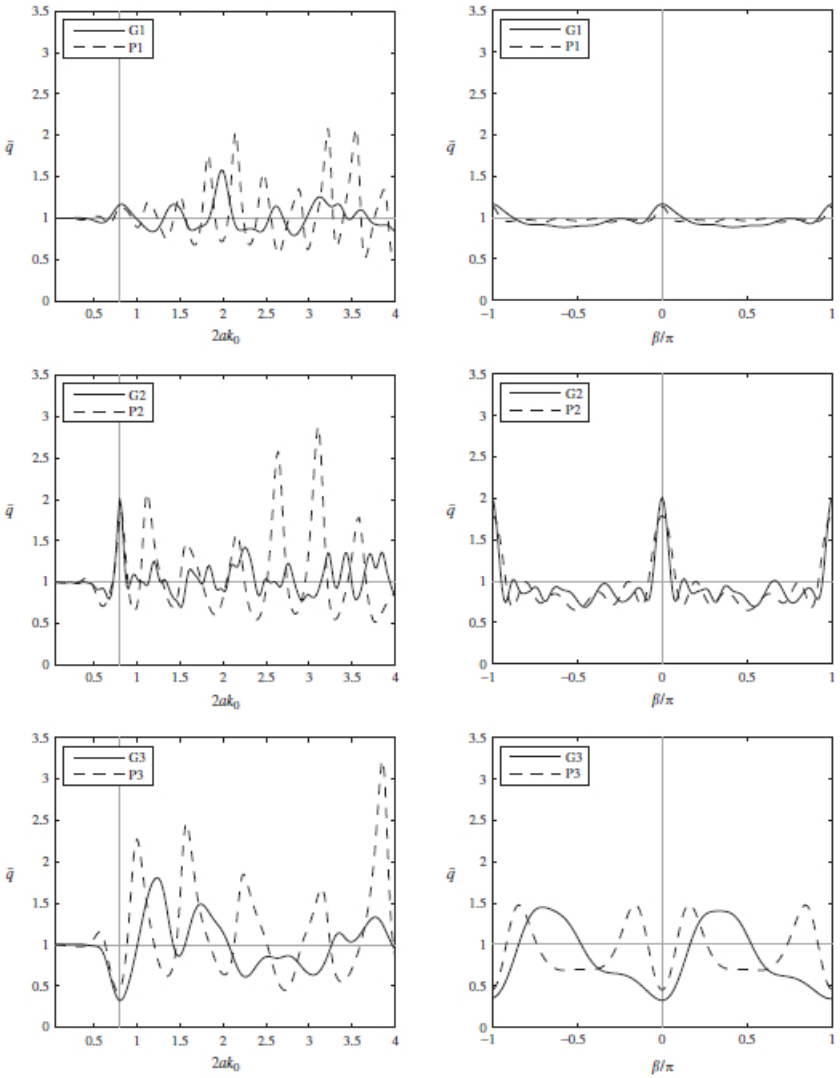

Figure 2.3: Variation of interaction factor q with non-dimensional wavenumber $2ak_0$ for fixed angle of attack $\beta = 0$ (left) and with angle of attack β for non-dimensional wavenumber $2ak = 0.8$ (right). Vertical grey lines show tuning wavenumbers $2ak_0 = 0.8$ (left) and incident wave angle $\beta = 0$ (right) [40].

The plots in figure 2.3 are illustrative in that they show the general pattern seen in most array configuration studies, with q oscillating about unity, with areas of both destructive and constructive interference for a given con-

figuration that depends on both the wavenumber and wave incidence angle. On the left hand side in figure 2.3, we remark that an array optimized at a certain κa, shown by the vertical line, can provide the opposite effect for a different wave environment. On the right in the same figure, we can see a visual verification of condition (2.5.2), with a strong benefit at a given β offset by a detriment at others. In the study [40], Child and Venugopal also verified the consistency condition equation (2.5.2), under less restrictive assumptions than those in [27], and found it to hold true for a range of array configurations. Child [69], extended the work in [40], which considered optimization in regular seas only, to the case of irregular seas. He implemented a GA optimization for a 5-member heaving cylinder array for the same tasks as mentioned in subsection 2.5.2 , maximizing the q value for real (passive) and reactively-tuned devices, and minimizing the q for reactively-tuned devices, Child utilized a JONSWAP spectrum with directional spreading as the input sea state. The results, as expected, show much less increase in power production compared with the regular wave case, with a q-max of only 1.044 for passive-tuned devices and 1.176 for reactive-tuned ones. Although optimization in the JONSWAP input case offers a net benefit, the benefit is not very significant. The result does, however, point to the need to explore this line of investigation further, particularly by looking at optimization with real sea climates.

2.6 Control of arrays of WECs

2.6.1 Array control

Control of arrays of WECs has only recently become an active area of research. The chief reason is that simulating control requires extensive com-

puting resources that only recently became available. To achieve optimal control, that is to extract the greatest possible power from the array, both the mass and damping of all devices need to be modified so that the WEC impedance is the complex conjugate of the impedance of the incoming wave force [10]. No devices currently in development offer this possibility, so the maximum power absorbed using optimal control serves more as a benchmark against which real device performance can be measured. We can consider two main classes of arrays of devices, those generally known as closely-spaced arrays attached to a fixed structure and those that are sparsely spaced and individually moored. For the closely-spaced devices, both the mass and the damping can be modified in operation while for the individually-moored devices, the modification of the floater mass is much more difficult to effectuate and therefore any form of control currently under development only optimizes the Power Take-Off (PTO) damping. Before we look in detail at array control, we take a brief step back and examine individual device control to appreciate the difficulty in investigating and implementing array control as well as classifying existing control schemes.

2.6.2 A Brief overview of WEC control

The need for dynamic control of individual WECs was established in the mid-1970s, only a few years after the initial investigations into the possibility of converting wave energy into electricity for the electric grid [70]. The need for control arises because most devices' resonant frequency and the predominant frequency of incident waves in the ocean. For a vast majority of WECs, maximization of power output necessitates a match between the motion of the wave and the motion of the device. To achieve this, the phases of the WEC oscillation and the wave oscillation must match (see section 3.5

for details). For wave energy devices, and in particular for heaving buoys, to achieve phase matching in average ocean frequencies without dynamic control to modify their oscillations, their physical dimensions exceed those that are currently economically feasible [71].

We note that, in the context of wave energy, the term *control* has a meaning different from that used in control engineering. It is an energy optimization problem, as opposed to *closed loop control* where the difference between the desired state and measurements of an actual state are used to determine the controlled inputs. More specifically, *control* in published wave energy literature is used to mean optimization of the power take off (PTO) force which in the majority of cases has a goal of maximization of the power captured [72], although other objectives like power smoothing can be pursued [61]. The latter objective may be desirable from the standpoint of the power grid, which needs to minimize disturbances in the power supply [61]. Within the scope of these definitions, a review of some of the control strategies for a single wave energy converter with a view toward their implementation in an array is carried out.

2.6.3 Overview of control methods for a single WEC

With the abundance of control strategies available for control of a single device of the point absorber type, it is important to classify them in a systematic way, as shown in figure 2.6.3. At the highest classification level, we shall make a distinction between the ideal unconstrained control, which is useful only as a theoretical benchmark, as this limit is impossible to reach in a real life operating scenario, as we shall see below.

For these operational scenarios we have the constrained optimal case and the suboptimal case, where the latter usually does not seek a maximum

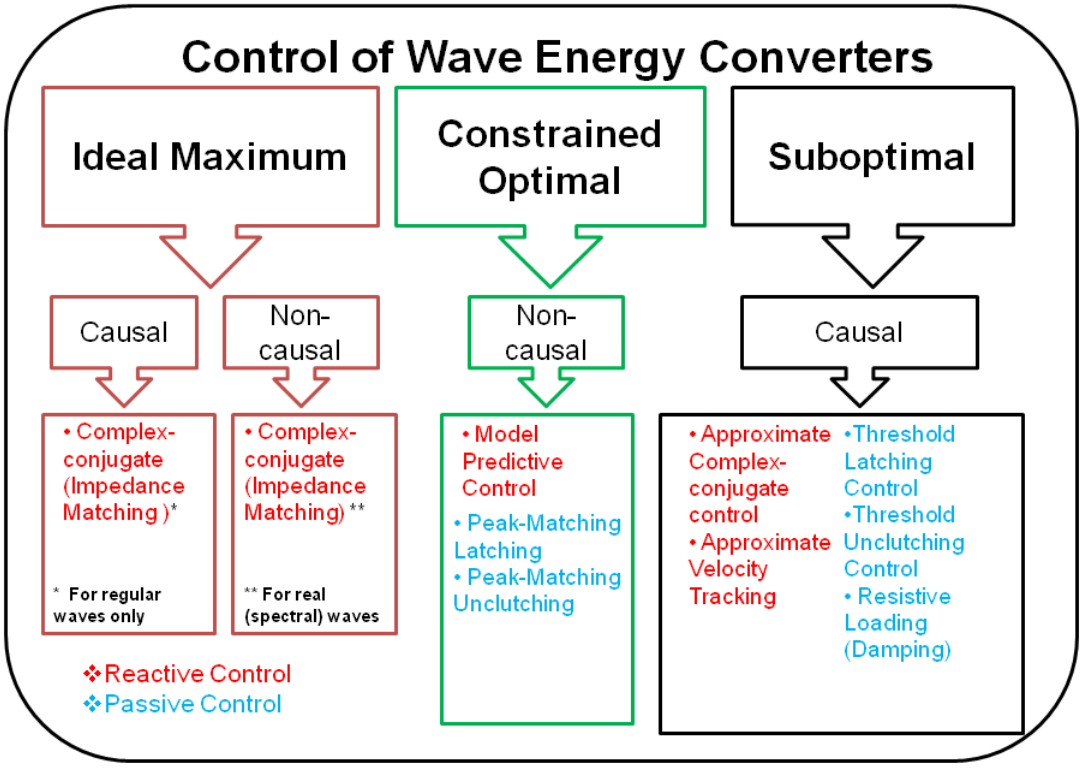

Figure 2.4: Different categories of control strategies for WECs

power capture but is often easier to implement in practice. Following the work of Falnes [10], and Price [72] we shall make a distinction between causal and non-causal control at the next level down. The theoretical optimal case is only causal in the case of regular waves. As a consequence, one of the reasons that the ideal scenario of complex conjugate control at all frequencies is impossible to realize in practice is that, for a real sea state (irregular waves), it requires infinite knowledge of the future values of the incident waves [73]. Still, it is possible to approach this theoretical power capture limit within the limits of operating constraints; such is the aim of constrained control. For example, for control methods that require prediction, it is

possible to forecast the incident wave elevation into the future for a half to two periods for a majority of sea states using a simple auto regressive model [74]. In the case of small devices, this forecast might enable the power capture to be maximized to within 10% of the theoretical maximum [74, 75]. Some examples of this constrained optimal strategy are model-predictive control, peak matching latching and declutching, all of which require a future prediction for the implementation of the optimal control force. These methods are described in detail and compared for both regular and irregular waves in a recent paper by Hals *et al.* [76]. The influence of array device interactions on prediction requirements is an important topic for future investigation and will have implications for whether constrained optimal control strategies are appropriate for arrays of WECs.

Except for the purely theoretical case of regular seas, all of the methods that are causal, that is those not requiring future knowledge, are classified as sub-optimal since they, by necessity of simplification, always capture less power in theory than optimal methods. These include the majority of currently implemented control approaches, including simple resistive damping, the only control method hitherto simulated in published studies to date for arrays of WECs [28, 46, 47]. An important point to note here is that some control methods require a reactive force from the PTO, that is for some part of the cycle power will have to be extracted from the system, a capability which many devices do not have. Therefore, in practice, sub-optimal methods may be preferred over optimal methods for some cases even though the total power output may be lower [76]. Moreover, control can be applied continuously or only at certain points in time, therefore the distinction between discrete and continuous control is sometimes made, for example by Falnes [10]. Two important methods of discrete control are latching and

declutching control. In heave where the two are applied as follows: for some time interval the device is held fixed for an in latching, and heaving motion is greatly slowed in declutching, then released [76]. However, not all control schemes can be easily classified. For example, a recent hybrid control system proposed by Tedeschi and Molinas [77] combines reactive and passive control that changes regimes depending on the energy of incident waves, and the difference between discrete and continuous control is somewhat arbitrary as most control algorithms require calculations and are applied at discrete intervals, albeit very short ones. Owing to the difficulty of calculating hydrodynamic responses of individual devices in an array, it remains to be seen which of the control schemes presented in this paragraph, if any, will be most appropriate when applied to arrays of WECs.

2.6.4 Control methods applied to arrays of WECs

For a regular wave input, Bellew *et al.* [58] varied the supplementary mass and damping for a linear array of 5 devices with inter-device spacing $4r$ where r is the device radius. The investigators found that, over most of the operating frequency range, a diagonalised optimal damping matrix provides the best power output, noting however that close to the resonance frequency of an isolated device an iterative approach to finding the damping matrices for the devices is better. They note however, that this increase is mitigated when a restriction is placed on the possible values of the damping [58]. De Backer et al. [47] investigated two rectangular arrays of 12 and 21 buoys with roughly one diameter inter-device spacing varying both the supplementary mass m_{sub} and damping B_{ext}. The authors considered three control strategies: the first strategy applies the optimal control parameters for a single body to all devices in an array, the second optimizes the power

for an array and applies the resulting m_{sub} and B_{ext} to each device, the final method determines separate values of m_{sub} and B_{ext} for each device (individual optimization). Running the simulation for a range of simulated real sea states, the investigators noted a significant increase in performance for the individually optimized devices versus the other two methods, while noting, that in the unconstrained case the individual optimisation converged to an unrealistic solution. In practical operating conditions, with multiple constraints on the motions and forces on the devices, individual control provides the best solution, with a q-value of 0.79 compared to 0.70 for the diagonal and single-device optimal cases.

Child and Venugopal [41] looked at the difference in performance between reactively tuned devices and real tuned ones, for a two-body array with a separation distance of $8r$. They observed a large peak in the q-value for a reactively-tuned device noting, however, that despite the higher power produced in the reactive-control case, the motion required to achieve it may not be achievable in deployment [41]. Folley and Whittaker [28] studied two floating hemispheres of 10 m radius for heave and surge motion for two scenarios of suboptimal control. In the first case, the reactive control force applied to the system differs from the optimum control tuned to a particular frequency and in the second case only passive tuning is considered. There is a significant reduction in power compared to the optimally tuned case because in both cases the resulting array is not able to take advantage of the beneficial phase relationships between the indecent and radiated waves that leads to positive q-factors [28]. In addition, the authors studied the q for a real spectral wave climate, finding that for reactively controlled devices the optimal average q for arrays of 2, 3 and 5 bodies was 1.16, 1.15, and 1.19 when they allowed the distance between the devices to vary up to 300 meters

[28]. Cruz et al. [46] studied the effect of tuning a rectangular array of 4 cylinders with device separation $4r$ in irregular sea states. They tuned each device independently by iterating on a linear damping coefficient, achieving q-factors between 0.88 and 0.97 for a range of sea states and heading angles. Antonutti and Hearn [78] studied a configuration of semi-submerged heaving hemispheres of radius 1.2m and separation distance $4r$. They compared the annual power yield from an array of 2,3 and 4 devices for a site-specific wave climate, finding a significant decrease in array performance for both sea-state specific tuning and scatter diagram based tuning of B_{ext} [78]. Finally Annuar et al.[79] investigated and array of six devices in regular seas with real and reactive control, in addition modelling the PTO and generator system, finding a more than two-fold increase in power output with reactive control.

2.7 Conclusion

With the recent surge of investigation into many aspects of the WEC array problem, we finally can start to make tentative conclusions about the placement of devices in an array. However, because of the multi-faceted nature of the task, there is still considerable uncertainty in these conclusions. Furthermore, there are areas of investigation which have to date not been studied in any great detail, for example the influence of uneven bathymetry, non-linear waves, and interactions of arrays with currents and/or tides. All of these issues may become important for array projects located near-shore in water depth of less than 30 meters, which, because of the costs of electrical infrastructure, is currently the most attractive location to palace these arrays.

One fact has, however, become clear; even though, in theory, arrays

can be used to increase power output through constructive interference, for realistic operating conditions, that is multi-directional real seas, PTO force motion restrictions, plus friction in the mechanical systems, it will be hard to achieve an output much greater than that of unity. In fact, a more approachable goal, stated as far back as 1994 by McIver [22], will be to use knowledge of hydrodynamics to minimize destructive interference. This is still a worthwhile goal, as a difference in the q-value of 0.5 can mean the difference between economic success and failure of a project.

One particular area which still needs to be further explored is the possibility of using real-time control, such as that presented in [80] to optimize array power output. It may be possible to use control to offset some of the negative effects of hydrodynamic interactions and utilizes constructive interference via coordinated radiation to improve array performance. Results along this trajectory will be presented in 5.

Chapter 3

Modelling WEC Arrays with Potential Flow Methods

In this chapter the theoretical modelling background for the results presented in the thesis is presented. This work is presented within the framework of linear wave theory. This chapter is brief overview of the subject, a much more thorough analysis can be found in the following references [81, 10, 82]. Linear potential theory rests on two key assumptions, namely that the fluid is assumed to be irrotational and that the free surface and body motions are relatively small compared to the wavelength and the water depth. Moreover, we assume the wetted area of the body is constant and that the fluid is everywhere incompressible. Section 3.1 describes the hydrodynamics of the linear boundary value problem, whilst subsection 3.1.1 describes the pressure and force relations. Section 3.2 characterizes irregular seas, sections 3.3 and 3.4 develop the equations of motion in the frequency and time domains, respectively. Section 3.5 outlines the power absorption by an array. Finally, section 3.6 outlines the control strategies investigated in this thesis.

3.1 Boundary Value Problem

In this section, a right-handed Cartesian coordinated system with three orthogonal axes: x y and z is adopted. The z axis is pointing upward. Assuming irrotational flow, we can write the velocity of a fluid particle as

$$\mathbf{v} = \nabla\phi \tag{3.1}$$

where ϕ is the velocity potential of the fluid. Combining equation (3.1) with the equation of continuity for an incompressible fluid results in the Laplace equation [82]

$$\nabla^2\phi = \frac{\partial^2\phi}{\partial x^2} + \frac{\partial^2\phi}{\partial y^2} + \frac{\partial^2\phi}{\partial z^2} = 0 \tag{3.2}$$

The solution of Laplace's equation gives the velocity potential ϕ everywhere in the fluid. The hydrodynamic pressure is then obtained from Bernoulli's equation. In linear wave theory this equation is equal to

$$p = -\rho\frac{\partial\phi}{\partial t} - \rho g z + p_0(t). \tag{3.3}$$

The first and the second term are known as the hydrodynamic and hydrostatic part, while the third part is nominally the atmospheric pressure but is often taken to be zero since it is simply an additive constant.

The boundary conditions required to solve Laplace's equation consist of the kinematic and dynamic part. The kinematic boundary condition requires that fluid particle cannot cross a solid boundary. This means that the normal velocity component on any body in the fluid and on the sea floor is equal to zero:

$$\frac{\partial\phi}{\partial\mathbf{n}} = 0 \tag{3.4}$$

where **n** is the unit vector normal to the body surface or the sea bed. On the free surface, the linearized kinematic boundary condition states that any particle lying on the free surface will remain there. Assuming the particle velocity components are small compared to the wave velocity and that the wave elevation is small compared to the wavelength, the linearized kinematic boundary condition can be stated as:

$$\frac{\partial \eta}{\partial t} = \frac{\partial \phi}{\partial z} \text{ at } z = \eta. \tag{3.5}$$

where η is the wave elevation. The dynamic boundary condition on the free surface rests on the assumption that the pressure outside the fluid is constant. Substituting the pressure from equation

$$\frac{D}{Dt}\left(-\rho\frac{\partial \phi}{\partial t} - \rho g z + p_0(t)\right) = 0 \tag{3.6}$$

and combining with the free surface kinematic condition (equation 3.5) results in the following condition on the free surface.

$$\frac{\partial^2 \phi}{\partial t^2} + g\frac{\partial \eta}{\partial t} = 0 \text{ at } z = 0. \tag{3.7}$$

Here $\frac{D}{Dt}$ is the total derivative operator equal to $\frac{\partial x}{\partial t}+\frac{\partial}{\partial x}(\frac{\partial x}{\partial t})+\frac{\partial}{\partial y}(\frac{\partial y}{\partial t})+\frac{\partial}{\partial z}(\frac{\partial z}{\partial t})$ for $x(t)$, $y(t)$, and $z(t)$. Again, in linear wave theory, we assume that the wave amplitude is small and therefore we simplify the equation 3.7 by setting the free surface at $z = 0$ instead of $z = \eta$. Because linear theory allows for the principle of superposition, the total velocity potential ϕ can be written as a sum of three different potentials which can be calculated separately.

$$\phi = \phi_I + \phi_D + \phi_R. \tag{3.8}$$

ϕ_I is the incident wave potential, ϕ_D is the diffracted wave potential (sometimes known as the scattered wave potential) and ϕ_R is the radiated wave potential. The incident potential of a regular plane progressive wave of amplitude A and zero phase is given by:

$$\phi_I = A\frac{g}{\omega}\frac{\cosh(k(z+h))}{\cosh(\kappa h)}\sin(\beta\kappa x + \beta\kappa y - \omega t) \tag{3.9}$$

where β is the direction of wave propagation relative to the x-axis and h is the water depth, and ω is the angular frequency. κ, the wavenumber is defined by

$$\kappa = \frac{2\pi}{\lambda} \tag{3.10}$$

for wavelength λ. κ is related to ω by the well-known dispersion relation

$$\omega^2 = g\kappa\tanh(\kappa h). \tag{3.11}$$

The diffraction potential is found by solving Laplace's equation on the body whilst it is kept still in a regular wave field. In addition to satisfying the dynamic boundary conditions on the free surface and sea bed, the sum of the incident and diffracted potentials must satisfy the kinematic boundary condition on the submerged body surface S_b

$$\frac{\partial\phi_D}{\partial n} = -\frac{\partial\phi_I}{\partial n} \text{ on } S_b \tag{3.12}$$

The diffraction potential must also satisfy the far-field condition that satisfies the conservation of energy [82]:

$$\phi_D = \frac{\sin(\kappa r - \omega t)}{\sqrt{\kappa r}} \text{ as } r \to \infty \tag{3.13}$$

The radiation potential is the wave field generated by body forced into motion in still water. For the most general case of a body moving in six degrees of freedom, this is expressed as:

$$\phi_R = \sum_{j=1}^{6} \xi_j \phi_j(t) \tag{3.14}$$

where ϕ_j is the potential per unit displacement amplitude, and ξ_j is the amplitude of the motion in mode j. The radiation potential must satisfy all aforementioned boundary conditions: equations (3.7) (3.12) (3.13) plus the kinematic boundary condition (equation (3.4)) on each body for each mode of motion:

$$\frac{\partial \phi_j}{\partial n} = \frac{dx_j}{dt} n_j \text{ on } S_b. \tag{3.15}$$

where x_j is the body displacement in each mode of motion and is equal to:

$$x_j = \xi_j e^{i\omega t} \tag{3.16}$$

and n_j is the normal force component in that mode. Assuming that all time varying quantities oscillate with the same frequency ω we can write the time-dependent potential as the real part of the complex time-independent potential $\hat{\phi}$. For the rest of the chapter we will use complex notation unless explicitly stated otherwise.

$$\phi(x, y, z, t) = \Re\Big[\hat{\phi}(x, y, z) e^{-i\omega t}\Big] \tag{3.17}$$

3.1.1 Pressure and force

After the total velocity potential of all bodies is found, the pressure below the free surface is calculated from Bernoulli's equation, (3.3) , assuming $p_0(t) = 0$. Using the complex amplitudes of the velocity potential allows us to write the pressure explicitly:

$$p = -\rho\frac{\partial\phi}{\partial t}(x, y, z, t) - \rho gz = -\rho\Re\left[i\omega\hat{\phi}(x, y, z)e^{-i\omega t}\right] - \rho gz. \tag{3.18}$$

The wave elevation can derived from equation and (3.7) and is equal to

$$\eta = \frac{1}{\rho g}p|_{z=0}. \tag{3.19}$$

The hydrostatic and hydrodynamic forces and moments are then determined by the integration of pressure on the submerged body surface S_b. Here we focus on the hydrodynamic forces, leaving the hydrostatic part ρgz for section 3.3

$$\mathbf{F_{hyd}} = \iint_{S_b} p\mathbf{n}d\mathbf{S}. \tag{3.20}$$

$$\mathbf{M_{hyd}} = \iint_{S_b} p(\mathbf{r} \times \mathbf{n})d\mathbf{S}. \tag{3.21}$$

where $\mathbf{n}$ is the generalised normal vector on S_b and $\mathbf{r}$ is the position vector. Often times, the forces and moments are expressed in one generalized force vector $\mathbf{F}$ with six degrees of freedom. Just as with the potential, we can divide the calculation of the hydrodynamic forces into two parts, one where the bodies are held fixed and the second one where they are moving in still water in all modes of motion. The first part, combining the integrals of the excitation and diffraction potentials, is termed the excitation force (or

moment) and is equal to:

$$\begin{aligned} F_{ex}^{j} &= \Re\left[\hat{F}_{ex}^{j} e^{i\omega t}\right] \\ \hat{F}_{ex}^{j} &= i\omega\rho \iint_{S_b} (\hat{\phi_I} + \hat{\phi_D})\mathbf{n}^j dS. \end{aligned} \tag{3.22}$$

The first part of equation (3.22), namely the integral of $\hat{\phi_I}$, is known as the *Froude-Krylov* force and represents the force experiences from the oncoming wave, ignoring perturbations on it by the body. The second part of equation (3.22) is oftentimes termed the *diffraction force*.

The radiation force in mode j, F_{rad}^{j}, the integral of the radiation potential in equation (3.14) results in two terms in equation (3.23), the first of which is in phase with the acceleration and the second in phase with the velocity (see [82] p. 359):

$$\begin{aligned} F_{rad}^{j} &= \Re\left[\hat{F}_{rad}^{j} e^{i\omega t}\right] \\ \hat{F}_{rad}^{j} &= \sum_{k=1}^{6} -\mathbf{A}^{jk}\frac{d^2 x_j}{dt^2} - \mathbf{B}^{jk}\frac{dx_j}{dt}. \end{aligned} \tag{3.23}$$

Differentiating the x with time we get:

$$\hat{F}_{rad}^{j} = \sum_{k=1}^{6} \left(-\omega^2 \mathbf{A}^{jk} + i\omega\mathbf{B}^{jk}\right)\xi_k. \tag{3.24}$$

A and **B** are coefficients known as the added mass and radiation damping, respectively. The index jk indicates the force component in the direction of j that is induced by an oscillation in mode k.

3.2 Irregular Waves

The analysis of regular harmonic waves, as presented in section 3.1, provides clarification into the fundamental properties of ocean waves. Real ocean waves where we expect to deploy wave energy conversion systems, however, are not regular nor harmonic. As a consequence, one needs to introduce tools to simulate real ocean sea states, whether in the laboratory or as in the case of this thesis, in numerical modelling tools. Ideally, this simulated wave train is assumed to be statistically stationary and homogeneous in time and space [83].

Given the assumptions in the previous paragraph, irregular sea states are most often described by the short term variance spectrum, or the power spectral density $S(f)$ or $S(\omega)$, where f and ω are the frequency in Hz and angular frequency in rad/sec, respectively The power spectral density $S(\omega)$ can be defined as:

$$S(\omega) = \lim_{T\to\infty} \frac{1}{2\pi T}|\Xi(\omega)|^2 \tag{3.25}$$

where $\Xi(\omega)$ is the Fourier transform of the wave elevation $\eta(t)$. It represents the distribution of the average power or variance of the wave elevation in the frequency domain. If a random wave is defined as a stochastic process, we can define the n_{th} moment m_n as:

$$m_n = \int_0^\infty \omega^n S(\omega) d\omega. \tag{3.26}$$

Using the moment definition we can express quantities that define the average characteristics of a random sea. The two most frequently used parameters are the significant wave height H_s and the wave energy period T_e.

Using the spectral moments, these are equal to:

$$H_s = 4\sqrt{m_0} \tag{3.27}$$

$$T_e = 4\frac{m_{-1}}{m_0}. \tag{3.28}$$

The significant wave height, approximately equal to the highest one third of the measured wave heights, corresponds to the observational definition of a wave height of a real sea state. The wave energy period is the mean wave period with respect to the spectral distribution of energy. Another useful quantity that defines an irregular sea is the peak period T_p, defined as the value at which $S(\omega)$ is at a maximum. The power, in W/m, of an irregular wave in deep water is given by the following convenient expression:

$$P = \frac{\rho g^2}{64\pi} H_s^2 T_e \tag{3.29}$$

It is important to mention that irregular waves also vary according to their direction of propagation. To describe this, the directional spectrum $S(\omega, \theta)$, where θ represents the direction of the spectrum, is defined. Usually, the directional spreading is assumed independent of the frequency distribution and the directional spectrum $S(\omega, \theta)$ is defined as the product of the non-directional spectrum $S(\omega)$ and the spreading function $G(\theta)$. In the results in this thesis in chapters 5 and 6, we focus on isolating the directional effects, therefore, we assume no directional spreading, meaning that all the energy is assumed coming from a given direction.

3.2.1 Commonly used spectral shapes

Based on sea data collected over the last fifty years, there are a number of different spectral formulations $S(\omega)$ that parametrize a given sea state (for a table of the most commonly used ones see [83]. They are most commonly parametrized in terms of sea state parameters such as H_s and T_p or the wind speed at 10 m of elevation such as in the case of the Pierson-Moskowitz spectrum [83]. Two of the most commonly used spectra in wave energy studies are the JONSWAP spectrum and the Bretschneider spectrum or the generalized Pierson-Moskowitz spectrum. The former, introduced by Hasselman *et al.* in 1973 based on data collected in the North Sea, is generally used to model fetch-limited wind seas in closed basins [83]. The latter, introduced by Bretschneider in 1959 with later modifications by Mitsuyasu, is the most commonly used spectral formulations for modelling open-ocean conditions [84]. The Bretschneider spectrum for a fully-developed sea is given by the following equation:

$$S(\omega) = 0.257 {H_s}^2 T_p^{-4} \omega^{-5} e^{-1.03(T_p\omega)^{-4}}. \tag{3.30}$$

Here H_s is the significant wave height and T_p is the peak period of the sea state. Because of its ubiquity and because it most accurately represents the sea conditions encountered at sites proposed for future full-scale commercial WEC farms, the Bretschneider spectrum will be used henceforth in this thesis to represent a real sea state. The surface wave elevation η, for an irregular sea state can be produced from the power spectrum by performing an inverse Fourier transform on each of the frequency bins. This is possible because in linear wave theory all frequencies are assumed to be independent of each other. This is the procedure followed in this thesis, using the sea-

keeping package WAFO ®. The phase effects do not affect the results: therefore a random phase is chosen to seed each of the sea state components.

3.3 Equations of motions in the frequency domain

In order to determine the power absorbed by an array of bodies, we need to know the motion of each body in the system. Before looking at the time-domain equation it is instructive to look at the simpler frequency domain case where we assume that all motions are steady-state. Once all the forces on all the bodies are known, their motions can be derived by applying Newton's second law of motion to the system:

$$\mathbf{M}\frac{d^2\mathbf{x}}{dt^2} = \mathbf{F_h} + \mathbf{F_{hs}} + \mathbf{F_v} + \mathbf{F_f} \tag{3.31}$$

For the most general case of an array of N bodies with 6 degrees of freedom, $\mathbf{M}$ is a $6N \times 6N$ matrix of masses or moments of inertia and $d\mathbf{x}^2/dt^2$ is a $6N \times 1$ vector of accelerations. All forces are $6N \times 1$ vectors: F_{hyd} are the hydrodynamic forces, F_{hs} is the hydrostatic buoyancy force, F_v is the viscous damping force, and F_f is a frictional force term that includes mechanical losses as well as constraints like mooring. Since the last term depends on the internal structure of the PTO system and not on the body hydrodynamics, and in most cases is strongly non-linear, we shall disregard it further in the thesis.

The hydrodynamic force is the sum of the excitation and radiation forces and can be written, following eqns. (3.22) (3.24) as:

$$F_h = F_{ex} - \mathbf{A}\frac{d^2\mathbf{x}}{dt^2} - \mathbf{B}\frac{d\mathbf{x}}{dt}. \tag{3.32}$$

Here F_{ex} is the $6N \times 1$ vector of exciting forces, $\mathbf{A}$ is the $6N \times 6N$ generalized added mass matrix and $\mathbf{B}$ is the generalized damping matrix. ξ is the $6N \times 1$ vector of displacements whose $6 \times N$th component is the displacement of the Nth body in the k_{th} mode of motion. In linear theory, the hydrostatic buoyancy force can be modelled as the product of the stiffness matrix C and the displacement x of the body from the equilibrium position:

$$F_{hs} = -\mathbf{C}\mathbf{x}. \tag{3.33}$$

Here $\mathbf{C}$ is a $6N \times 6N$ matrix and $\mathbf{x}$ is a $6N \times 1$ vector. The viscous damping force is most accurately modelled as a quadratic term in velocity but in this thesis we shall linearise it to the following:

$$\mathbf{F}_v = -\mathbf{B_v}\frac{d\mathbf{x}}{dt}. \tag{3.34}$$

$\mathbf{B_v}$ is the linearized damping coefficient and $\dfrac{d\mathbf{x}}{dt}$ is the vector of the velocities of each device. For details on the derivation of $\mathbf{B_v}$ see ch. 4. Rearranging Newton's law equation (3.31) so that all the terms including the body motion are on the left side, we get a familiar 2^{nd} order non-homogenous differential equation with constant coefficients:

$$(\mathbf{M} + \mathbf{A})\frac{d^2\mathbf{x}}{dt^2} + (\mathbf{B} + \mathbf{B_v})\frac{d\mathbf{x}}{dt} + \mathbf{C}\mathbf{x} = \mathbf{F_{ex}}. \tag{3.35}$$

Making the same assumption, as in equation (3.17) that the forces and motions are harmonic with a frequency ω, one can write a time-invariant version of equation (3.35) in terms of complex amplitudes:

$$[-\omega^2(\mathbf{M} + \mathbf{A}) + i\omega(\mathbf{B_v} + \mathbf{B}) + \mathbf{C}]\xi = \hat{\mathbf{F}}_{ex}. \tag{3.36}$$

Here $\mathbf{F}_{ex} = \Re\left[\hat{\mathbf{F}}_{ex}e^{i\omega t}\right]$ and $\mathbf{x} = \Re\left[\xi e^{i\omega t}\right]$. Then the complex amplitude vector ξ for each mode of motion is found to be:

$$\xi = [-\omega^2(\mathbf{M}+\mathbf{A}) + i\omega(\mathbf{B_v}+\mathbf{B}) + \mathbf{C}]^{-1}\hat{\mathbf{F}}_{ex}. \tag{3.37}$$

3.4 Equations of motions in the time domain

As we saw in chapter 2, there are some applications which require us to model non-stationary and non-linear phenomena of the system. Within the framework of linear potential theory, we can model use a time-domain formulation equivalent of equation (3.36) by taking the inverse Fourier transform. Including the linearised viscosity and the PTO force,the resulting equation for an array of N floating bodies, introduced by Cummins in 1962 [85], is the following:

$$[\mathbf{M}+\mathbf{A}(\infty)]\,\ddot{\mathbf{x}}(t)+\mathbf{B_v}\dot{\mathbf{x}}(t)+\int_0^T \mathbf{K}(t-\tau)\dot{\mathbf{x}}(\tau)d\tau+\mathbf{C}\mathbf{x}(t) = \mathbf{F}_{ex}(t)+\mathbf{F}_{pto}(t). \tag{3.38}$$

Here $\mathbf{M}$ is the generalized mass matrix, $\mathbf{A}_\infty$ is the added mass at infinite frequency, $\mathbf{B_v}$ is the matrix of viscous damping coefficients for each body,$\mathbf{K}(\mathbf{t})$ is the radiation damping response function, $\mathbf{C}$ is the stiffness matrix, and $\mathbf{F}_{pto}$ is the PTO force. All the matrices are assumed to be time-invariant and are the same as those in equation (3.35). The excitation force is the convolution of the time-domain impulse response function $\mathbf{f}_{ex}(t)$ with the wave elevation η [86]:

$$\mathbf{F}_{ex}(t) = \int_{-\infty}^{\infty} \mathbf{f}_{ex}(\tau)\eta(t-\tau)d\tau. \tag{3.39}$$

$\mathbf{f}_{ex}(t)$, the excitation force impulse response function is, in turn, the inverse Fourier transform of the frequency domain excitation force $\hat{\mathbf{F}}_{ex}$ (3.22),

$$\mathbf{f}_{ex}(t) = \frac{1}{2\pi}\int_{-\infty}^{\infty} \hat{\mathbf{F}}_{ex}(\omega)e^{i\omega t}d\omega. \tag{3.40}$$

The radiation impulse response function $\mathbf{K}(t)$ represents the effects of an radiation impulse by the body on the free surface [86]. $\mathbf{K}(t)$ is the inverse Fourier transform of the complex radiation impedance matrix, which can be represented as the sum of the real radiation damping and the complex added mass terms.

$$\mathbf{K}(t) = \frac{2}{\pi}\int_{0}^{\infty} \left[\mathbf{B}(\omega) + i\omega\left(\mathbf{A}(\omega) - \mathbf{A}(\infty)\right)\right] e^{i\omega t}d\omega \tag{3.41}$$

As a consequence of causality, that is since $\mathbf{K}(t) = 0$ for $t < 0$, $\mathbf{K}(t)$ can also be obtained from the frequency domain radiation damping matrix $\mathbf{B}$:

$$\mathbf{K}(t) = \frac{2}{\pi}\int_{0}^{\infty} \mathbf{B}(\omega)\cos(\omega t)d\omega. \tag{3.42}$$

When working with potential flow methods, all hydrodynamic coefficients in equation (3.38), namely, $\mathbf{M}$, $\mathbf{A}$, $\mathbf{B}$, and $\mathbf{C}$ are obtained from frequency domain software such as WAMIT®, which we shall do in the following chapters, except for the special case of $\mathbf{B}_v$ which will be derived in chapter 4.

3.5 Energy and power absorption

We next look at some general results for power absorption, again returning to the frequency domain for simplicity, assuming that all motions are harmonic. We further suppose that there is a PTO mechanism, the details of which

are beyond the scope of this thesis, capable of absorbing power in one or more modes of motion. Following [16] and [15], we can define the total time-averaged power given by the waves to the array of devices as the product of the hydrodynamic forces and velocities of each body:

$$P_{av} = \frac{1}{2}\mathbf{F}_{hyd}^{\mathsf{T}}\frac{d\mathbf{x}}{dt}. \tag{3.43}$$

Here T indicates the matrix transpose. Equation (3.43) can be written in complex amplitude form as:

$$P_{av} = \frac{1}{2}\Re\left[\hat{\mathbf{F}}_{hyd}^{*} i\omega\xi\right], \tag{3.44}$$

where * indicates the complex conjugate. As in section 3.3, the average power can be separated into two consistent parts; it is equal to the power absorbed by the devices from the incident waves minus the power radiated out by the devices, and can be written as:

$$P_{av} = \overline{P}_{ex} - \overline{P}_{rad} \tag{3.45}$$

where $\overline{P}_{ex}$ is the average absorbed power and $\overline{P}_{rad}$ is the average radiated power. Equation (3.45) can be written as:

$$P_{av} = \frac{1}{2}\Re\left[\hat{\mathbf{F}}_{ex}^{*} i\omega\xi\right] - \frac{1}{2}\xi^{*}\mathbf{B}\omega^{2}\xi. \tag{3.46}$$

Here $\mathbf{B}$ is the complex radiation damping matrix with the dimensions $6N \times 6N$. Equation (3.46) can be re-written as (for details see [16]) as:

$$P_{av} = \frac{1}{8}\hat{\mathbf{F}}_{ex}^{*}\mathbf{B}^{-1}\hat{\mathbf{F}}_{ex} - \frac{1}{2}\left(\omega\xi - \frac{1}{2}\mathbf{B}^{-1}\hat{\mathbf{F}}_{\mathbf{ex}}\right)^{*}\mathbf{B}\left(\omega\xi - \frac{1}{2}\mathbf{B}^{-1}\hat{\mathbf{F}}_{\mathbf{ex}}\right) \tag{3.47}$$

Then, the maximum power is reached when the second term in equation (3.47) is equal to zero and the total average power is equal to the first term only:

$$P_{max} = \frac{1}{8}\hat{\mathbf{F}}_{ex}^{*}\mathbf{B}^{-1}\hat{\mathbf{F}}_{ex}. \tag{3.48}$$

The condition is satisfied when the body motions are equal to the following:

$$\frac{d\mathbf{x}}{dt} = \frac{1}{2}\mathbf{B}^{-1}\hat{\mathbf{F}}_{ex}. \tag{3.49}$$

This equation (3.48) however, entails that all motions x are optimal, meaning that the value of the complex conjugate of the radiation damping matrix $\mathbf{B}$ is required for all frequencies for all bodies. As we saw in Chapter 2 this is impossible in practice in real seas. Equations. (3.48) and (3.49), however, are useful as a theoretical upper limit to the power absorbed by an array and its motions. As we will see in next section, a power-maximizing control algorithm will seek this maximum.

3.6 Energy-maximizing control

The array control methods as presented in this thesis, are an extension a control method first proposed in [87] for a wave-powered desalination plant. This was extended in [80] to a two-body self-reacting point absorber, and to arrays of two point absorbers in [88]. The results for controlled arrays in this thesis are an extension of the work presented in [89]. The control problem as defined in this thesis seeks to find the PTO force profile which maximises the total energy absorbed by the array whose equation of motion is given by equation 3.38 over a time interval T. The total energy absorbed

by the arrau is given by the following equation:

$$W = -\sum_{k=1}^{n} \int_0^T \dot{z}^k(t)\ F_{pto}^k(t)\ dt, \tag{3.50}$$

where $\dot{z}^k(t)$ and $F_{pto}^k(t)$ are, respectively, the heave velocity and the PTO force of the k-th device. Although in practise, the wave excitation force estimation will introduce an additional source of error into the results, for the purposes of this thesis it is assumed that the wave excitation is known completely into the future. The following three subsections describe the two control schemes, as presented in [89].

3.6.1 Discretization

The control problem is descritized by approximation the velocity and PTO forces with a linear combination of basis functions, resulting in a finite-dimension optimization problem. As in [89], the PTO force and velocity are approximated with truncated zero-mean Fourier series:

$$\dot{x}^k(t) \approx \sum_{n=1}^{N/2} x_{n,c}^k \cos(n\omega_0 t) + x_{n,s}^k \sin(n\omega_0 t) \tag{3.51}$$

$$f_{pto}^k(t) \approx \sum_{n=1}^{N/2} p_{n,c}^k \cos(n\omega_0 t) + p_{n,s}^k \sin(n\omega_0 t) \tag{3.52}$$

where ω_0 is the fundamental frequency of discretizaion. The best approximation of the solution of the equation of motion (3.38) is sought by applying the Galerkin method, the details of which are presented in [80], and the result is the linear system

$$\mathbf{GX} = \mathbf{P} + \mathbf{E} \tag{3.53}$$

where $\mathbf{X}$, $\mathbf{P}$, $\mathbf{E}$ and $\mathbf{G}$ are defined as

$$\mathbf{X} = \begin{bmatrix} X^1 \\ X^2 \end{bmatrix} \quad \mathbf{P} = \begin{bmatrix} P^1 \\ P^2 \end{bmatrix} \quad \mathbf{E} = \begin{bmatrix} \mathrm{E}^1 \\ \mathrm{E}^2 \end{bmatrix} \quad \mathbf{G} = \begin{bmatrix} \mathrm{G}_{11} & \mathrm{G}_{12} \\ \mathrm{G}_{21} & \mathrm{G}_{22} \end{bmatrix}.$$

The vectors X^k and P^k, for $k = 1, 2$, are the vectors of the Fourier coefficients of the velocity and PTO force of the k-th device, and are arranged as

$$\begin{aligned} X^k &= \left[x^k_{1,c}, x^k_{1,s}, x^k_{2,c}, x^k_{2,s}, \ldots, x^k_{\frac{N}{2},c}, x^k_{\frac{N}{2},s}\right]^T \\ P^k &= \left[p^k_{1,c}, p^k_{1,s}, p^k_{2,c}, p^k_{2,s}, \ldots, p^k_{\frac{N}{2},c}, p^k_{\frac{N}{2},s}\right]^T \end{aligned} \quad \text{for } k = 1, 2.$$

The elements of the vectors E^k are the Fourier coefficients of the excitation force on the k-th device and are arranged in the same manner as the vectors X^k and P^k. The matrices $\mathrm{G}_{ij} \in \mathbb{R}^{N \times N}$ composing the matrix $\mathbf{G}$ are block diagonal, where each of the $N/2$ blocks is of size two and the l-th block is defined as

$$\begin{aligned} \mathrm{G}^l_{ij} &= \begin{bmatrix} \mathrm{D}^l_{ij} & \mathrm{M}^l_{ij} \\ -\mathrm{M}^l_{ij} & \mathrm{D}^l_{ij} \end{bmatrix} \qquad \text{for } l = 1, \ldots, N/2 \\ \mathrm{D}^l_{ij} &= \mathrm{B}_{ij}(l\omega_0) + \mathrm{B}_{ij} \\ \mathrm{M}^l_{ij} &= l\omega_0 \left(\mathrm{M}_{ij} + \mathrm{A}_{ij}(l\omega_0)\right) - \mathrm{C}_{ij}/(l\omega_0). \end{aligned} \tag{3.54}$$

B_{ij}, M_{ij} and C_{ij} are, respectively, the elements of the matrices $\mathbf{B}$, $\mathbf{M}$ and $\mathbf{C}$, while $\mathbf{m}_{ij}(\omega)$ and $\mathrm{A}_{ij}(\omega)$ and $\mathrm{B}_{ij}(\omega)$ are elements the added mass and damping matrices. As first mentioned in 3.4, these matrices are calculated by the hydrodynamic software package WAMIT®.

3.6.2 Global control

The control system of the GC strategy is aware of the whole configuration of the array; the resulting optimisation problem is defined by the cost function

$\mathrm{W} = -P^T X$, which is obtained by substituting (3.51) and (3.52) into the definition of the total absorbed energy in (3.50). If G is non-singular, the cost function can be expressed as a function of P by solving (3.53) for X, and the coefficients $P^\star$ of the optimal PTO forces that maximise the absorbed energy for the array are obtained by solving the optimisation problem

$$P^\star = \arg\max_P -P^T X = -P^T \mathrm{G}^{-1} P - P^T \mathrm{G}^{-1} \mathrm{E}. \tag{3.55}$$

3.6.3 Independent control

For the IC case, it is assumed that each device is equipped with its own controller and excitation force estimator. It is also assumed that no communication occurs between the devices, and each controller uses the model of a single isolated device; that is, the controller of the k-th device uses the model (3.38) where $x(t)$, $f(t)$, M, A, B, K(t), and C are scalars and parameters of a single isolated device of the same geometry as the corresponding array. For the example of a two-device array the two cost functions are:

$$\begin{aligned} \mathbf{G_s X_1} &= \mathbf{P_1} + \bar{\mathbf{E}}_\mathbf{1} \\ \mathbf{G_s X_2} &= \mathbf{P_2} + \bar{\mathbf{E}}_\mathbf{2} \end{aligned} \tag{3.56}$$

The matrix $\mathbf{G}_s$ is the equivalent of the matrix $\mathbf{G}$ in the approximated equation of motion of the array in (3.53); however, in this case, $\mathbf{G}_s$ is calculated using the hydrodynamic coefficients of a single isolated device and $\bar{\mathbf{E}}_k$ is the excitation force measured by the estimator on device k. Each of the independent controllers calculates the optimal PTO force that maximizes the energy absorbed by the corresponding WEC using the models in (3.56).

The resulting optimisation problems are:

$$\begin{aligned} P_1^\star &= \arg\max_{P_1} = -P_1^T \mathrm{G_s}^{-1} P_1 - P_1^T \mathrm{G_s}^{-1} \bar{\mathrm{E}}_1 \\ P_2^\star &= \arg\max_{P_2} = -P_2^T \mathrm{G_s}^{-1} P_2 - P_2^T \mathrm{G_s}^{-1} \bar{\mathrm{E}}_2, \end{aligned} \tag{3.57}$$

the cost functions of which are the energy absorbed by each device. Because the two equations are coupled, they are solved by an iteration procedure detailed in [89].

3.6.4 Passive tuning

In this section, a passive tuning scheme for device control is examined. While not a energy-maximizing control scheme *per se*, PT will serve as a useful benchmark against which we can measure performance of the control schemes presented in the following sections as well as enable us to compare our results to previously published data [41, 46]. Following the work of Child and Venugopal [41, 39] the damping is set constant B_{pto} to maximize the power extracted at a given frequency ω. However, instead of choosing ω_0, the peak frequency of the wave spectrum, as in [69], we set the damping constant $\mathrm{B_{pto}}$ to maximize power at the wave energy frequency ω_e, which is equal to $2\pi/T_e$, as defined in equation (3.28). This is because the wave energy frequency represents the area in the spectral distribution of the wave field where the greatest energy is present. It therefore is sensible that the devices be tuned to this frequency. To accomplish this task in the array, each device is tuned individually, with the PTO force in the right-hand site of equation (3.38) set to the product of the device heave velocity $\dot{z}$ and $\mathrm{B_{pto}}$ where

$$\mathrm{B_{pto}} = \sqrt{[\mathbf{B}(\omega_e)]^2 + \omega_e^2 \left[\mathbf{M} + \mathbf{A}(\omega_e) - \frac{\mathbf{C}}{(\omega_e)^2}\right]^2}. \tag{3.58}$$

Here $\mathbf{M}$ is the generalized mass matrix, $\mathbf{C}$ is the hydrodynamic stiffness, $\mathbf{B}(\omega_e)$ and $\mathbf{A}(\omega_\mathbf{e})$ are the values of the radiation damping and added mass at ω_e. All matrices are 6×1 matrices where only the heave mode is non-zero. The energy for each device is then calculated from equation (3.43) where $\mathbf{F_{hyd}}$ in this case is equal to the force exerted by the PTO:

$$\mathrm{F_{pto}} = \mathrm{B}_{pto}\dot{z}(t) \tag{3.59}$$

where $\dot{z}$ is the heave velocity of each body. The total energy absorbed by the array is then equal to the sum of the energy extracted by each device k in the array:

$$\mathrm{W} = \sum_{k=1}^{N} \mathbf{B}_{pto^k} |\dot{z}(t)^k|^2 \tag{3.60}$$

Chapter 4

Linearized Viscous Damping Correction

4.1 Introduction

While the majority of currently published studies in the realm of wave energy conversion use the approximation of an inviscid fluid to calculate device motions (for a comprehensive overview see [86]), sea water does have viscosity. At 20° celsius its value is equal to $1.002 \times 10^{-3} NS/m^2$, and it decreases slightly with increasing water temperature. Although the effects of viscous losses are of the same order of magnitude as other simplifications used in wave energy conversion studies, for example the assumption of a static hydrodynamic stiffness, with increased wave amplitude larger device displacements incur larger velocities that tend to increase the drag due to viscous damping [90]. Therefore, viscosity should be included in any nonlinear WEC model. Furthermore, the addition of a viscosity term will also improve a linear model where the device motion is expected to be significant, for example in the case of reactive control. Indeed, several recent

wave energy studies have included a viscous damping term in the equation of motion of a WEC, including [91, 92, 58, 78].

For many applications however, the equation of motion 3.35 needs to be linear, which presents a problem in that viscosity is modelled as a quadratic term in velocity (see eq. 4.2) [93]. One solution is to linearize the quadratic term in velocity so that we get the linear equivalent of the quadratic damping term. This will be the line of thought followed in this chapter. In 4.2 we begin by defining the appropriate flow regimes, then in 4.3 Morison's equation of viscous damping is presented. In sec 4.4 the drag coefficient in Morison's equation is examined, in 4.5 the linearisation procedure of Morison equation is outlined, and finally in 4.6 some numerical examples are presented that show the how including the linearized viscosity term improves the WEC motion modelling. In this chapter the focus will be focusing on heave motions only, therefore all motions and velocities are in the z direction.

4.2 Dimensionless parameters defining fluid flow regimes

We begin this discussion by looking at the relative importance of viscosity to other fluid properties. For a body of diameter D oscillating about mean water level, the three important dimensionless parameters which determine

the fluid flow regimes are:

$$\text{Keulegan-Carpenter number: KC} = \frac{\dot{X}_m T}{D} = \frac{(\omega\alpha)(2\pi T/\omega)}{D} = \frac{2\pi\alpha T}{D} \tag{4.1a}$$

$$\text{Frequency parameter: } \beta_s = \frac{\rho D^2}{\mu T} \tag{4.1b}$$

$$\text{Reynolds number: Re} = \text{KC } * \beta_s = \frac{\rho \dot{X}_m D}{\mu}. \tag{4.1c}$$

For an oscillating flow past a stationary cylinder, $\dot{X}_m$ is the fluid velocity amplitude, T is the oscillation period and ω the frequency, D is the cylinder diameter, α is the water displacement amplitude, ρ is the water density and μ is the dynamic of absolute viscosity of water. The Keulegan-Carpenter number is a measure of the relative importance of drag forces over inertia forces in an oscillatory flow. The Reynolds number measures whether the flow is laminar or turbulent. The frequency parameter, also known as the Stokes parameter β_s, represents the ratio of the diffusion normal to the flow to diffusion parallel to it. β_s measures the applicability of boundary layer theory, which describes the interaction of a moving fluid and a boundary and is fundamental to all calculations of viscous forces [94]. Of note is that only two of the three numbers are independent, that is in knowing two of the dimensionless numbers, one can derive the third one.

4.3 Morison's equation

The most common form of parameterizing the loss of kinetic energy due to viscosity is a force proportional to the square of the velocity [95]. A

semi-empirical equation to account for the drag force due to the viscosity of water was developed by J.E. Morison *et al.* in 1950 [96]. For the case of 3-D oscillatory motion it is equal to:

$$F(t) = \frac{1}{2}\rho C_D \mathcal{A} x(t)|\dot{x}(t)| \tag{4.2}$$

where $\dot{x}(t)$ is the velocity of the oscillating fluid and C_D is a dimensionless drag coefficient that is dependent on both **KC** and β_s, and $\mathcal{A}$ is the cross-sectional area of the body perpendicular to the fluid motion. The Morison equation has been extensively used in engineering practice and has been experimentally verified in a number of studies involving structures in oscillating fluids [95, 97, 98]. However, due to the difficulty of recreating in laboratory settings the high Reynolds, high β_s conditions that are inherent in the open ocean, there is still a high degree of uncertainty in the value of C_D [99]. Unfortunately, these are precisely the conditions encountered in the study of wave energy conversion systems; because of this lack of experimental data any values of C_D need to be scrutinized to see if they apply to this flow regime. For example, if we look at figure 4.1 we can see that the flow regime at high Reynolds numbers and low **KC** numbers is not clearly delimited based on existing laboratory data.

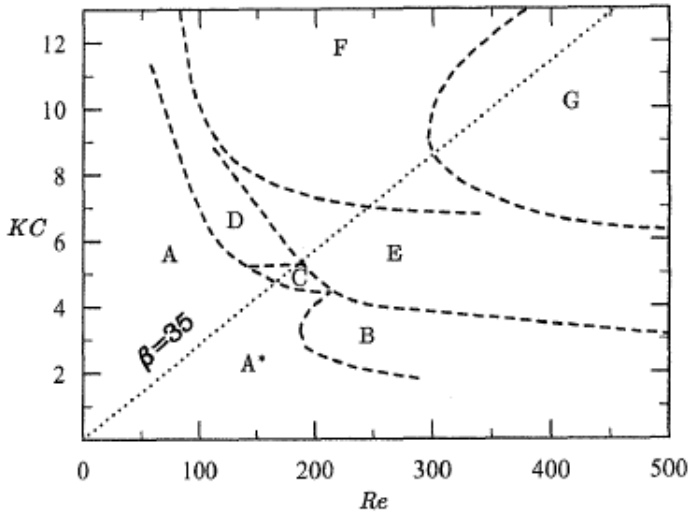

Figure 4.1: Flow regimes: The principal features of the regions are: (A *) No flow separation, secondary streaming, two dimensional; (A) two vortices shed symmetrically per half cycle, two dimensional; (B) three-dimensional instability, longitudinal vortices; (C) rearrangement of large vortices, three dimensional; (D) flow convected obliquely to one side of the axis of oscillation, three dimensional; (E) irregular switching of flow convection direction, three dimensional; (F) flow convected diagonally, three dimensional; (G) transverse vortex street, three dimensional. [98]

For the case of a heaving wave energy converter (WEC), there is an additional source of uncertainty in defining the reference frame for the velocity terms in the equation 4.2. Since the drag force depends upon the relative motion between the moving cylinder and the moving water, the drag component in Morison's equation should be, in the case of an oscillating cylinder in waves, proportional to the relative velocity:

$$F(t) = \frac{1}{2}\rho C_D \mathcal{A}(\dot{x}(t) - \dot{z}(t))|\dot{x}(t) - \dot{z}(t)| \tag{4.3}$$

where $\dot{x}(t)$ is water velocity and $\dot{z}(t)$ the velocity of the heaving cylinder [93]. However, in the case of a WEC, the viscous effects will be most significant

around the resonance frequency, or the peak frequency of the incident waves in the case the device is controlled to resonate at the peak wave frequency. Therefore $\dot{z}(t)$, the velocity of the device, will generally be higher than $\dot{x}(t)$, the velocity of the flow. Because $\dot{x}(t)$ and $\dot{z}(t)$ will have the same sign for the greater part of the time, the cross-terms and the $\dot{x}(t)^2$ term in equation (4.3) will largely be of the opposite sign. In addition, around the forcing frequency of the cylinder, both cross-terms will be much smaller than the $\dot{z}(t)^2$ term. Hence the cross-terms and the $\dot{x}(t)^2$ term are comparable to second-order effects and can hence be ignored. The equation (4.3) can then be simplified to:

$$F(t) = \frac{1}{2}\rho C_D \mathcal{A} \dot{z}(t)|\dot{z}(t)| \tag{4.4}$$

4.4 Determining the value of the drag coefficient

The biggest potential source of error in this formulation is the value of C_D, the viscous drag coefficient. Several different studies have looked at its value over a range of KC and β, but there is no definitive set of values because they are highly dependent on laboratory testing conditions. For an example heaving cylinder WEC with diameter of 10 m operating in seas of 2 m at an average peak period of 10 s the approximate values of the three numbers are: **KC** $\simeq$ 1-2, **Re** $\simeq 0.5 - 1 \times 10^7$, and $\beta \simeq 1 - 2 \times 10^7$. For **KC** < 10 and a Reynolds number greater than 10^5 a value of 0.6 is suggested in [93]. This corroborates well with numerical data from [100] where the authors looked at values of **Re** up to 1×10^8. Their results for $\beta = 5.787 \times 10^6$ and $\beta = 1 \times 10^{10}$ for a range of **KC** between .001 and 10 are presented in figures 4.2 and 4.3. One can see that for **KC** of around one, C_d is close to 0.6 and that an assumption of laminar flow shown by the straight line underestimates the drag coefficient for higher values of **KC**.

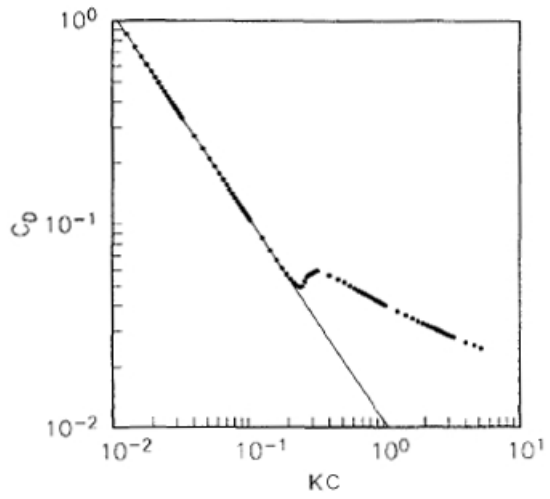

Figure 4.2: The coefficient of drag as a function of the Keulegan-Carpenter number for $P = 5.787 \times 106$, Wang's laminar formulation [101] (line) and the numerical results (*) from [100].

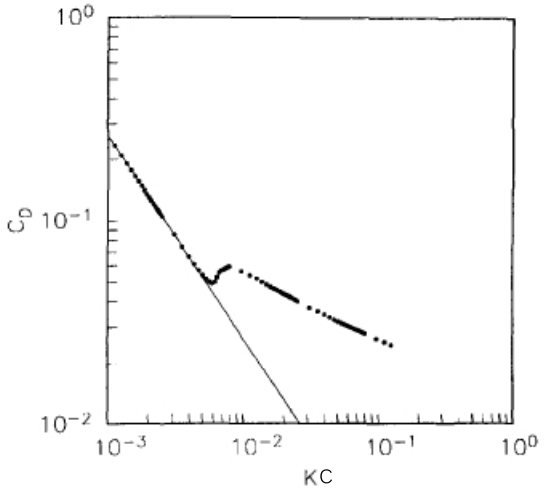

Figure 4.3: The coefficient of drag as a function of the Keulegan-Carpenter number for $P = I \times 1010$. Wang's laminar formulation [101] (line) and the numerical results (*) from [100].

Regrettably experimental data for high β and low **KC** numbers are not available due to the difficulty in obtaining these conditions in laboratory

settings. However, one can see in figures 4.4 and 4.5 from experiments by Sarpkaya in 1976 that a value for C_d between 0.5 and 1 is hinted at by the data as one focuses on the low **KC** numbers on the left hand side [95].

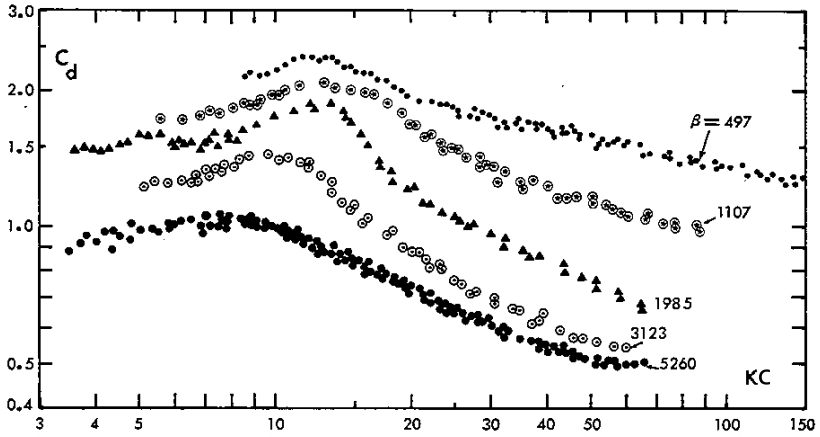

Figure 4.4: C_d versus **KC** for various values of the frequency parameter [95]

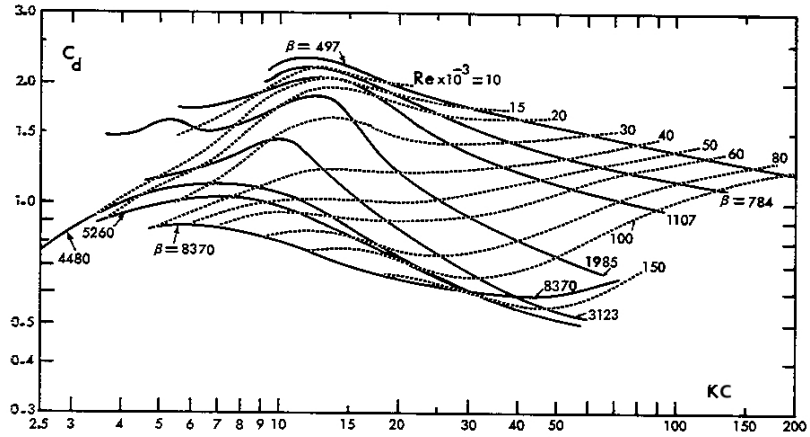

Figure 4.5: C_d versus **KC** for various values of the Reynolds number and the frequency parameter [95]

In conclusion, assuming a smooth cylinder, in the operational regime of a WEC, a value of C_d between .5 and .8 seems the best reasonable approximation based on the current understanding of viscous flow. Nevertheless, this

value will need to be increased if we are to consider a non-smooth cylinder [95], a case that will need to be looked at in future studies.

An alternative to using previously published C_D values was recently proposed by Bhinder *et al.* [56], where the authors used a CFD model to empirically determine the viscous drag coefficient of an oscillating body in a fluid at rest. Their results for a heaving cylinder of diameter of 15 m and a 20 m height for a range of simulated sea states converged to C_D equal to 1.7, which is in line with several published values, such as those in figure 4.9 in [102], however, this estimate is higher than the values used elsewhere such as in [95]. In the present work we will use a compromise value of $C_D = 0.8$, which is also in line with the results presented in [94] as shown below in figure 4.6 for a cylinder with flow perpendicular to its axis of motion.

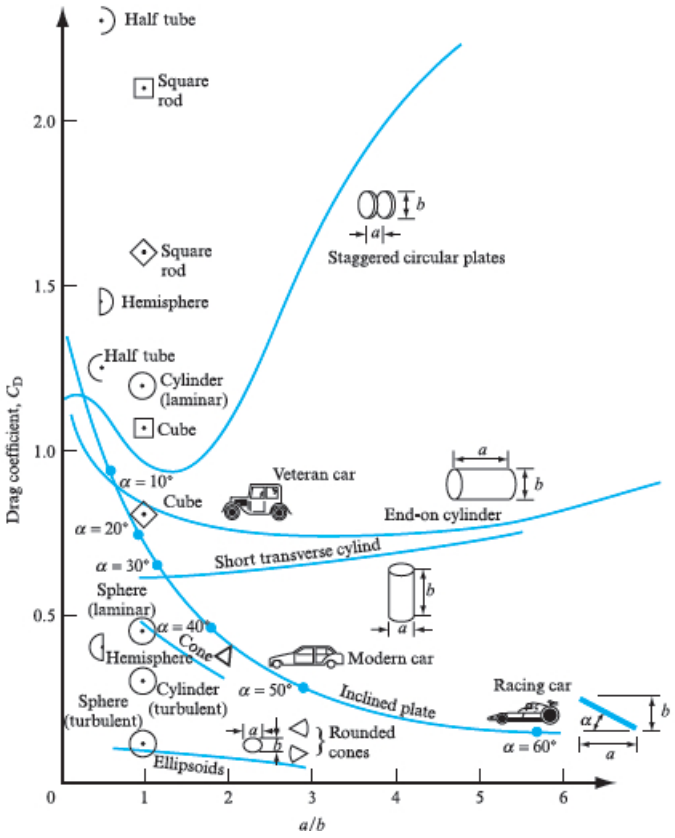

Figure 4.6: C_D for various body shapes at $\mathbf{Re} \approx 10^5$, based on frontal area. [94]

4.5 Lorentz's linearisation of Morison's equation

Although Morison's equation is the best available parametrization for measuring viscous effects, it contains a pitfall in the form of a non-linear term in the velocity (see eq. 4.2). In many applications of wave energy conversion where we need to assume system linearity for computational simplification such a term in the force equation will not be acceptable. While there is no method to accurately capture the non-linear behaviour of a fully non-linear system with a linear coefficient, for relatively small drag forces experienced

by WECs it is possible to satisfactorily linearize the quadratic term using several different methods, as has been done in [92, 90, 52, 78]. These investigations employed an additive damping term that is assumed to include viscous effects. In the case of periodic motion, such as that of a WEC, a good approach to use is termed *Lorentz linearisation* after H. Lorentz who first applied it in the 1920s to the case of an oscillating frictional flow in a tidal channel [103, 104]. This procedure uses an energy equivalence principle where the energy over a cycle dissipated in the quadratic relation is set equal to that dissipated in the linear relation. The coefficient of the linear velocity term is then derived. Because Morison's equation has the same quadratic form in velocity as the equation of tidal friction, Lorentz linearization can be applied in the case of modelling viscous effects, provided that the motion is periodic. This strategy has been experimentally verified in [105, 103] and was first used in the study of WECs in 2007 [92] for the case of a flap-type hinged converter. Although the assumption of periodicity is not strictly true in the case of irregular wave excitation, for a majority of operating conditions the motion can be approximated as periodic. To begin the procedure, we make assumption first advanced by Lorentz [106, 107], that the energy dissipated in one period of oscillation by the quadratic term is equal to that dissipated by the yet to be linear one. This is equivalent to the work done by the oscillating system, that is $W = \int_0^{2pi/\omega} F\dot{z}dt$ where the force is given in 4.4. We then equate the work done below:

$$B_v \int_0^{2\pi/\omega} \dot{z}^2 dt = \frac{1}{2} C_d A \rho \int_0^{2\pi/\omega} \dot{z}^2 |\dot{z}| dt, \tag{4.5}$$

where B_v is linear damping constant to be determined. We then insert the expression for the velocity, $\dot{z}(t) = \dot{z}_a \cos(\omega t)$, into (4.5). The cylinder

has vertical displacement $z(t) = \alpha sin(\omega t)$, and therefore $\dot{z}_a$, the maximum heave velocity amplitude, is equal to $\omega\alpha$ for a maximum heave displacement α. The cross-sectional area of a heaving cylinder is equal to $\mathcal{A} = \pi r^2$. After some algebra we get:

$$B_v = \frac{4}{3} C_D \rho r^2 \omega \dot{z}_a \tag{4.6}$$

Here r is the cylinder radius, ρ is the water density, $\dot{z}_a$ is the maximum heave velocity amplitude, and C_D is the same drag coefficient as in the quadratic form of Morison's equation. The linearized viscous force term then becomes:

$$F(t) = \frac{4}{3} \rho C_D r^2 \dot{z}_a \dot{z}(t) \tag{4.7}$$

In certain cases, for example when displacement amplitudes constraints are invoked, it is easier to handle equation (4.7) in terms of the maximum displacement amplitude α:

$$F(t) = \frac{4}{3} \rho C_D r^2 \omega \alpha \dot{z}(t) \tag{4.8}$$

Hence, the linear damping coefficient can be determined knowing either the maximum heave oscillation amplitude or the maximum heave displacement and period of oscillation. For device motion in a regular wave these quantities are easily determined. For motion in irregular waves the situation is more complicated but using time series techniques it is possible to derive both the frequency and amplitude information from a record of the device motion [108]. For a time-invariant or slowly varying system these parameters can be estimated in advance, while for a system whose response changes rapidly they can be estimated and updated online by including an active tuner in the system [108].

4.6 Examples of motion including linearized viscous term

In deriving the results to follow (chapters 5 and 6), this thesis will make use of the Lorentz linearisation method presented in 4.5 as an additional damping term in the equation of motion 3.38. In this section the procedure deriving a value for B_v as well as some example results are demonstrated. Here, the device motion in the array is calculated using the energy-maximizing control schemes presented in 3.6. The value of B_v is passed to the controller as a parameter which then adds it as a damping term in calculating the motion of each device. In this thesis an iterative procedure is used to derive a viscous damping coefficient, B_v, for each device in the array, based on the viscous damping value for an isolated device for a given input sea state. Then, in an array of N equivalent devices, all devices have the same coefficients B. The procedure beings by using (4.8) with the value of the sea state's wave energy period T_e and significant wave height H_s. This first guess is an approximate estimation, whose validity is discussed at the end of section 4.5. Next this value is inserted into the controller whence we calculate the displacement and velocity of the device. Then, knowing the velocity we can use the more accurate formula eq. (4.7) in deriving the next value of B_v in the procedure. We repeat the process until the upper and lower bounds of the damping value converge within 1 % of each other or the 100th iteration in the case that they oscillate about a common point. An example iteration is shown for the case of a 2.5 m radius 6 m draft cylinder in a 2 m 10 s Bretschneider sea state is shown in fig. 4.7.

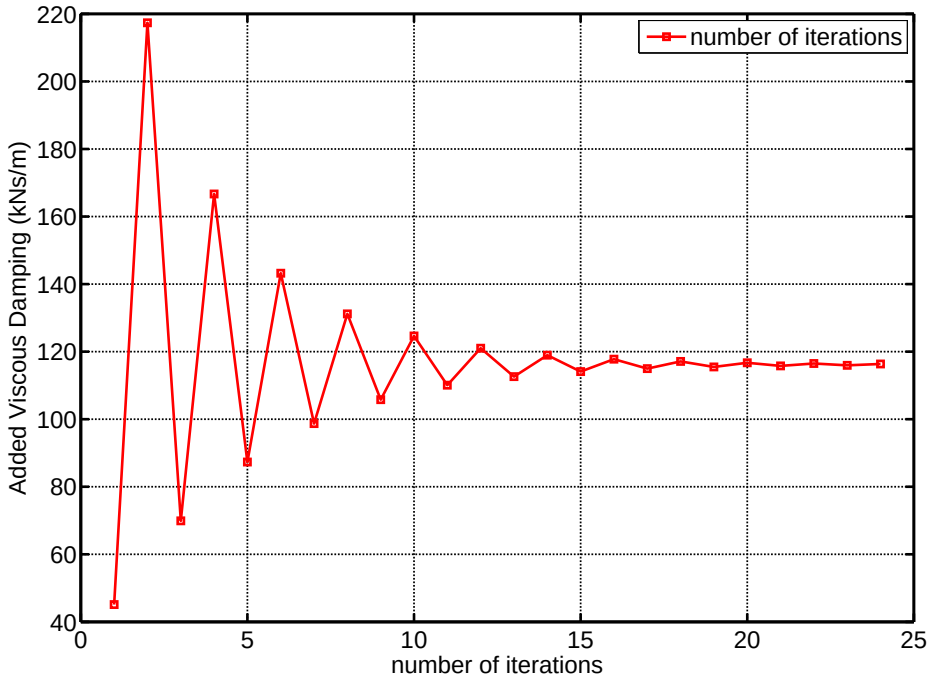

Figure 4.7: Viscous Damping term in kNs/m shown for each iteration in the procedure outline in section 4.6. 5 m radius 6 m draft cylinder operating in heave in a 2 m 10 s Bretschneider sea state

One can see that in this case the value of Bv rapidly converges to 116 kNs/m. The resulting motion of the device is shown in figure 4.8 where the vertical displacement is shown for the value of B_v determined using the iterative procedure, along with the motion without an additional damping term (in practice a negligibly small value of $B_v < 10Ns/m$). One can clearly see the effect of viscous damping in that the motion is decreased by an order of magnitude. In fact, without the damping term, the motion is unrealistically large in this case, with the 6 m draft device clearing the water, undoubtedly an unrealistic scenario.

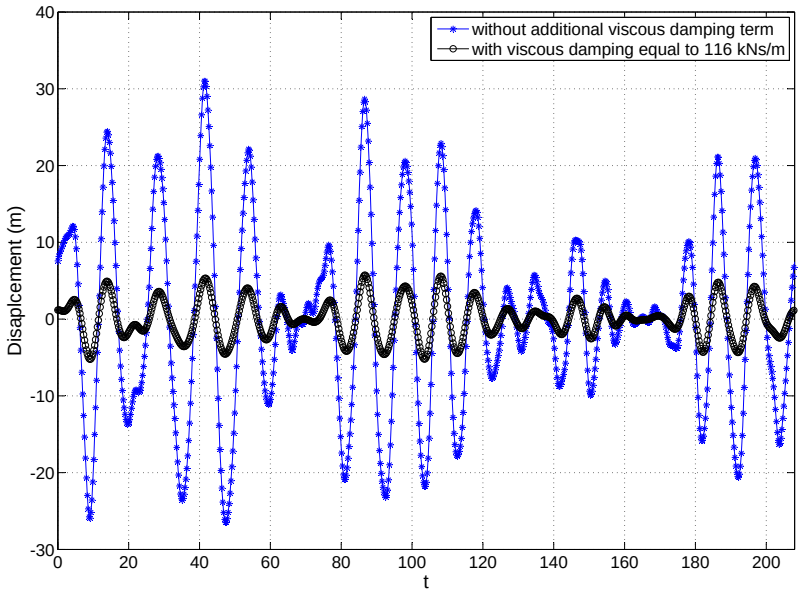

Figure 4.8: Comparison of heave displacement of a 5 m radius 6 m draft cylinder operating in heave in a 2 m 10 s Bretschneider sea with and without an added viscous damping of 116 kNs/m

4.7 Conclusion

The effect of viscous damping, while small enough to be ignored in many linear models of the WEC motion, can present a source of error comparable to the change in the added damping term due to small variations in device spacing [58]. In certain applications like modelling of arrays of WEC, linear theory greatly overpredicts the amplification of the free surface compared with experimental results [58]. This is particularly so in the case of a reactive controller which seeks to approximate the resonance condition by pushing the device to maximize displacement [10]. This overestimation in turn leads to unrealistic predictions for both device heave amplitudes and the power production. In the case of arrays this is especially important because without restriction on motion there can be significant displacements incurred by

devices caused by radiation of surrounding WECs in an array [18]. Including a non-linear friction term in the model will result in a more realistic motion for each individual unit and a better estimate of the total power produced by the array. While viscous damping is not the only source of error in linear WEC models, for example the issue of a fixed wetted surface presumed under linear theory can present a similar magnitude of error, the addition of a linearized viscosity term to the equation of motion is a simple way to improve model accuracy. Moreover, including this term in the model will serve to provide a more accurate estimate of device motion for a real-time controller, where it may noticeably improve the controller's performance. In the specific case of an array, the viscous damping term will prevent an overestimate of the power production of an array in cases where constructive interference from radiation causes large displacements that might be over-predicted by strict linear equations of motion.

Chapter 5

Comparison of Control Strategies

As was demonstrated in chapter 2, given the cost of current technology and the challenges inherent in wave energy conversion, to make wave energy economically feasible, some form of a control scheme will have to be implemented that modifies the motion of the device. Although a variety of control schemes have been implemented to date for single devices [109], for arrays of wave energy devices only the simplest technique, namely variation of the linear damping B_{PTO} in the frequency-domain equation (3.35), has been simulated in studies modelling arrays of WECs in real seas [110, 78, 111, 46]. While theoretical studies of arrays with complex-conjugate control have been performed since the framework of array control was established by Falnes in 1980 [15], these papers [15, 18, 9] have dealt exclusively with regular seas, which while simplifying the problem, cannot be applied directly to real-world control schemes for devices deployed in the ocean. In this chapter we will therefore apply three different control schemes to an array of two and three devices in irregular sea states, comparing their performance and appli-

cability to an array of WEC. While the modelling set-up is also simplified, with device motion restricted to heave only, and with only the Bretschneider spectral representation of an input sea state, it will enable one to test the relative performance of the control schemes and make conclusions about their applicability to arrays of WECs.

5.1 Modelling and control Setup

In this chapter the focus is on the application of different control strategies to an array of heaving, cylindrical WECs. We will assume that the energy can be extracted in heave only and that the mechanical system is frictionless. An example of such a system can be seen in figure 5.1, with the restriction that the rope is assumed to move only in heave. Viscous damping is taken into account, however, as outlined in chapter 4. Our attention is focused on example arrays of two and three devices, whose layout is shown in the diagram 5.2. The schematic diagram of the two-device array is shown in fig. 5.3. The three different control schemes analysed in this chapter, detailed in 3.6, are summarized below:

1. Passive Tuning (PT) to the wave energy frequency of the incoming irregular sea state for each device in the array

2. Independent Control (IC) where array energy is maximized using the hydrodynamic model of a single isolated device

3. Global Control (GC) which maximizes the energy given a complete hydrodynamic model of the array

The 8 input simulated sea states are shown in table 5.1, where for regular seas H is the height and T is the period. For Bretschneider seas, described

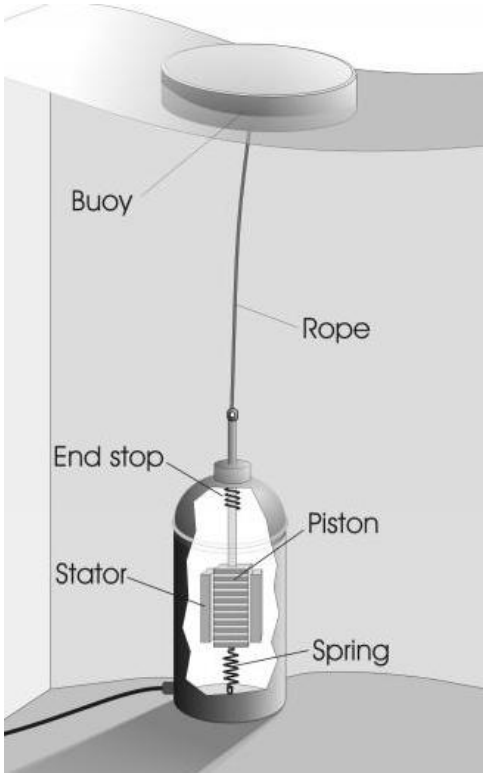

Figure 5.1: An example WEC as modelled in this thesis

in 3.2, H_s is the significant wave height, and T_p is the spectral peak period. The regular sea states simple sinusoidal waves simulated at the period shown, while the Bretschneider seas (equation (3.30)) are simulated by the sea-keeping package WAFO ® over the range of frequencies .0151 to 2.461 rad/sec in steps of .0151 rad/sec. The masses of the devices **M** and the hydrodynamic coefficients, namely **A**, **B**, and **C** are calculated by WAMIT® for the same range of frequencies .0151 to 2.461 rad/sec in steps of .0151 rad/sec as the input sea state. All devices modelled are heaving circular cylinders. The modelled device parameters are shown in table 5.2. The cylinders modelled range from a long thin solid tube to a flat disk, with the shape changing the device's radiative properties while the volume stays approximately the same. A total of 7 cylinder geometries were simulated,

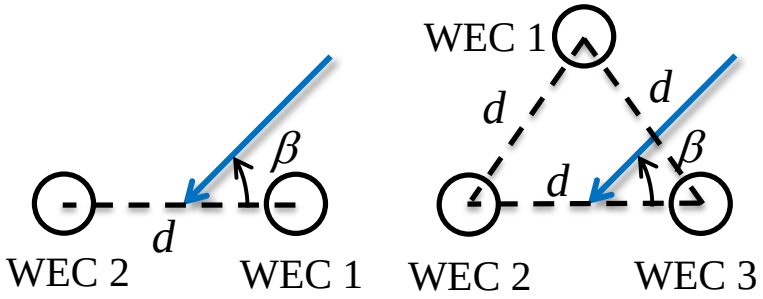

Figure 5.2: Top view of 2 and 3 body array. All devices are separated by d

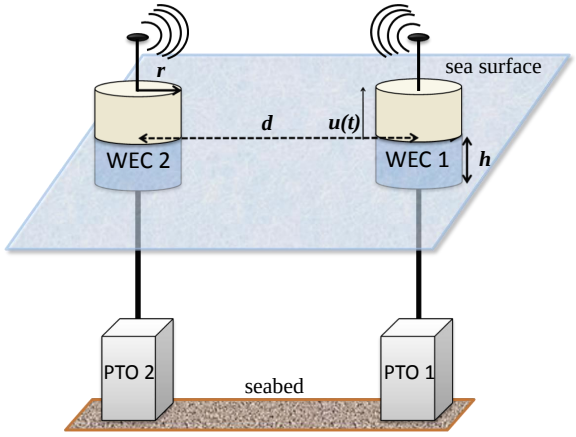

Figure 5.3: Layout for a 2-body array. Motion and PTO force is restricted to heave only

these are shown in table 5.2 sorted by increasing radius and decreasing draft. The unforced heaving resonance period is given by the formula 5.1:

$$T_0 = \frac{2\pi}{\sqrt{\frac{C_{33}}{M+A_{33}}}}. \tag{5.1}$$

where M is the mass of the cylinder, A_{33} is the added mass in heave, and C_{33} is the hydrodynamic stiffness in heave. We can see that as the cylinder gets flatter in shape, the natural resonance period decreases. Each configuration is modelled for a set of distances d from a minimum of $4r$ where r is the radius in meters, to $d = 500m$, with logarithmically increasing spacing. The

Table 5.1: Simulated sea states

type	H [m]	T [s]	type	H_s [m]	T_p [s]
Regular wave	1.0	6.0	Bretschneider	1.0	6.0
Regular wave	1.0	8.0	Bretschneider	1.0	8.0
Regular wave	1.0	10.0	Bretschneider	1.0	10.0
Regular wave	1.0	12.0	Bretschneider	1.0	12.0

angle of wave incidence β is only varied from 0° to 90° in increments of 5°. On the account of the symmetry of the layouts, this provides a complete description for all directional effects.

Table 5.2: Modelled cylinder parameters

name	Radius [m]	Draft [m]	Natural Period [s]
I	2.5	25	10.34
II	3.5	13	7.80
III	4	10	7.05
IV	5	6	5.92
V	6.25	4	5.36
VI	7.25	3	5.08
VII	8	2.5	4.99

5.1.1 Control problem solution

The total energy converted is shown in section 5.2 for an array of 2 and 3 devices for each of the three control methods introduced in 3.6. The discretization procedure outlined in 3.6.1 is utilized, with the fundamental discretization frequency ω_0 set to .0151, resulting in the same frequency resolution as the input sea state and the hydrodynamic coefficients. The simulation time T in equation (3.50) is set to $208s$, a period sufficient to approximate optimal control, as outlined in [89]. For PT, the energy is simply calculated using equation (3.60). For GC and IC, the quadratic programming problems equations (3.55) and (3.57) are solved in MATLAB® by the function `quadprog`. Further detail on the problem setup us given in [80] and

[89]

5.2 Control results

The total energy output (in MJ) for the arrays of 2 and 3 devices with different control strategies are presented in this section. In each table, the rows are the simulated sea states while the columns are selected geometries (for key see table 5.2). Two regular and four irregular sea states are represented. For each sea state illustrative results are shown for 3 incoming wave angles $\beta = 0°, 45°$, and $90°$, where E_{min} and E_{max} is the lowest and highest value, respectively, of the converted energy out of all the simulated distances, for a given β. The data shown in the tables is for two regular and four irregular sea states. The data for PT is shown in tables 5.3 and 5.4, data for GC is shown in tables 5.5 and 5.6, and data for IC is shown in 5.7 and 5.8. Three of the seven geometries as defined in table 5.2 in section 5.1 are considered here, in order of increasing radius and decreasing draft. The tabular data demonstrates the significant increase in the converted energy for GC and IC controlled array, compared with a passively tuned one. The variation between $E_{min}$and E_{max} shows the effects of inter-body separation distance d. Note the large variation in these values for regular seas. This is expected because the large variations ue to constructive and destructive interference are not smoothed out by spectral width as witnessed in the case of irregular seas.

In addition to tabular data, some illustrative graphs are presented which demonstrate the influence of distance on the total power output in a 2-body array as well as the difference between the three control schemes. First, the difference in power output between PT, GC and IC as well as three of the 7 geometries is shown in figure 5.4. Here a sample case is taken where for

Table 5.3: Energy Converted for Passive Tuning for a 2 body array (MJ)

sea	H	T	β	Body Geometry					
	(m)	(s)	(°)	II		IV		VI	
				E_{min}	E_{max}	E_{min}	E_{max}	E_{min}	E_{max}
			0°	1.430	1.835	33.454	44.560	46.040	57.464
R	1.0	6	45°	1.397	1.834	30.417	46.067	46.452	70.057
			90°	1430	1857	34 472	52 706	46 452	70 057
			0°	17.503	18.074	33.715	35.320	64.260	69.054
R	1.0	10	45°	17.460	18.784	33.762	35.169	65.061	70.133
			90°	17.503	18.074	33.083	35.711	64.835	72.642
			0°	0.7494	0.8259	8.5741	9.1448	15.21	15.93
B	1.0	6	45°	0.7362	0.8032	8.1208	9.3107	14.035	16.463
			90°	0.7555	0.81432	8.8868	10.394	15.697	17.651
			0°	5.4241	5.7577	12.79	13.263	23.212	24.225
B	1.0	8	45°	5.3775	5.6144	12.302	13.22	23.197	24.839
			90°	5.2979	5.6864	13.015	13.906	24.403	26.441
			0°	6.422	6.704	14.024	14.424	26.842	27.556
B	1.0	10	45°	6.365	6.565	13.911	14.235	27.183	28.141
			90°	6.266	6.620	14.108	14.509	27.824	29.042
			0°	6.265	6.372	14.088	14.279	28.109	28.582
B	1.0	12	45°	6.237	6.304	14.063	14.242	28.184	29.028
			90°	6.144	6.322	13.932	14.279	28.719	29.550

R = Regular Wave B= Bretschneider. Geometry (rad,draft): II (2.5,13), IV (5,6), VI (7.25,3)

one sea state, namely an irregular sea of $H_s = 1m$ and $T_p = 10s$ and for a head sea at $\beta = 90°$, the total converted power is shown for a 2-body array of three different cylinder Geometries: II, IV, and VI. The figure shows that relative value of the effect of different control schemes and different array body geometries on the total energy output. It is clear from the figure that the effect of array control is proportionally greater than the influence of body shape. However, these effects are superimposed and thus for the most radiative shape (Geometry VII), the difference in absolute magnitude of the total energy converted is much greater between PT and GC than for the low radiation shape (Geometry II). We also note that the array effect on

Table 5.4: Energy Converted for Passive Tuning for a 3 body array (MJ)

sea	H	T	β	Body Geometry					
	(m)	(s)	(°)	II		IV		VI	
				E_{min}	E_{max}	E_{min}	E_{max}	E_{min}	E_{max}
			0°	2.041	2.957	45.74	71.423	64.833	94.099
R	1.0	6	45°	2.115	2.985	50.068	65.715	69.484	89.474
			90°	2.064	2.922	42.804	71.592	58.450	87.392
			0°	25.974	26.956	49.799	52.772	97.156	105.600
R	1.0	10	45°	25.972	26.954	49.792	52.728	97.763	104.24
			90°	25.976	26.955	49.808	52.727	95.554	106.85
			0°	1.108	1.267	12.222	14.218	21.696	25.038
B	1.0	6	45°	1.120	1.274	12.612	13.855	21.798	23.648
			90°	1.126	1.261	12.637	13.951	21.284	24.704
			0°	8.058	8.524	18.505	19.962	35.128	36.876
B	1.0	8	45°	8.106	8.530	18 791	20 011	35 184	36 364
			90°	8.129	8.518	18.763	19.824	34.594	37.193
			0°	9.538	9.927	20.962	21.333	40.628	41.719
B	1.0	10	45°	9.586	9.935	20.982	21.382	40.813	41.521
			90°	9.618	9.922	20.862	21.334	40.470	42.159
			0°	9.321	9.495	20.924	21.314	91.280	99.859
B	1.0	12	45°	9.321	9.499	20.971	21.260	91.279	99.146
			90°	9.322	9.492	20.907	21.346	91.286	99.897

R = Regular Wave B= Bretschneider. Geometry (rad,draft): II (2.5,13), IV (5,6), VI (7.25,3)

energy output, that is the additional energy converted because of positive interference between array members, is much greater for the control schemes GC and IC than it is for PT. For the controlled arrays, this effect is also noticeable for larger separation distances, as even at a distance of $150m$ there is a positive gain in energy for Geometries IV and VII. Note however, that there is also a region of destructive interference at close separation distances, especially in the case of Geometry VII. In this case the control schemes are not able to counteract the phase relationships between radiated waves from either bodies that lead to cancellation of some of the incoming energy.

Table 5.5: Energy Converted for Global Control for a 2 body array (MJ)

sea	H	T	β	Body Geometry					
	(m)	(s)	(°)	II		IV		VI	
				E_{max}	E_{min}	E_{max}	E_{min}	E_{max}	E_{min}
			0°	8.7929	11.099	33.609	44.877	52.497	71.115
R	1.0	6	45°	8.4669	10.779	30.556	46.348	47.842	81.215
			90°	9.2909	11.357	34.507	53.872	52.089	102.5
			0°	50.98	56.335	116.05	134.53	181.93	234.31
R	1.0	10	45°	49.648	56.942	109.53	136.11	181.32	250.61
			90°	48.261	58.868	100.57	151.11	159.52	283.41
			0°	4.5177	4.7312	15.36	16.088	24.459	25.818
B	1.0	6	45°	4.3428	4.6593	14.347	16.549	23.753	27.776
			90°	4.3016	4.8015	15.789	17.921	26.221	31.661
			0°	12.25	12.637	32.351	33.947	51.319	56.386
B	1.0	8	45°	11.699	12.826	30.511	34.926	51.042	57.954
			90°	11.117	13.156	28.359	37.112	50.418	64.413
			0°	21.066	22.551	49.904	53.548	84.276	90.006
B	1.0	10	45°	20.47	22.916	46.422	55.434	78.809	93.731
			90°	19.838	23.384	43.106	58.025	70.825	101.69
			0°	29.311	31.663	63.39	70.477	112.25	122.25
B	1.0	12	45°	28.821	32.115	60.524	72.752	102.94	127.77
			90°	28.307	32.577	57.663	75.096	93.792	135.76

R = Regular Wave B= Bretschneider. Geometry (rad,draft): II (2.5,13), IV (5,6), VI (7.25,3)

Next the case of the three body array for the same cylinder shapes is examined in fig 5.5. In this example, for the same irregular sea state of $H_s = 1m T_p = 10s$, and for a incident wave angle of $\beta = 60°$, the difference in energy output between the two control schemes and PT is just as large, as is the difference between the different body shapes. And yet, in contrast to the two-body case, we see a pronounced effect of the distance on power output for GC and IC, where for Geometry VII the positive interaction is significant even at an inter-body separation distance of $500m$. In the PT case no such effect is observed, meaning this effect is due to the control schemes' ability to utilize the constructive radiation effect in the array. To further analyse the

Table 5.6: Energy Converted for Global Control for a 3 body array (MJ)

sea	H	T	β	Body Geometry					
	(m)	(s)	(°)	II		IV		VI	
				E_{max}	E_{min}	E_{max}	E_{min}	E_{max}	E_{min}
			0°	12.614	16.898	46.256	72.09	71.34	129.43
R	1.0	6	45°	13.145	16.967	51.006	66.15	86.259	116.03
			90°	12.757	16.814	43.193	72.17	62.389	112.53
			0°	67.878	85.933	144.77	211.66	265.1	384.16
R	1.0	10	45°	67.868	84.443	144.68	202.56	264.67	362.86
			90°	67.892	83.252	144.9	200.77	246.98	360.31
			0°	6.5181	7.0476	21.788	25.133	34.798	37.98
B	1.0	6	45°	6.6168	6.8677	22.411	23.634	33.877	42.387
			90°	6.5468	6.989	21.586	24.811	39.462	51.518
			0°	16.495	19.236	42.902	52.214	74.921	86.458
B	1.0	8	45°	16.502	18.932	43.126	50.417	75.724	82.106
			90°	16.499	19.207	43.203	52.396	76.071	86.827
			0°	28.143	34.278	62.285	82.418	108.72	139.27
B	1.0	10	45°	28.141	33.919	62.348	80.682	109.02	134.16
			90°	28.15	34.194	62.456	82.62	109.33	139.38
			0°	39.558	48.001	79.671	108.17	135.85	189.48
B	1.0	12	45°	39.556	47.662	79.693	106.63	135.96	184.51
			90°	39.563	47.722	79.761	107.52	136.17	186.84

R = Regular Wave B= Bretschneider. Geometry (rad,draft): II (2.5,13), IV (5,6), VI (7.25,3)

difference between PT, GC and IC , it is instructive to compare regular wave examples to irregular wave ones. We start by focusing on PT, where in figure 5.6, the converted energy is plotted over distance for 5 regular sea states for a two body array of cylinders of Geometry V. Power output for irregular sea states with H_s and T_p set at the same values as H and T in the regular wave cases are shown in figure 5.7. A clear difference in behaviour between the regular and irregular seas is noted: whereas in the regular sea case the largest absolute peak in power is found at $T = 6s$, for the irregular wave case, it is at the highest T_p of $12s$. This is because at a period of $T = 6s$ the resonance frequency of the device, $5.94s$, is very close to the tuning period,

Table 5.7: Energy Converted for Independent Control for a 2 body array (MJ)

sea	H	T	β	Body Geometry					
	(m)	(s)	(°)	II		IV		VI	
				E_{max}	E_{min}	E_{max}	E_{min}	E_{max}	E_{min}
			0°	8.792	11.093	33.438	44.508	51.589	69.629
R	1.0	6	45°	8.465	10.777	30.219	46.172	47.218	80.363
			90°	9.2868	11.354	34.367	53.024	51.705	96.913
			0°	50.716	56.24	115.54	133.17	180.02	227.54
R	1.0	10	45°	49.394	56.922	107.64	135.91	179.47	249.49
			90°	48.019	58.816	98.983	150.3	154.57	278.87
			0°	39.558	48.001	79.671	108.17	135.85	189.48
B	1.0	6	45°	39.556	47.662	79.693	106.63	135.96	184.51
			90°	39.563	47.722	79.761	107.52	136.17	186.84
			0°	4.509	4.695	15.215	15.762	23.862	25.761
B	1.0	8	45°	4.335	4.6572	14.166	16.491	23.124	27.55
			90°	4.267	4.7921	15.702	17.664	25.907	30.545
			0°	20.935	22.545	48.879	53.28	83.246	87.431
B	1.0	10	45°	20.343	22.91	45.503	55.345	75.743	93.329
			90°	19.716	23.36	42.296	57.708	68.445	100.13
			0°	29.15	31.658	62.316	70.401	108.17	120.36
B	1.0	10	45°	28.663	32.109	59.534	72.683	99.546	127.41
			90°	28.154	32.557	56.76	74.861	91.093	134.44

R = Regular Wave B= Bretschneider. Geometry (rad,draft): II (2.5,13), IV (5,6), VI (7.25,3)

$T = 6s$. This is also evidenced by the large peaks and troughs in the curve of the power output at $T = 6s$ that are the result of the device oscillations producing relatively large constructive and destructive interference. The resonance effect is also visible in the $T = 5s$ curve, which is also not far removed from the natural period of the device. The higher period sea states, by contrast, show comparatively less power modification, meaning that the the device is primarily forced by the incoming waves. For the irregular wave case in figure 5.7, we still see the influence of resonance at $T_p = 6s$, especially in the $\beta = 90°$ case (circle markers), where there is a marked increase in the power output at close distances. Still, the overall effect is muted, with the

Table 5.8: Energy Converted for Independent Control for a 3 body array (MJ)

sea	H	T	β	Body Geometry					
	(m)	(s)	(°)	II		IV		VI	
				E_{max}	E_{min}	E_{max}	E_{min}	E_{max}	E_{min}
			0°	12.612	16.76	45.535	71.384	70.65	125.85
R	1.0	6	45°	13.14	16.69	49.991	65.827	81.276	114.59
			90°	12.741	16.561	42.646	71.811	60.949	111.69
			0°	66.727	85.88	138.35	211.11	246.34	380.87
R	1.0	10	45°	66.717	84.421	138.26	202.18	245.92	360.96
			90°	66.741	83.195	138.48	199.53	241.95	355.61
			0°	6.4872	7.0409	20.593	24.936	34.383	41.172
B	1.0	6	45°	6.5796	6.8635	21.082	23.528	34.932	38.717
			90°	6.5195	6.9851	21.194	24.708	34.595	41.319
			0°	16.162	19.219	40.616	51.92	68.984	85.15
B	1.0	8	45°	16.168	18.922	40.776	50.257	69.398	81.384
			90°	16.169	19.197	40.964	52.223	69.727	86.093
			0°	27.569	34.255	59.111	82.111	100.16	137.82
B	1.0	10	45°	27.566	33.906	59.147	80.504	100.29	133.38
			90°	27.577	34.177	59.306	82.405	100.63	138.36
			0°	38.817	47.98	75.998	107.9	125.77	188.18
B	1.0	10	45°	38.815	47.649	76.007	106.49	125.8	183.79
			90°	38.822	47.702	76.099	107.3	126.03	185.68

R = Regular Wave B= Bretschneider. Geometry (rad,draft): II (2.5,13), IV (5,6), VI (7.25,3)

influence of distance very slight and the total power converted on average a third of that converted for the regular wave case. Next, the instance of GC and IC is examined for the same configuration of a 2-body array of Geometry V for regular waves 5.8 and irregular waves 5.9, where both IC and GC are plotted for $\beta = 0°, \beta = 45°$, and $\beta = 90°$ for periods of 6,8, and $10s$. As in the PT case, there are notable differences between the regular and irregular wave cases, with the regular wave case understandably exhibiting more interaction. Nonetheless, there is still considerable interference in the irregular wave state for IC and GC, where there is almost none for PT, with most of it constructive beyond the first 50 meters of separation distance.

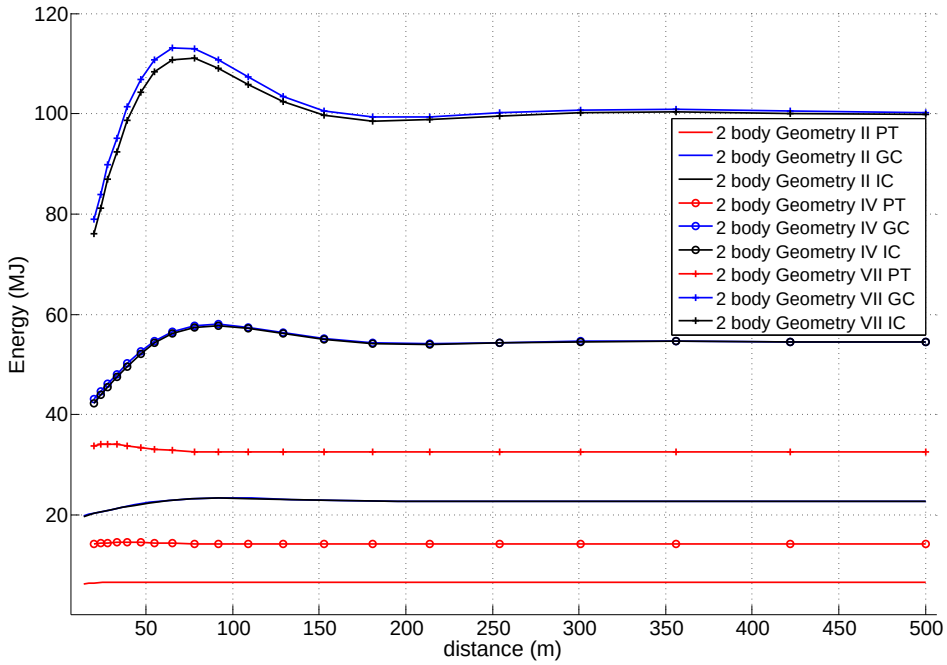

Figure 5.4: Total Energy Converted for 2-body arrays of 3 different geometries and 3 control schemes. Sea State: Bretschneider $H_s = 1m$ $T_p = 10s$, $\beta = 90°$

If we now look at a similar graphs for the less radiative Geometry II, in figures 5.11 and 5.10, with a longer draft and shorter radius, we can see that the essential features of the graph remain the same, but that the absolute magnitudes of the interference effects are diminished. This is, again, due to the fact that interference is due to scattering and radiation, and with a thinner, longer shape, scattering decreases while at the same time the body does not have as favourable radiation properties as a thinner cylinder and therefore is not radiate out to the other body in the array.

5.3 Discussion

From the tabular data we see increase in the power converted by the controlled array versus a passively tuned one for every sea state and configu-

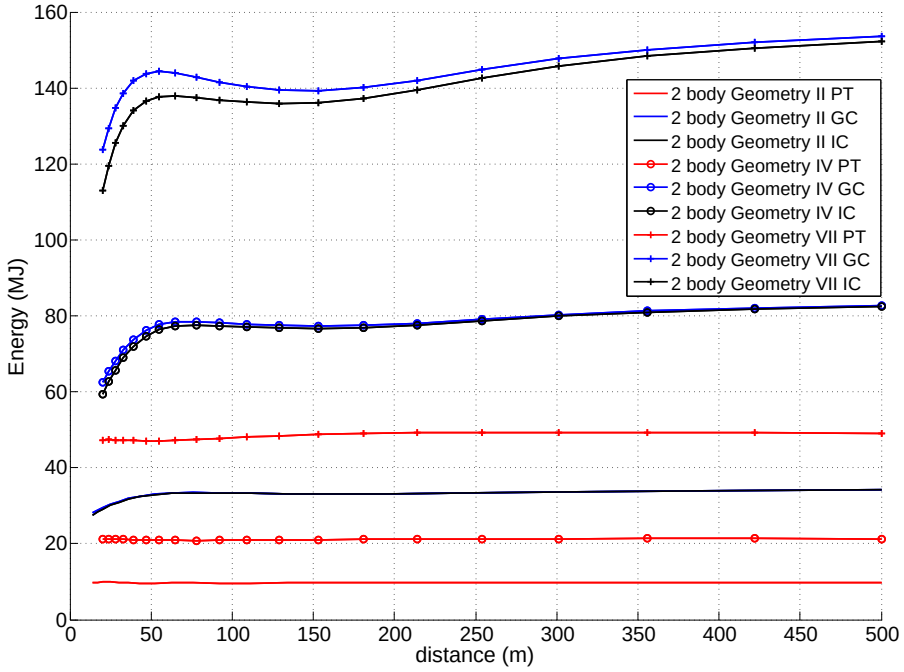

Figure 5.5: Total Energy Converted for 3-body arrays of 3 different geometries and 3 control schemes. Sea State: Bretschneider $H_s = 1m$ $T_p = 10s$, $\beta = 90°$

ration, approaching an order of magnitude difference in some cases. This increase, however, is not uniform between different body geometries and sea states. Because PT tunes the device to a single frequency, in regular seas where the wave energy frequency is close to the natural frequency of the cylinder, PT will tune the device to oscillate close to its optimal profile for maximum power extraction. As an example, in table 5.3 for Geometry VI which has a natural period of $5.94s$, (see 5.2), in the case of a 2 body array oriented at $\beta = 45°$ PT converts 86% of the energy that GC converts and 88% of what IC converts. This however is close to an ideal situation for PT, and in a real life operating scenario with real seas which may be far away from the device's natural period the performance of PT is, as one can presume, poor. To illustrate, we take the same cylinder (Geometry VI) but

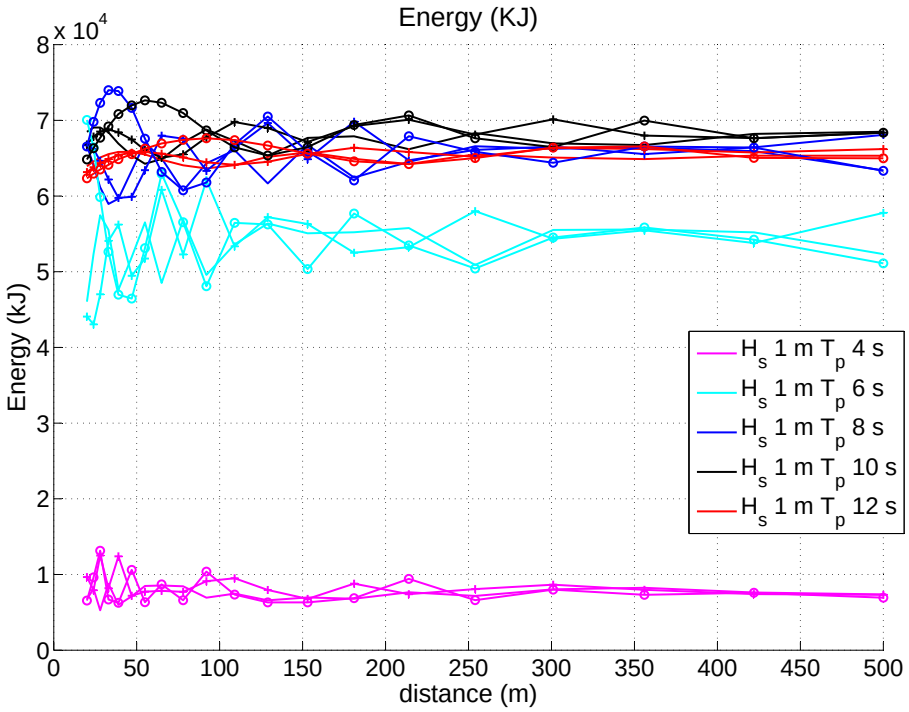

Figure 5.6: Total Energy Converted by a 2 body array for PT for regular wave case. Geometry V

place is in an irregular sea state with the peak period far removed from the natural period, $T_p = 12s$. In this case, for $\beta = 45°$ the maximum energy converted by PT is only 22% of the energy converted by GC and IC. The result should not be surprising as it shows the effectiveness of array control where control can not only modify the oscillation period of each of the devices but also take advantage of the radiative properties of the devices to increase the power captured. Because a flatter body with a smaller draft and bigger radius is able to radiate more energy, and by extension capture more energy from the incoming wave, an increase in captured energy can be observed in all the data tables from left to right, with decreasing radius and increasing draft. This difference can also be seen between figures 5.10 and 5.11 and figures 5.8 and 5.9 where the former are for the thinner, longer Ge-

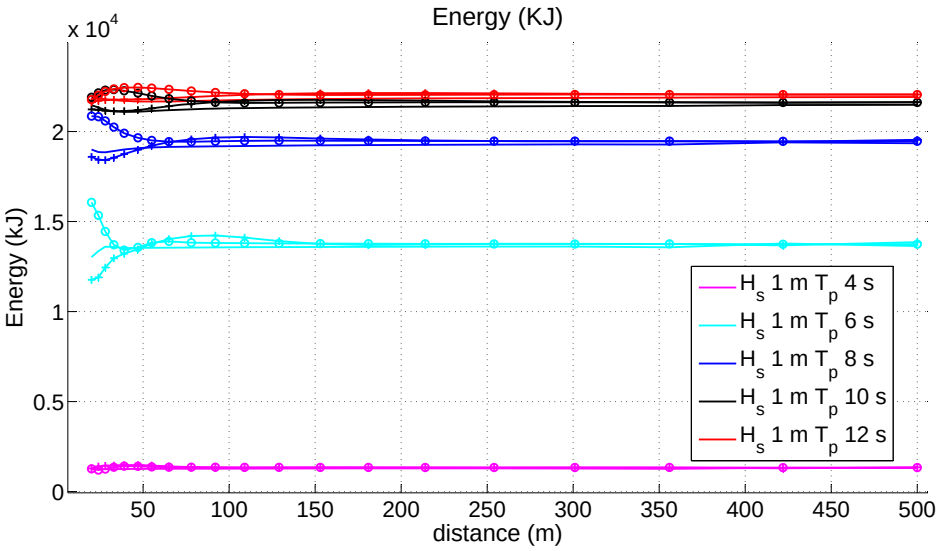

Figure 5.7: Total Energy Converted by a 2 body array for PT for irregular wave case. Geometry V

ometry II and the latter for the flatter Geometry V. This is true of both PT and active control. However, active control is not only effective for highly radiative bodies and large sea states. For example, for Geometry II, for the irregular sea state of $T_p = 6s$ at all angles β, the maximum converted energy for PT is less than .08 MJ while for GC and IC this figure is between 4.7 and 4.8 MJ, a five-fold increase. For Geometry VI there is less than a two-fold difference between the maximum converted energy by PT and GC. For arrays of devices operating in small sea states, the difference between the energy converted by GC and PT might make the difference between the device sitting idle and operating, which would ultimately affect the economic performance of a WEC array project.

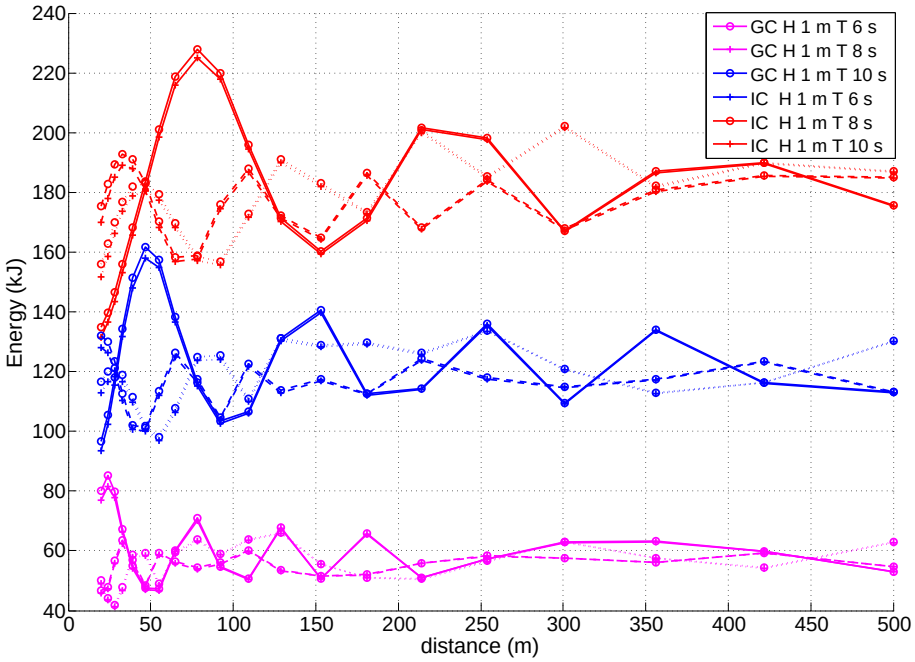

Figure 5.8: Total Energy Converted by a 2 body array for GC (o) and IC (+) for regular wave case. $\beta = 0°$ (solid line), $\beta = 45°$ (dotted line), $\beta = 90°$ (dashed line). Geometry V

5.3.1 Difference between GC and IC

As is witnessed in figures 5.11, 5.10 , 5.9, and 5.8, showing both GC and IC for a range of sea states for two different-shaped cylinders, the difference between GC and IC is not very large, especially compared to the difference in converted energy between PT and both control schemes. It is however, worthy to examine this dissimilarity further. As can be seen in these graphs, the difference, while small, grows with increasing radiative interference, both negative and positive, and is especially apparent in the large peak in the curves at $\beta = 90°$ at the region of maximum power capture. To further look into this matter, plots of the percentage difference in converted power between GI and IC over inter-body distance are presented in figures 5.12 and 5.13 for a 2-body and 3-body array, respectively, for an irregular sea

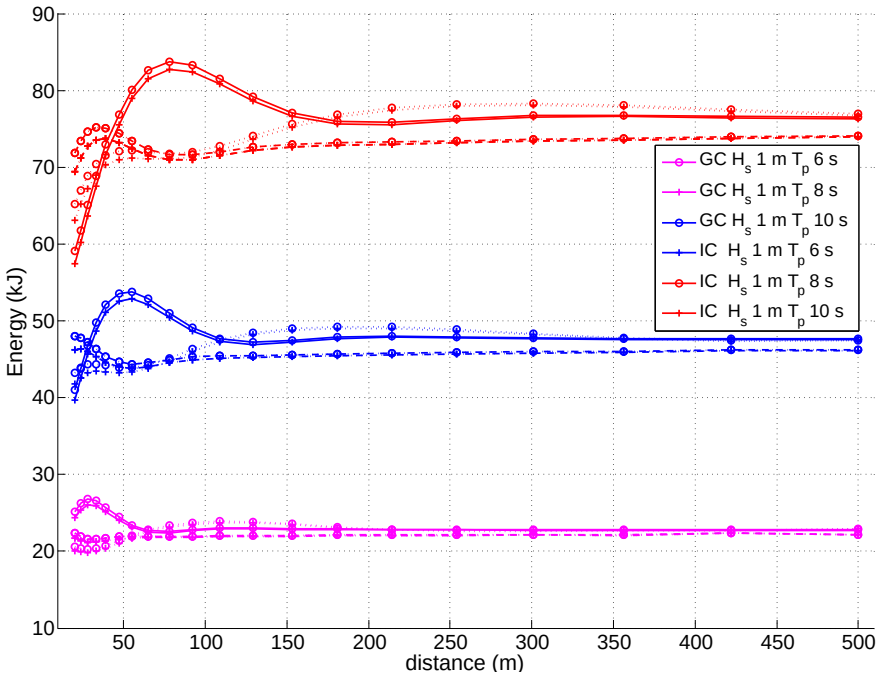

Figure 5.9: Total Energy Converted by a 2 body array for GC (o) and IC (+) for Bretschneider wave case. $\beta = 0°$ (solid line), $\beta = 45°$ (dotted line), $\beta = 90°$ (dashed line). Geometry V

state of $H_s = 1m$ and $T_p = 10s$ for all 7 geometries. The results clearly show that the difference is small, at most one percent for the two-body case and three percent for the three-body case. As anticipated, the effect is most pronounced for the most radiative geometries and is almost negligible for the thin long geometries. The magnitude of the effect for regular seas is the same, with 1% and 3% difference between GC and IC for the 2-body and 3-body array, respectively. Based on these results it can be asserted that the discrepancy between GC and IC is not significant enough in terms of its effect on power output to chose one scheme over the other, especially in light of the other significant effects such as body geometry, incoming sea state, separation distance, and wave incidence angle. The latter two effects will be examined for additional array configurations in more detail in chapter 6.

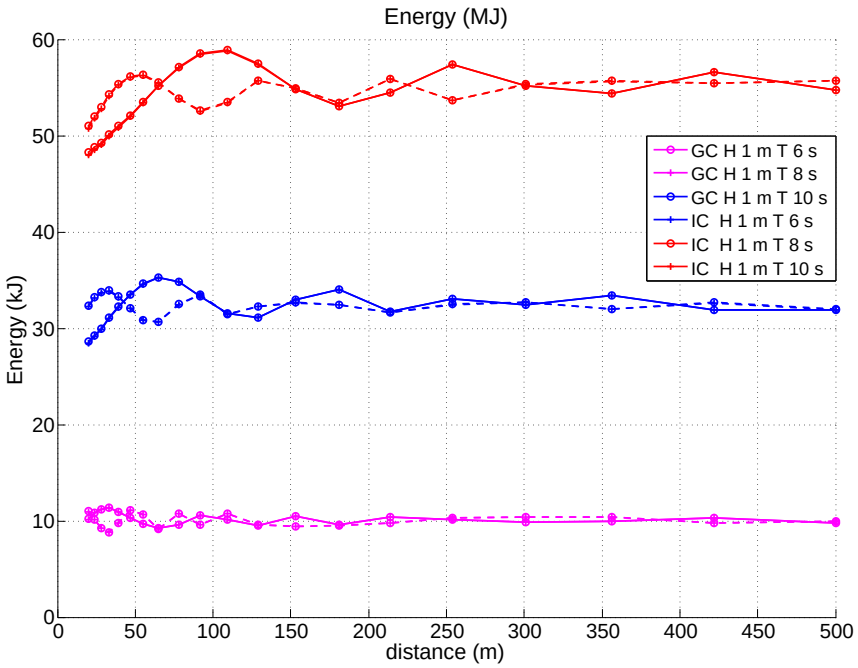

Figure 5.10: Total Energy Converted by a 2 body array for PT for regular wave case. Geometry II

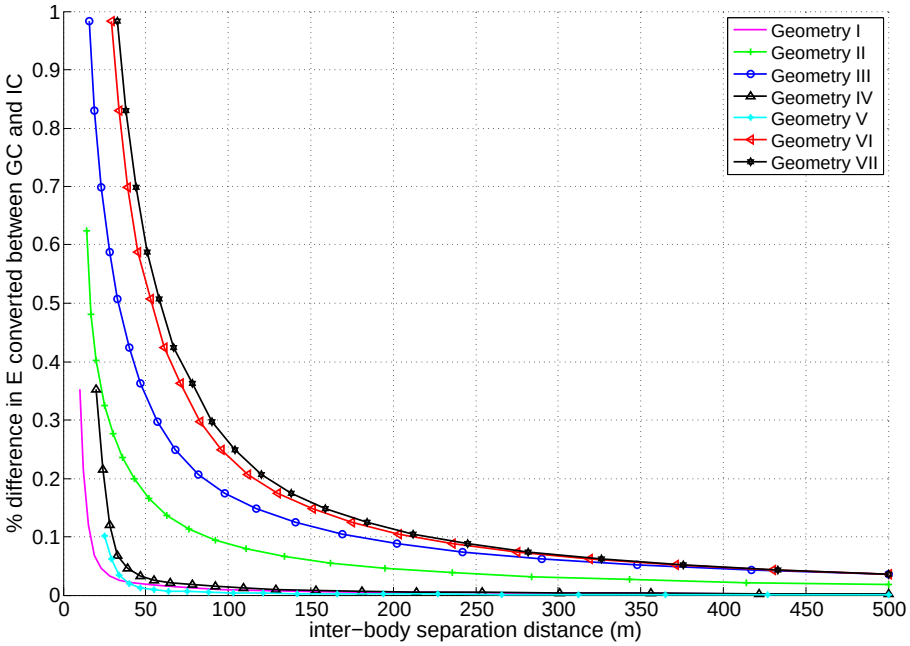

Figure 5.12: % difference between GC and IC for a 2-body array for Bretschneider sea H_s= 1 m T_p = 10s , β = 90°, for 7 Geometries listed in table 5.2

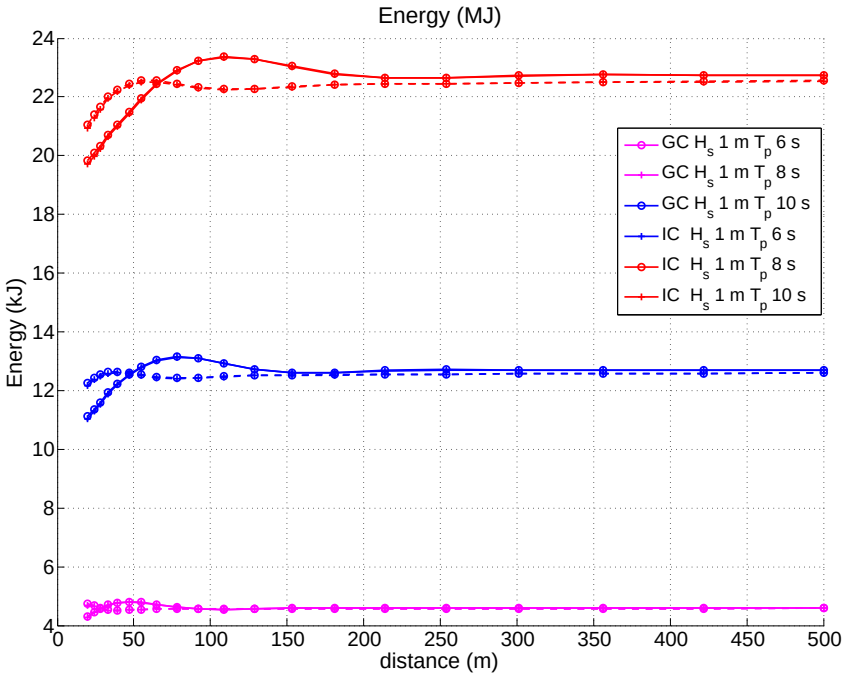

Figure 5.11: Total Energy Converted by a 2 body array for PT for irregular wave case. Geometry II

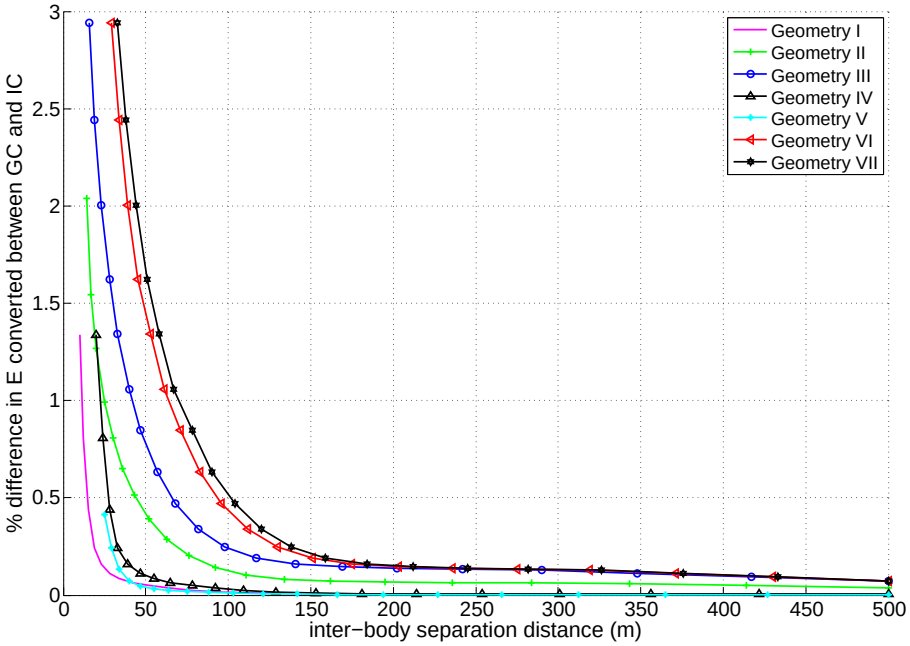

Figure 5.13: % difference between GC and IC for a 3-body array for Bretschneider sea H_s= 1 m $T_p = 10s$, $\beta = 90°$, for 7 Geometries listed in table 5.2

5.4 Conclusions

The effect of different control schemes on the power output of devices was investigated in this chapter. It was shown that adaptive control schemes such as GC and IC show superior performance over a simple tuning scheme such as PT, with a at least a three-fold increase in the energy converted for every sea state and configuration examined. In examining PT, it is worth remarking that alternative tuning regimes exist, such as diagonilization of the optimal damping matrix as is done in [47, 78], or choosing the value of $\mathbf{B_{pto}}$ based on an optimization procedure [47, 44]. While these schemes might produce better power output under certain conditions, they are more difficult to implement than simple tuning. At the same time, is is not possible to adapt them on a continuous basis, as is possible with control schemes. One additional point worth noting is that GC and IC both involve the use of reactive power, that in certain cases would not be possible to implement because of the nature of the specific PTO system. Furthermore, in some cases the cost of designing a PTO system that allows for high flows of reactive power would be prohibitive to a WEC project. There exist some possible solutions to this problem, one can implement constraints on the reactive power and or the PTO force to fit the specifications of the particular device. Alternatively, one can make the control system passive, that is force the PTO force in (3.38) to always have a positive sign. Finally, as we have seen in chapter 2, alternative objective functions for the control system can be implemented, such as those which seek to smooth the power output of a WEC array over a certain time interval as opposed to maximizing it at every time step.

Chapter 6

Clustered Array Optimization

As was shown in chapter 5, array layout is one of the primary determinants of a WEC array's energy output. There are many factors which determine the placement of devices in WEC array project, such as the electrical cabling, site bathymetry, navigation corridors, and project area size restrictions, some of these were elaborated on in 2.4.6. In this chapter, the focus will be solely on hydrodynamic factors that influence the array power output, that is the modification of the power output of devices in an array by other devices through scattering and radiation as well as modification of incoming waves. As was demonstrated in chapter5, a controlled array exhibits quite a different response to incoming waves than a passively tuned one, specifically in that significant energy output modification may occur at separation distances of up to $200m$. In this chapter the effect of the array layout on the power output on a controlled array of devices will be examined, with a focus on closely-spaced circular arrays of devices, because radiation, the means through which active control can create constructive

interference, is proportional to the inverse square root of the inter-device separation distance d.

6.1 Modelling setup

Analogous to chapter 5, the focus is on arrays heaving cylinders whose motion is described by 3.38. Linear wave theory applies to all the motions, and a linearised viscous damping term is added, as detailed in chapter 4. The cylinders modelled are shown in table 6.1, in order of increasing radius and decreasing draft.

Table 6.1: Modelled cylinder parameters

name	Radius [m]	Draft [m]	Natural Period [s]
I	2.5	25	10.34
II	3.5	13	7.80
III	4	10	7.05
IV	5	6	5.92
V	6.25	4	5.36
VI	7.25	3	5.08
VII	8	2.5	4.99

The sea states examined are shown in table 6.2, where the sea-keeping package WAFO® over the range of frequencies .0151 to 2.461 in steps of .0151, is used to calculate the irregular Bretschneider spectra. Symmetric array configurations of 2,3,4,5, and 6 bodies are examined. The array configurations are shown in figure 6.1 and for a schematic diagram of the setup the reader is referred back to figure 5.3 in chapter 5. A total of 20 separation distances d between the elements is varied from $4r$ to 500 m on a logarithmic scale.

Table 6.2: Modelled sea states

type	H [m]	T [s]	type	H_s [m]	T_p [s]
Regular wave	1.0	6.0	Bretschneider	1.0	6.0
Regular wave	1.0	8.0	Bretschneider	1.0	8.0
Regular wave	1.0	10.0	Bretschneider	1.0	10.0
Regular wave	1.0	12.0	Bretschneider	1.0	12.0

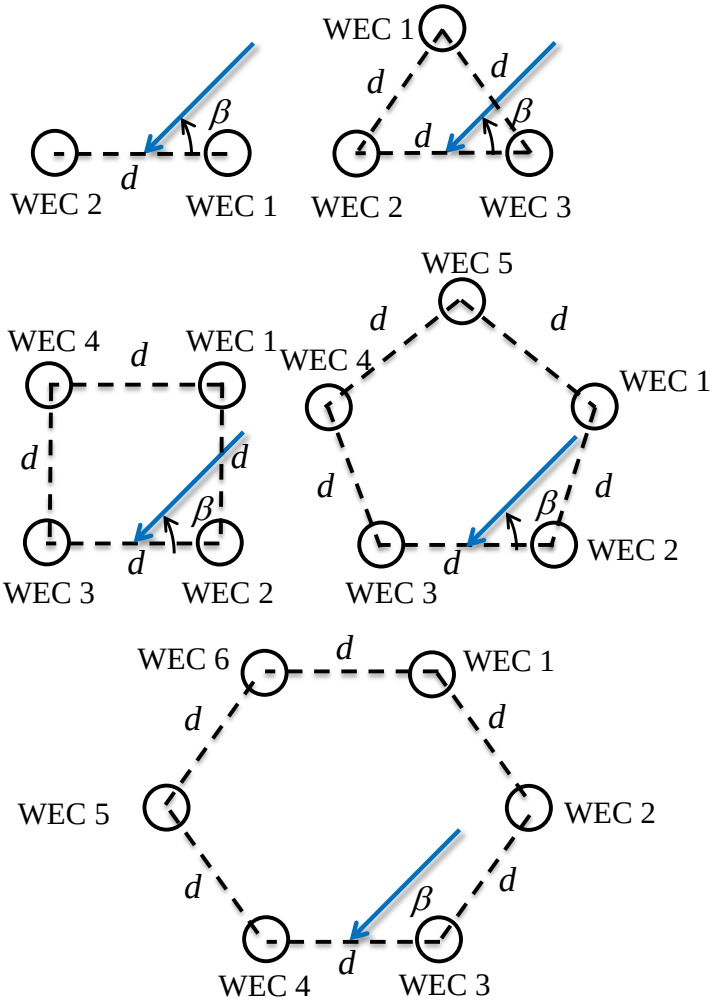

Figure 6.1: Top view of 2, 3 , 4 ,5 , and 6-body circular array. All separation distances d are regular polygon sides.

Because the array configurations are symmetric, the incident wave head-

ing angle β is only varied from 0° to 90° in increments of 5°. The excitation force $\mathbf{f}_{ex}$ is calculated from the sea profile and the hydrodynamic coefficients **A**, **B**, and **C** are calculated by WAMIT® for the range of frequencies .0151 to 2.461 in steps of .0151 . As was demonstrated in the previous chapter 5, the difference in the power output of the devices between the control schemes GC and IC is not meaningful enough to chose one control over the other to optimize power production. Therefore in this chapter GC is chosen on the basis of its more generalized objective function, which includes all the hydrodynamic interactions in the system, and its more straightforward implementation. Consequently, all controlled simulation in this chapter will be performed using global control.

As was observed in chapter 5, automatic control such as GC modifies the behaviour of devices by forcing them to radiate more with the aim of absorbing more power. In an array the radiation emitted by one body can subsequently enhance the energy uptake of another body. The strength of this radiation depends on the strength of the radiated wave field and the distance from the radiating object. Radiation strength depends on the body shape, and as was shown for cylinders in 5.2 in chapter 5, given a constant volume, the greater the radius and smaller the draft, the more a cylinder will be able to radiate waves. The dependence of radiation on distance is given by the following formula [82].

$$\phi_R \sim \frac{-ig\mathcal{A}(\theta)}{\omega}\left(\frac{2}{\pi\kappa r}\right)^{\frac{1}{2}} e^{i\kappa r - i\pi/4}\frac{\cosh\kappa(z+h)}{\cosh(\kappa h)} \ , \ \kappa r \to \infty, \tag{6.1}$$

where $\mathcal{A}(\theta)$ is the angular variation of the radially spreading wave. From this formula it is apparent that the radiation potential decreases as the square root of the distance r from the radiating object. In our case this is

the inter-device spacing r: as it increases one expects the interaction effects to decrease. Consequently, we would expect the greatest modification of array behaviour for highly radiative bodies for the closest spacing. However, this interaction is also dependent on the wavenumber κ. As we see in (6.1), the behaviour of the radiation potential also depends on κ. Because of the dispersion relation (3.11), the greater the period of the wave, the smaller the wave number. Therefore, because κ serves as a multiplying factor on r, as is readily apparent from 6.1, for greater period waves, one would expect stronger interaction effects to occur at greater inter-device spacing d. The hydrodynamics of array interaction is a complicated problem, and often times it is very difficult to distinguish the influence of different variables that affect the power output. In this chapter, the influence of the number of bodies, sea state, device geometry, input sea state, wave incidence angle β, and inter-body spacing d will be considered. Therefore an attempt shall be made to present the results as cross-sections of the different variables, with an emphasis on 3-D and contour graphs to present the results. As was shown in section 2.2 in chapter 2, the array interaction value q is the most commonly used benchmark of WEC array performance. As we are utilizing only one control scheme, GC, for all simulations, the energy converted by a single, isolated device will be the same for each geometry and sea state. Therefore q will be an appropriate measure of the effects of multi-body interactions on the power output of a WEC array.

6.2 Layout study in regular seas

6.2.1 2-body array

To begin the investigation, it is helpful to look at the simplest case, namely a 2-body array in regular seas. Although this is not a realistic operating scenario, with this simplified system it is possible to understand the nature of interactions in the array that will not be readily apparent from a study of more complicated, realistic WEC arrays. We start by simulating a regular wave with $H = 1m$ and $T = 10s$, plotting the contour plot of the q-value versus wave incidence angle β and separation distance d for Geometry VII in figure 6.2. Following [69], the interaction distance L for two devices placed on the x-axis is $(L = 2\pi d)/\lambda(1 \pm cos\beta)$ where the negative cosine is from the first body to the second and the positive in the opposite direction for incident wave length λ. From this one can plot a set of hyperbolas which are a solution to

$$\frac{\lambda}{2\pi} = \frac{d(1 \pm cos\beta)}{c} \tag{6.2}$$

where c is a constant for which the phase of the interaction is the same. A set of curves for the peak interaction for the first three areas of positive interaction are plotted in figure 6.2. The first peak is primarily due to the radiation while the second and following are due to scattering. We note good agreement with the contours of maximum q, especially for larger separation distances where the assumptions in deriving (6.2) hold (see [69] for more details). A maximum q of 1.15 is found near the intersection of the first two interaction curves at 90° where the radiated waves from both bodies are in phase and no shadowing occurs. A similar plot is next shown for Geometry III in figure 6.3 for the same sea state. The first thing we notice is a decrease in the range of the q values and the broadening out of the interaction peaks.

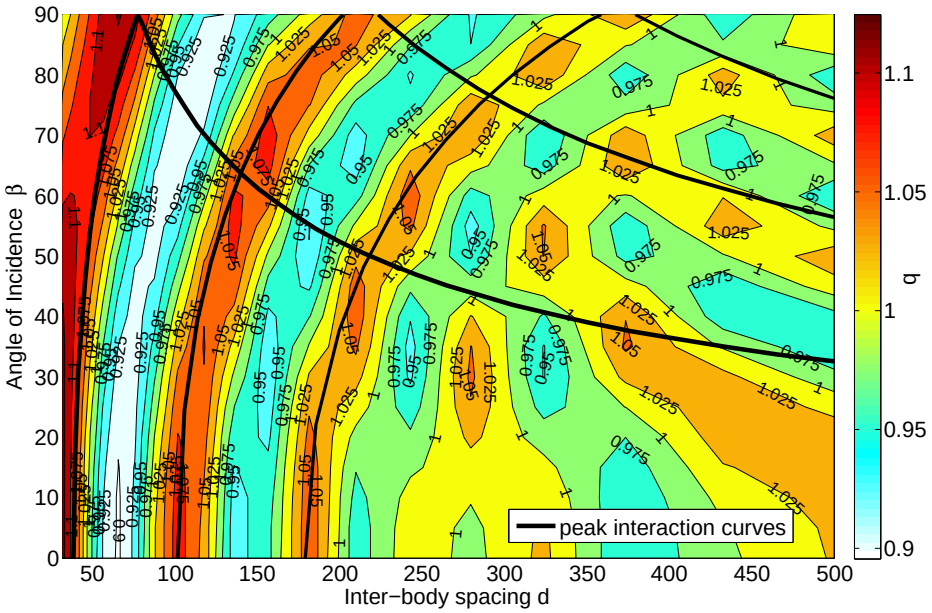

Figure 6.2: q-factor for 2-body array regular wave of 1 m height 10 s period, with eq. (6.2) plotted for the first three interaction maxima. Geometry VII

This is due to the less radiative shape of the cylinders, despite this, the relation 6.2 holds as evidenced from the interaction curves. To examine the influence of sea state, a 2-body array of the same geometries is chosen but in smaller and larger period sea states. First, a 2-body array of Geometry III is simulated in a $H = 1m$, $T = 6s$ regular sea state in figure 6.4. The plot for Geometry IV now resembles that for Geometry VII in a $1m$ $10s$ irregular sea because of the stronger interaction between the body geometry and the period of the sea. In addition, as T increases, λ decreases, so that the interaction curves are closer together than for the longer sea state. The opposite can be observed in figure 6.5 where a 2-body array of Geometry VII is placed in a $H = 1m$, $T = 12s$ regular sea. As expected, in this example, the interaction spread over a larger distance, both in r and in terms of the spread over the angles β. Because Geometry VII is a highly radiative body, there is clear interaction at this sea state, which is not true in the case of

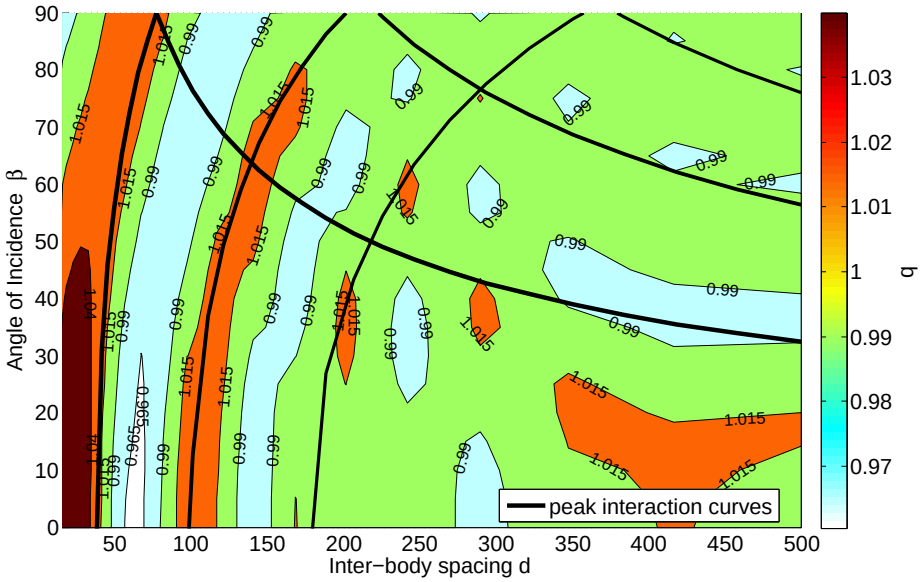

Figure 6.3: q-factor for 2-body array regular wave of 1 m height 10 s period, with eq. (6.2) plotted for the first three interaction maxima. Geometry III

Geometry IV, where in a $H = 1m$, $T = 12s$ sea the modification of q is an order of magnitude smaller (not shown).

6.2.2 Multi-body array

Next, the focus in shifted to multi-body arrays. Here the interaction is more complicated and cannot be described by a simple formula such as (6.2), the essential features of the contour plot of q show the same interplay of d,β, and λ as for the two body case. Again, contour plots of q versus d and β will be shown for various regular sea states and body geometries. The essential features of array interaction for multiple bodies are demonstrated in contour plots of the interaction factor, shown here for a regular sea state of $H = 1m$, $T = 12s$ for Geometry V, which is a flat cylinder with a ratio of radius to draft approximately 3 to 2. In figures 6.6, 6.7, 6.8, and 6.9, q is shown for arrays of 3, 4, 5, and 6 cylinders, respectively. Overall, we note

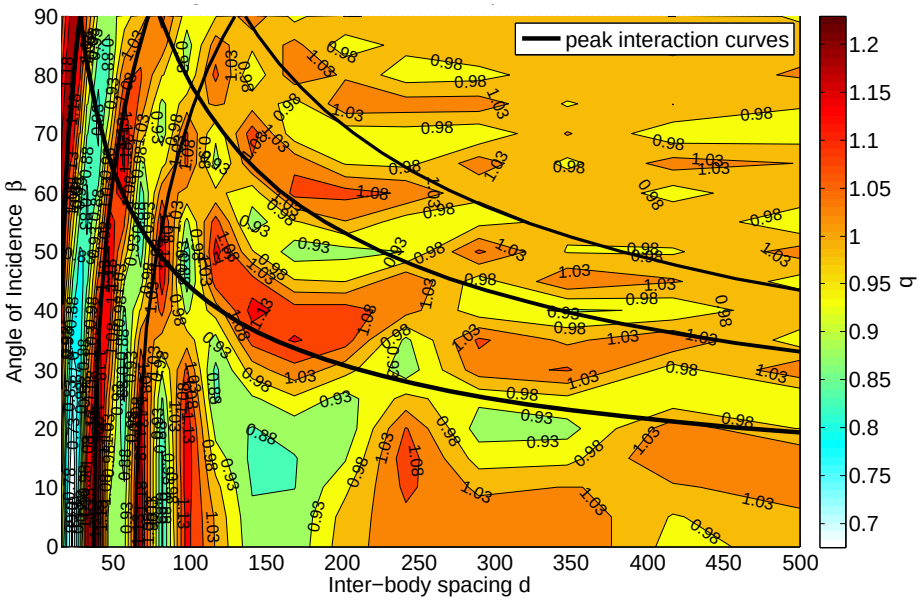

Figure 6.4: q-factor for 2-body array regular wave of 1 m height 6 s period, with eq. (6.2) plotted for the first three interaction maxima. Geometry III

that the graphs are not too dissimilar to figures 6.4 and 6.2 in subsection 6.2.1, especially in the 3 and 4 body array cases. In fact one can note the lines of contours of positive interaction where the two of the three devices are aligned, that is at $\beta = 30°$ and $60°$. For four bodies, one can clearly see the symmetry of the configuration in the areas of positive and negative interference. The superposition of the two sets of interaction lines from figure 6.2 are clearly visible, however in contrast to the 2-body case note the low values of q at close to the minimal distance $4r$. For 5 and 6 body arrays, the pattern is not easily discernible, with small areas of positive and negative interaction generally following the sloped hyperbolas of the relation in (6.2). As expected, the areas of strongest interaction are at closest r, and areas of similar q become larger in area and smaller in magnitude as d increases. An important point to keep in mind in observing these curves is that for this regular wave cases, each individual scattered and radiated component

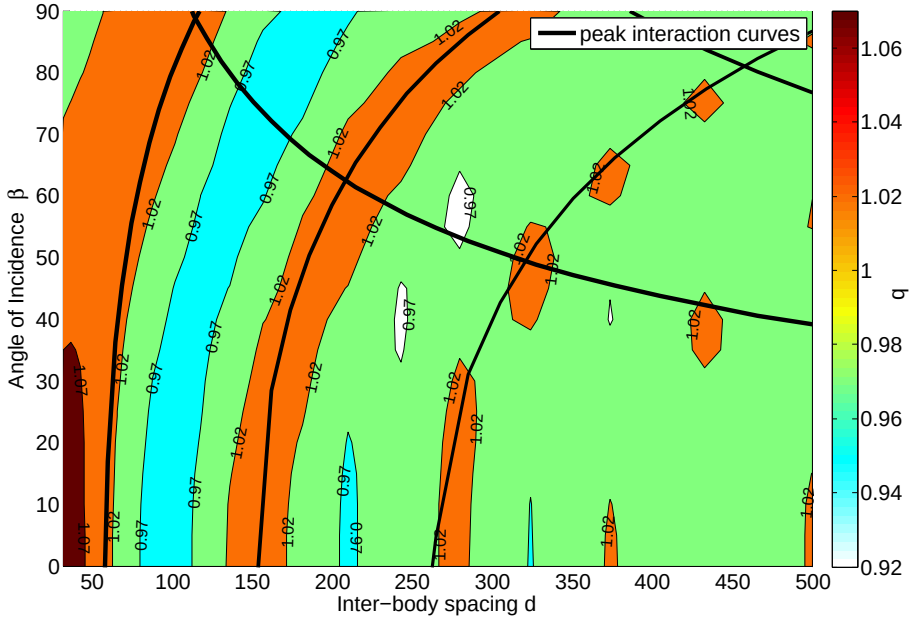

Figure 6.5: q-factor for 2-body array regular wave of 1 m height 12 s period, with eq.(6.2) plotted for the first three interaction maxima. Geometry VII

is easily distinguishable, hence the patchwork appearance of the graph. As will be shown in section 6.3, in irregular seas because of spectral spreading, the incident, scattered, and radiated waves often blend together, leading to a smoother larger areas of similar power output.

6.3 Layout study in irregular seas

6.3.1 2-body array

Although the regular wave case is instructive in examining the nature of the interactions in a WEC array, all commercial WEC array projects will operate in real seas. Therefore any study to determine the best configuration of a WEC array will need to be performed in irregular sea states. In this thesis, the first step to that end is taken, with an examination of 2, 3, 4, 5,

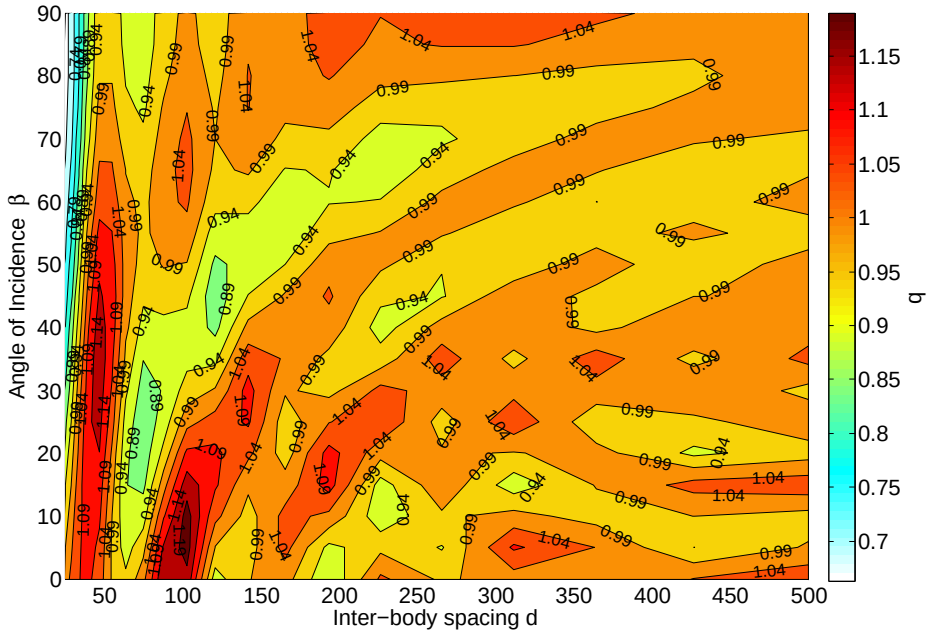

Figure 6.6: q-factor for 3-body array regular wave of 1 m height 8 s period, Geometry V

and 6 body circular arrays in four Bretschneider sea states shown in table 6.2. While not as accurate as using real site wave data, the Bretschneider spectrum was chosen as the most representative spectrum of the exposed ocean coast climate, where the majority of current WEC array projects are currently under development. As will be elaborated in chapter 7, any future WEC array project will need to have detailed site wave data available, because wave climates are very site-dependant. To begin the analysis, a q contour plot of a 2-body array of Geometry II in a typical Bretschneider $H_s = 1m$ $T_p = 10s$ is shown in 6.10. Clearly, the behaviour of q is very different from the regular wave 2-body cases shown in figures 6.2, 6.3, 6.4, and 6.5. Because the energy in the incident wave is spread out over a range of frequencies, the areas of similar q are likewise spread out over larger areas of d and β, because the dispersion relation (3.11) links λ in (6.2) to the frequency. However, the main crest of the interaction curve remains

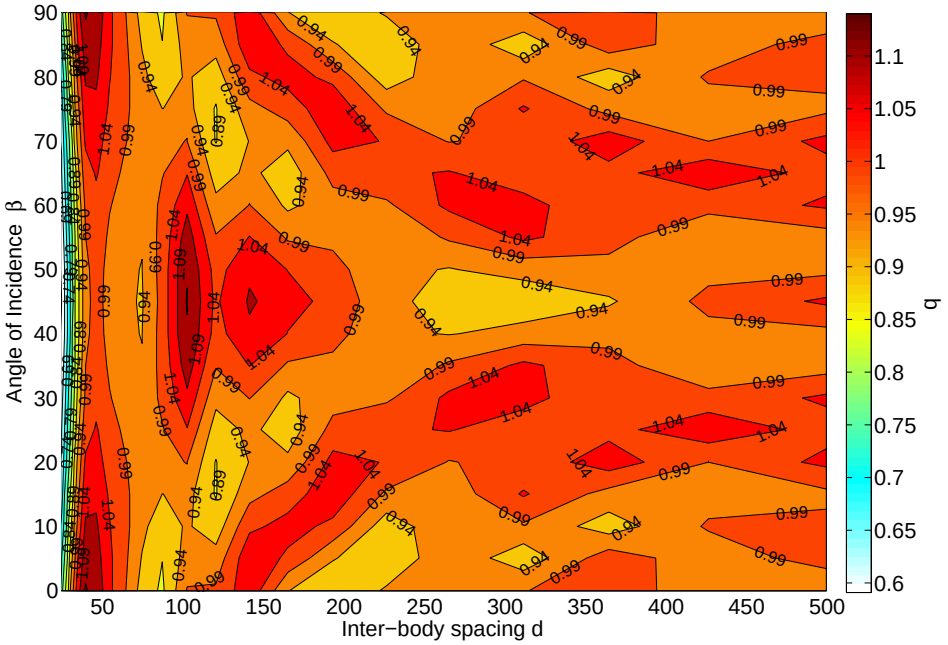

Figure 6.7: q-factor for 4-body array regular wave of 1 m height 8 s period, Geometry V

the same as in the regular wave case, with the hyperbolic curve clearly expressed in the curve. Furthermore, the highest interaction occurs at 90° at a septation distance slightly less than the λ, where no shadowing and only constructive interference from radiated waves from each of the bodies occurs. Note, however, that unlike the regular wave case, value of the peak in q is much lower, around 1.085. If we next look at the flatter shape Geometry VI for same $H_s = 1m$ $T_p = 10s$ irregular sea state in figure 6.11, we see that while the shape of the curve is the same, the constructive interference is stronger, with a q-max of around 1.23. Even so, the value of q-min remains about the same for Geometry II and VII for this case, indicating a net benefit of control in this case.

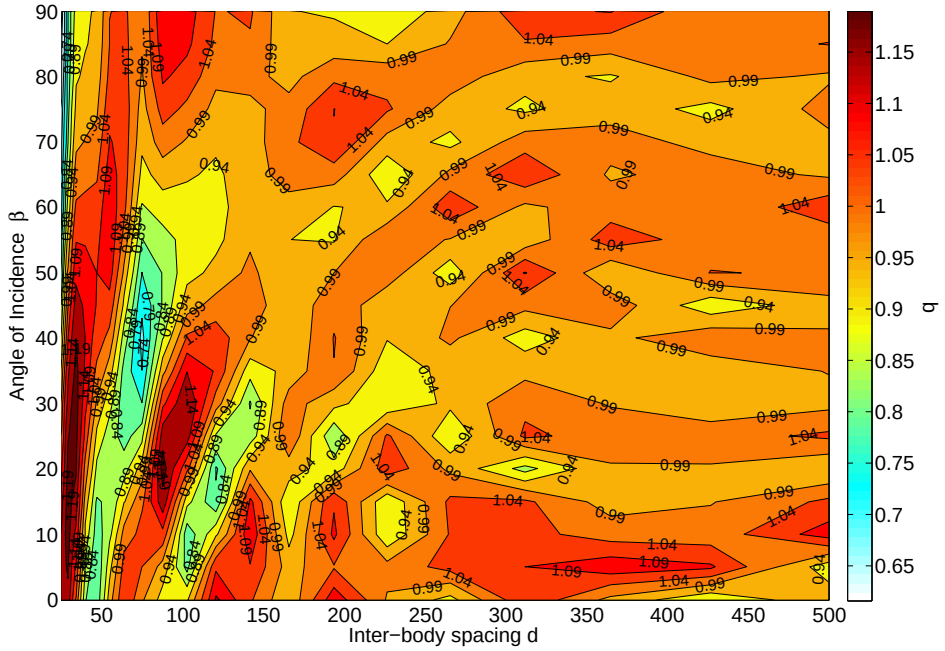

Figure 6.8: q-factor for 5-body array regular wave of 1 m height 8 s period, Geometry V

6.3.2 Multi-body array

Looking at a surface plot the 3-body array for the Geometry VI in fig 6.12, the symmetry of the configuration is apparent: the maximum q s are at $\beta = 30°$ and $60°$, which where 2 of the 3 bodies are aligned to minimize shadowing. Note that a significant portion of the graph is above the grey surface at $q = 1$, which indicates that the configuration is beneficial from a power maximization viewpoint. The graphs for 4 and 5 bodies show similar features, the four body graph showing the superposition of the positive interaction area in the 2-body case shown in figure 6.11. To look at the difference between different body geometries, we contrast two 6-body arrays shown in figures 6.13 and 6.14 for a H_s= 1 m $T_p = 10s$ Bretschneider sea state. The first shows the q values of a 6-body array of the long, thin Geometry I. In this surface plot, it is apparent that most of the interaction is

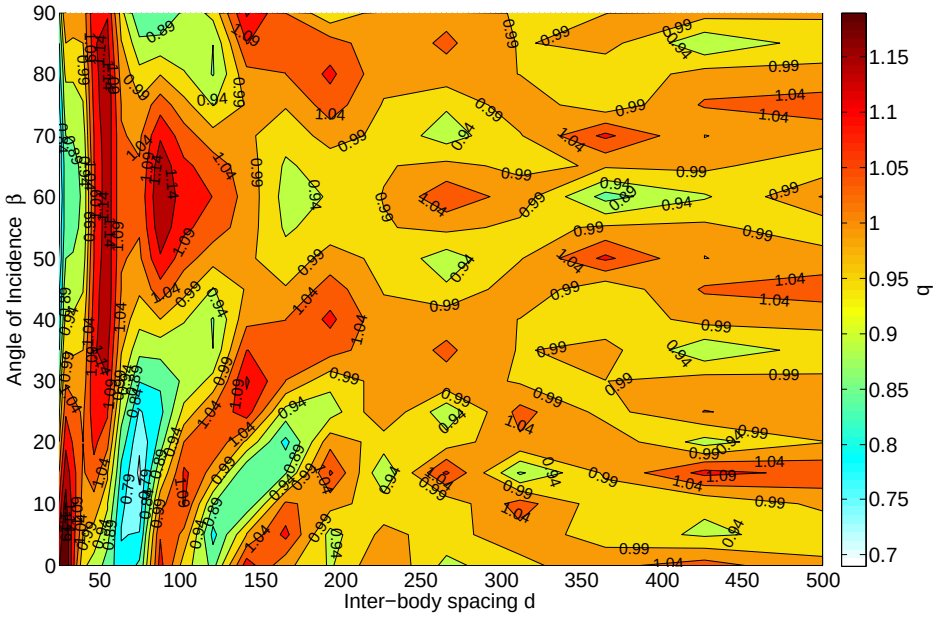

Figure 6.9: q-factor for 6-body array regular wave of 1 m height 8 s period, Geometry V

negative, with all but a few small areas below the $q = 1$ surface. The graph also shown that regardless of the incident angle, at a spacing closer than $200m$ all interaction is highly negative, indicating that such configurations should be avoided if power maximization is the project goal. By contrast, in figure 6.14, the majority of the q values are positive, with the angular variation much more strongly expressed. Even at close distances there are some areas of positive interaction at β around 10° and 50°. Hence one can conclude that for multi-body arrays, it is essential for a body to be able to radiate in order enable the controller to create a net positive effect of array interaction.

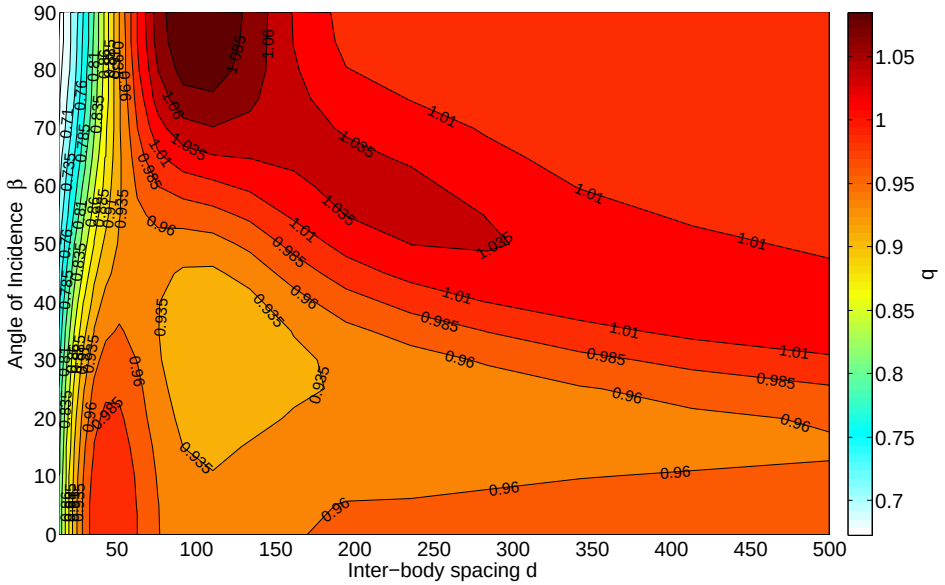

Figure 6.10: q-factor for 2-body array, Bretschneider wave of H_s= 1 m $T_p = 10s$, Geometry II

6.4 Conclusions

In this chapter we have seen demonstrated the effect of array layout on a WEC array whose devices are controlled by a global control scheme. Because the control scheme seeks to maximize the power output, which for the heaving WEC is proportional to the device velocity, the power output is greatly influenced by the effect of other devices. While these effects can be both positive and negative, the advantage of GC is that it can minimise the negative effects that are brought about by shadowing and destructive scattering, whilst at the same time maximizing the power produced on each device by producing constructive interference through phase matching. This is the case where the radiation from one or more devices is in phase with the incoming wave such that the motion of a give device is increased. As expected from theory, elaborated in [82], we have seen this effect to be especially significant at short distances. However, this constructive interference is greatly

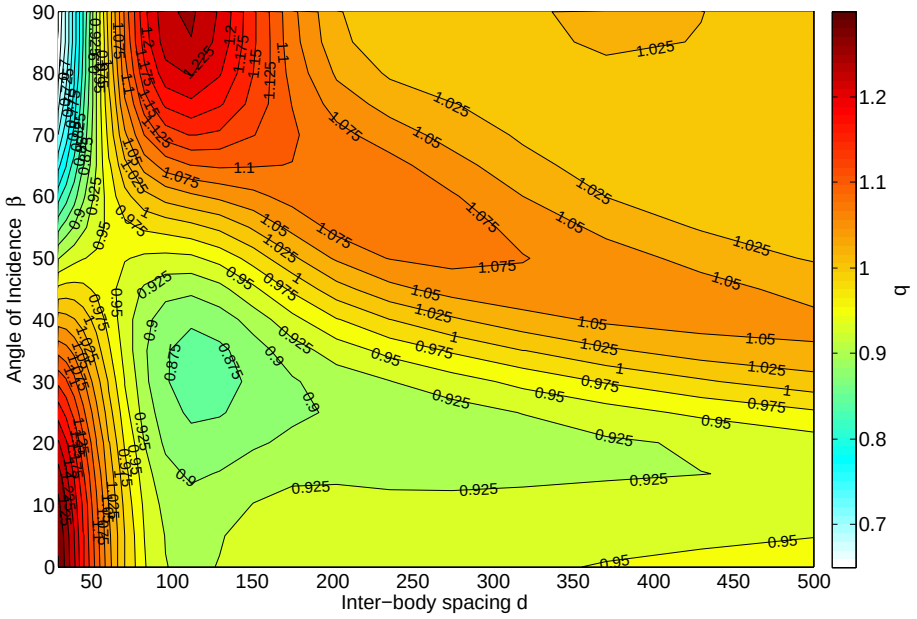

Figure 6.11: q-factor for 2-body array, Bretschneider wave of H_s= 1 m $T_p = 10s$, Geometry VI

dependent on the device shape, and the influence of shape is magnified as the number of devices increases. Evidence of this is clearly demonstrated in the qualitative difference between figures 6.13 and 6.14. Unlike the guidelines presented in [112], even for small controlled arrays, there are significant interactions, both positive and negative, to a distance of well beyond 20 r or 10 diameters, that should not be disregarded. Moreover, given a sufficiently suitable device shape, that is one that is an efficient radiator, one can not only mitigate negative effects of wave shadowing from dense arrays, but can produce a net benefit even in irregular seas. This can be seen for example in fir 6.11 for close distances for angles of incidence $\beta = 0°$ to 45°. Therefore, if the objective of a WEC array project is power maximization, it is imperative that not only is an array control scheme implemented, but that the control is considered before a decision on the array layout is made. While it may be possible to use control *a posteriori* to improve an existing

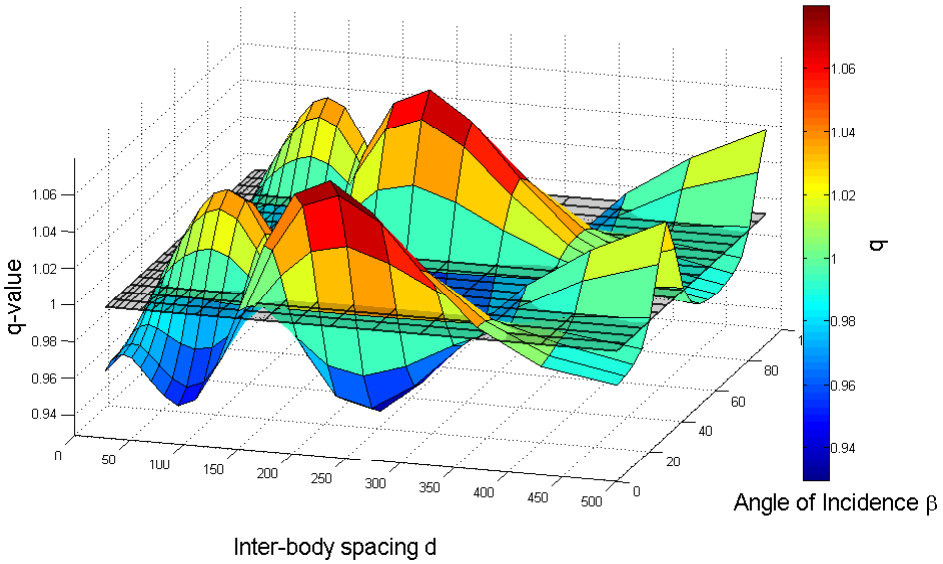

Figure 6.12: q-factor for 3-body array, Bretschneider wave of H_s= 1 m $T_p = 10s$, Geometry VI

layout's performance, it will be of much value to design the most advantageous layout at the initial design stages, especially given the enormous costs of a commercial WEC array project.

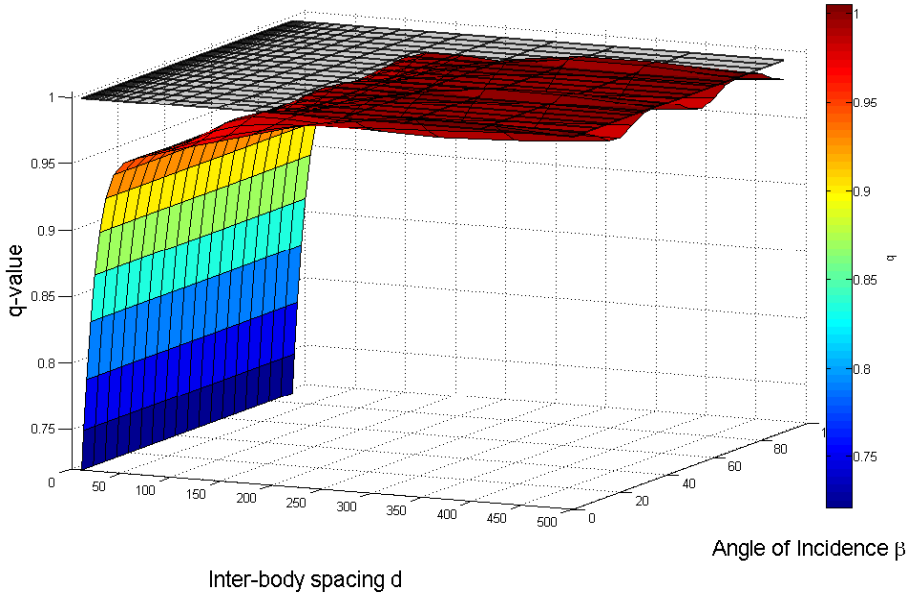

Figure 6.13: q-factor for 6-body array, Bretschneider wave of H_s= 1 m $T_p = 10s$, Geometry I

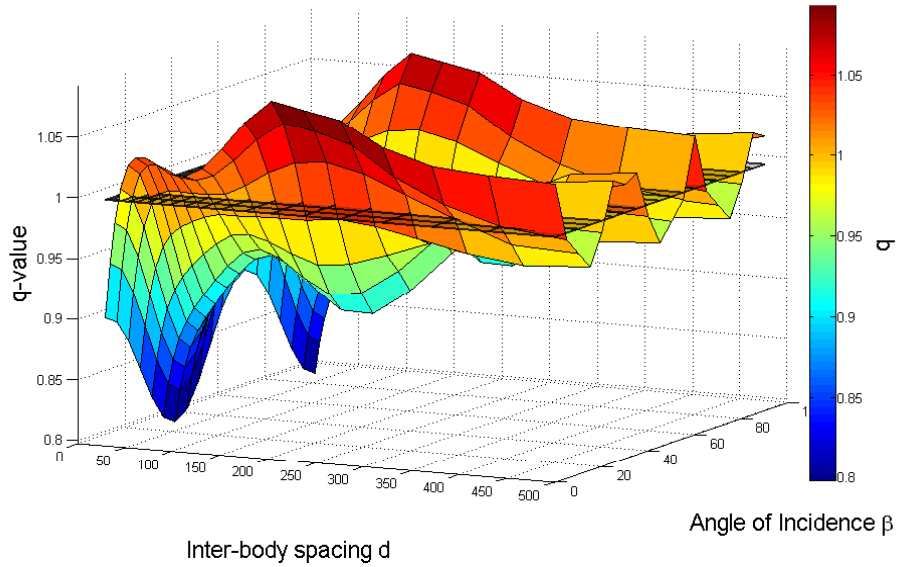

Figure 6.14: q-factor for 6-body array, Bretschneider wave of H_s= 1 m $T_p = 10s$, Geometry VI

Chapter 7

Conclusions

The hydrodynamic interactions of controlled arrays of WEC have been the focus of research of this thesis. In this chapter the important findings are summarized in 7.1. Remarks on future research directions are given in 7.2.

7.1 Discussion and conclusions

The global theoretical potential of wave energy, currently estimated at 2.11 TW, is great enough to pursue this source of renewable energy, despite the difficulties associated with wave energy conversion. As was shown in chapter 1, there are several countries in the world currently pursuing wave energy conversion projects, particularly in Europe. Because of the small scale of most single WECs, most proposed projects are to consist of multiple units or arrays WECs placed in a specific area in the ocean. In the review in chapter 2 it was shown that despite the long history of research into the problem of hydrodynamics of WEC arrays, there are still many questions that remain to be answered in terms of the layout of the devices, their type, and the controller of the PTO of the devices. Control of arrays, in particular, is an area of research that only recently has become active, with investigations

into control of arrays of devices in realistic operating scenarios. This is due, in particular, to the necessity for modelling adaptive control in the time domain, as was shown in 2.6.4. The computing power required for modelling and simulating the hydrodynamic equations of multiple bodies has only recently become available. As computer hardware and software continues to improve, more accurate modelling of control of arrays will become possible, specifically with CFD software packages, as was discussed in section 2.4.4.

With a view toward implementation of the controllers in chapter 5, in chapter 4 it was shown that adding a viscous damping term to the equation of motion (3.38) improves the accuracy of the hydrodynamic model. In particular, the addition of the viscous damping term decreased the heaving motion for devices at large velocities, where without the viscous damping term, the motion would have violated linear wave theory. Moreover, in section 4.5, the validity of linearizing the quadratic damping term in the case of heaving surface-piercing devices was shown. This linearization method is particularly useful in cases where the equation of motion must be linear, as in the case of a low level velocity-tracking controller of a device.

The performance of three control schemes, Passive Tuning (PT), Global Control (GC), and Independent Controller (IC), was analysed for arrays of two and three heaving cylinders of different radius to draft ratios in chapter 5. The overall benefit of adaptive control, such as GC and IC, in terms of maximizing the power capture was shown for all instances. In particular, it was shown that the relative performance of an adaptive controller such as GC and IC improves in an irregular sea state, compared with a fixed tuning such as PT. This is significant in that most studies on WEC array control to date [46, 47, 78], which have shown an overall negative effect on power capture by an array in real seas, have utilized a fixed tuning regime.

Therefore we can conclude that an appropriate control scheme for an array will be able, at least in part, to offset the destructive interference, by forcing the devices to maximize beneficial phase relationships.

In chapter 6, the effect of array layout on controlled multiple-body arrays of various cylinder shapes was investigated. The difference between array performance in regular and irregular seas was highlighted, specifically in terms of the spatial variation of the interaction factor q, which measures the relative power capture of an array. It was shown that for controlled array, for devices shapes which are able to radiate, for a majority of inter-device spacing and heading angles of the incoming waves, the value of q is greater than one. Conversely, for devices that radiate poorly, the overall array performance was shown to be negative, that is a net decrease in power compared to isolated devices, notably at close spacings less than $100m$. It can therefore be concluded that array control offsets the shadowing and destructive interference that results from dense packing of multiple WECs in an array, provided that the particular WEC shape can radiate strongly at the given sea state. Moreover, as was shown in section 6.3, in irregular sea states, array control gives freedom of device placing, with relatively broad areas of constructive interference. Given the expected movement of devices that are moored to the sea bottom, this will enable an accurate estimate of a WEC array project's power output, in spite of the position uncertainty.

7.2 Future research perspectives

In this thesis, in particularly in chapters 5 and 6, there became apparent a need for further investigation into several areas. Firstly, throughout this thesis no restriction was placed on the device motion. While the addition of the viscous damping term derived in 4 makes the device motions in this

thesis realistic, they still could be large enough to violate linear wave theory, in particularly near the resonance period of the device. In addition, both GC and IC are reactive control schemes, that is they can use reactive power to drive the device to match the phase of the incoming wave. Consequently, without restrictions and with the stated aim of maximizing power, such control schemes can push a device beyond its operating range. In summary, future investigations into array control need to take constraints into consideration, whether they be on stroke length, device motion or the total PTO force. Naturally, these restrictions will depend on a particular device, yet a more realistic model will need to include them as a restriction on device motion will modify the power absorption and radiative behaviours of the device and thus the power output of an array. Furthermore, as was mentioned in 5.4, it would be particularly useful to implement an adaptive control scheme which is passive, in other words that excludes the possibility of using reactive power. Although such a control scheme will necessarily have a lower power output, having device which can employ reactive power might be prohibitive from a materials and maintenance perspective, thus making it an economically attractive option.

The investigations carried out in this thesis modelled one particular type of device, a heaving cylinder. Further work will need to consider other types of devices, in particularly surging flap-type devices, as several of these are currently candidates for commercial WEC array projects. Because such devices typically operate in shallow water, the effect of water depth h will also need to be included in future work.

The passive tuning scheme considered in this thesis maximized the power for by tuning each individual device to the wave energy frequency ω_e. An alternative PT scheme, where the devices are tuned to other sea state pa-

rameters, such as ω_p, will need to be considered to see if an improvement in performance can be obtained. Such an improvement has been shown for the case of single devices in [108].

In chapter 6, we have considered symmetrical array configurations of 2, 3, 4, 5, and 6 devices. These configurations were chosen because in an eventual WEC array project, such configurations will enable possible sharing of mooring and electrical infrastructure, as well as enable navigation access to each device for maintenance. Whilst having more device placed together will decrease the overall performance, as was shown in [45], there are other configurations of closely-packed arrays of WEC that can be considered which are linear or non symmetrical. One possible direction of future research is to run an optimization with multiple parameters to find the optimal placing of device in an array, as was performed in [40] for an array of 5 devices in regular seas.

The irregular sea states investigated in this thesis have all been non-directional random spectral distributions, in particular Bretschneider spectra. While Bretschneider spectra give a good first approximation of the wave conditions that can be expected at an eventual WEC array project site, for a more accurate analysis, specific spectral wave data for a particular project site will be needed. Further work on array layout will need to use a specific set of wave data to investigate a given array's performance over a long-term period, for example a year. Because wave climates across the world vary greatly, the eventual best configuration for economic perforate of an array will vary for different areas of the ocean.

Bibliography

[1] Observ'ER, "Worldwide electricity production from renewable energy sources 14th inventory," tech. rep., Observ'ER, 2012.

[2] K. Gunn and C. Stock-Williams, "Quantifying the potential global market for wave power," *Renewable Energy*, vol. 44, pp. 296–304, 2012.

[3] International Energy Agency, "Key world energy statistics‘," tech. rep., International Energy Agency, 2012.

[4] Food and A. O. of the United Nations, "Un atlas of the oceans." online, February 2012.

[5] U.S. Department of Energy, "Marine and hydrodykinetic technology database." online, December 2012.

[6] Carbon Trust, "Accelerating marine energy," tech. rep., Carbon Trust, 2011.

[7] CSIRO, "Ocean renewable energy: 2015-2050 an analysis of ocean energy in australia," tech. rep., Commonwealth Scientific 1 Industrial Research Organisation (CSIRO), 2012.

[8] Sustainable Energy Authority of Ireland, "Ocean energy roadmap 2010-2050," tech. rep., Sustainable Energy Authority of Irel1, 2010.

[9] K. Budal, J. Falnes, L. Iversen, Lillebekken, P. Oltedal, G. Hals, T. Onshus, and A. Hoy, "The norwegian wave-power buoy project," in *Proc. Second International Symposium on Wave Energy Utilization (H. Berge, ed)*, 1982.

[10] J. Falnes, "Optimum control of oscillation of wave-energy converters," in *Proceedings of the Eleventh (2001) International Offshore 1 Polar Engineering Conference,Stavanger, Norway, June 17-22.*, 2001.

[11] A. F. d. O. Falcão, "Phase control through load control of oscillating-body wave energy converters with hydraulic pto system," *Ocean Engineering*, vol. 35, pp. 358–366, 2008.

[12] A. Babarit and A. Clément, "Optimal latching control of a wave energy device in regular 1 irregular waves," *Applied Ocean Research*, vol. 28, pp. 77–91, 2006.

[13] A. Babarit, "Impact of long separating distances on the energy production of two interacting wave-energy converters," *Ocean Engineering*, vol. 37, pp. 718–729, 2010.

[14] K. Budal, "Theory for absorbtion of wave power by a system of interacting bodies," *Journal of Ship Research*, vol. 21, pp. 248–253, 1977.

[15] J. Falnes, "Radiation impedance matrix 1 optimum power absorbtion for interacting oscillators in surface waves," *Applied Ocean Research*, vol. 2, pp. 75–80, 1980.

[16] D. Evans, "Some theoretical aspects of three-dimensional wave-energy absorbers," in *Sympoisum on Ocean Wave Energy Utliziation*, (Gothenburg, Sweden), 1979.

[17] J. Falnes and K. Budal, "Wave-power absorbtion by parallel rows of interacting oscillating bodies," *Applied Ocean Research*, vol. 4, no. 4, pp. 194–207, 1982.

[18] G. P. Thomas and D. Evans, "Arrays of three-dimensional wave-energy absorbers," *Journal of Fluid Mechanics*, vol. 108, pp. 67–88, 1981.

[19] T. Thorpe, "A brief review of wave energy," tech. rep., The UK Department of Trade 1 Industry, 1999.

[20] H. Kagemoto and D. K. P. Yue, "Interactions among multiple three-dimensional bodies in water waves: an exact algebraic method," *Journal of Fluid Mechanics*, vol. 166, pp. 189–209, 1986.

[21] S. Mavrakos and P. Koumoutsakos, "Hydrodynamic interaction among vertical axisymmetric bodies restrained in waves," *Applied Ocean Research*, vol. 9, pp. 128–140, 1987.

[22] P. McIver, "Some hydrodynamic aspects of arrays of wave energy devices," *Applied Ocean Research*, vol. 16, pp. 61–69, 1994.

[23] http://www.ewtec.org/, 2011.

[24] J. Newman, *Wave Effects on Multiple Bodies*, pp. 3–26. RIAM, Kyushu University, 2001.

[25] D. Evans, "Maximum wave-power absorbtion under motion constraints," *Applied Ocean Research*, vol. 3, pp. 200–203, 1981.

[26] D. Pizer, "Maximum wave-power abosrbtion of point absorbers under motion constraints," *Applied Ocean Research*, vol. 15, pp. 227–234, 1993.

[27] C. Fitzgerald and G. P. Thomas, "A preliminary study of the optimal formation of an array of wave power devices," in *Proceedings of the 7th European Wave 1 Tidal Energy Conference,Porto, Portugal.*, 2007.

[28] M. Folley and T. Whittaker, "The effect of sub-optimal control and the spectral wave climate on the performance of wave energy converter arrays," *Applied Ocean Research*, vol. 31, no. 4, pp. 260–266, 2009.

[29] P. Ricci, J.-B. Saulnier, and A. F. de O. Falcão, "Point-absorber arrays: a configuration study off the portuguese west coast," in *Proceedings of the 7th European Wave 1 Tidal Energy Conference, Porto, Portugal*, 2007.

[30] M. J. Simon, "Multiple scattering in arrays of axisymmetric wave-energy devices. Part 1. A matrix method using a plane-wave approximation," *Journal of Fluid Mechanics*, vol. 120, pp. 1–25, 1982.

[31] P. McIver and D. Evans, "Approximation of wave forces on cylinder arrays," *Applied Ocean Research*, vol. 6, pp. 101–107, 1984.

[32] M. Okhusu, "Hydrodynamic forces on multiple cylinders in waves," in *Proceedings of the International Symposium on Dynamics of Marine Vehicles 1 Structures in Waves, London, U.K* (Institute of Mechanical Engineers, ed.), pp. 107–112, 1974.

[33] S. Mavrakos, "Hydrodynamic coefficients for groups of interacting vertical axisymmetric bodies," *Ocean Engineering*, vol. 18, pp. 485–515, 1991.

[34] P. McIver, S. Mavrakos, and G. Singh, "Wave-power absorption by arrays of devices," in *Proceedings of the 2nf European Wave Power Conference, Lisbon, Portugal*, 1996.

[35] S. Mavrakos and P. McIver, "Comparison of methods for computing hydrodynamic characteristics of arrays of wave power devices," *Applied Ocean Research*, vol. 19, pp. 283–291, 1997.

[36] H.Kagemoto and D. K.P.Yue, "Hydrodynamic interaction analyses of very large floating structures," *Journal of Marine Structures*, vol. Vol.6, p. 295322, 1993.

[37] O. Yilmaz and A. Incecik, "Analytical solutions of the diffraction problem of a group of truncated vertical cylinders," *Ocean Engineering*, vol. 25, pp. 385–394, 1998.

[38] B. Child and V. Venugopal, "Interaction of waves with an array of floating wave energy devices," in *Proceedings of the 7th European Wave 1 Tidal Energy Conference, Porto, Portugal*, 2007.

[39] B. Child and V. Venugopal, "Modification of power characteristics in an array of floating wave energy devices," in *Proceedings of the 8th European Wave and Title Energy Conference, Uppsala, Sweden*, 2009.

[40] B. Child and V. Venugopal, "Optimal configurations of wave energy devices," *Ocean Engineering*, vol. 37, pp. 1402–1417, 2010.

[41] B. Child and V. Venugopal, "Non-optimal tuning of wave energy device arrays," in *2nd International Conference on Ocean Energy (ICOE), 15th Brest, France*, 2008.

[42] C.-H. Lee and J. N. Newman, "Computation of wave effects using the panel method," in *Numerical Models in Fluid-Structure Interaction* (S. K. Chakrabarti, ed.), vol. 18 of *Advances in Fluid Mechanics*, Southampton: WIT Press, 2005.

[43] P. A. Justino and A. Clément, "Hydrodynamic performance for small arrays of submerged spheres," in *Proceedings of 5th European wave energy conference*, pp. 266–273, 2003.

[44] B. Borgarino, A. Babarit, and P. Ferrant, "Impact of the separating distance between interacting wave energy converters on the overall energy extraction of an array," in *Proceedings of the 9th European Wave 1 Tidal Energy Conference, Southampton, UK*, 2011.

[45] B. Borgarino, A. Babarit, and P. Ferrant, "Impact of wave interaction effects on energy absorbtion in large arrays of wave energy converters," *Ocean Engineering*, vol. 41, p. 7988, 2012.

[46] J. Cruz, R. Sykes, P. Siddorn, and R. Taylor, "Estimating the loads 1 energy yield of arrays of wave energy converters under realistic seas," *IET Renewable Power Generation*, vol. 4, pp. 488–497, 2010.

[47] G. De Backer, M. Vantorre, C. Beels, J. De Rouck, and P. Frigaard, "Power absorption by closely spaced point absorbers in constrained conditions," *IET Renewable Power Generation*, vol. 4, pp. 579–591, 2010.

[48] R. Taghipour, A. Arswendy, M. Devergez, and T. Moan, "Efficient frequencydomain analysis of dynamic response for the multi-body wave energy converter in multi-directional waves," in *18th International Offshore 1 Polar Engineering Conference*, 2008.

[49] B. Borgarino, A. Babarit, and P. Ferrant, "Extension of free-surface greens function multipole expansion for infinite water depth case," *International Journal of Offshore and Polar Engineering*, vol. 21, pp. 161–168, 2011.

[50] M. Folley, A. Babarit, B. Child, D. Forehand, L. OBoyle, K. Silverthorne, J. Spinneken, V. Stratigaki, and P. Troch, "A review of numerical modelling of wave energy converter arrays," in *Proceedings of the ASME 2012 31st International Conference on Ocean, Offshore 1 Arctic Engineering (OMAE), Rio de Janeiro, Brazil*, 2012.

[51] A. Merigaud, Gilloteaux, J.-C., and J. Ringwood, "A nonlinear extension for linear boundary element methods in wave energy device modelling," in *Proceedings of the ASME 2012 31st International Conference on Ocean, Offshore 1 Arctic Engineering (OMAE2012), Rio de Janeiro, Brazil*, 2012.

[52] M. Folley and T. Whittaker, "The adequacy of phase-averaged models for modelling wave farms," in *ASME 2011 30th International Conference on Ocean, Offshore 1 Arctic Engineering (OMAE2011) June 1924, 2011 , Rotterdam, The Netherl1s*, 2011.

[53] A. Alexandre, T. Stallard, and P. Stansby, "Transformation of wave spectra across a line of wave devices," in *Proceedings of the 8th European Wave and Title Energy Conference, Uppsala, Sweden*, 2009.

[54] J. A. Oskamp and H. T. Ozkan-Haller, "Wave predicitons at the site of a wave energy conversion array," in *Proceedings of 32nd Conference on Coastal Engineering, Shanghai, China, 2010*, 2010.

[55] E. B. Agamloh, A. K. Wallace, and A. von Jouanne, "Application of fluidstructure interaction simulation of an ocean wave energy extraction device," *Renewable Energy*, vol. 33, pp. 748–757, 2008.

[56] M. A. Bhinder, A. Babarit, L. Gentaz, and P. Ferrant, "Assessment of viscous damping via 3d-cfd modelling of a floating wave energy de-

vice," in *Proceedings of the 9th European Wave 1 Tidal Energy Conference, Southampton, UK*, 2011.

[57] Lejerskog, Erik and Gravråkmo, Halvar and Savin, Andreij and Strömstedt, Erland and Tyrberg, Simon and Haikonen, Kalle and Krishna, Remya and Boström, Cecilia and Rahm, Magnus and Ekström, Rickard and Svensson, Olle and Engström, Jens and Ekergård, Boel and Baudoin, Antoine and Kurupath, Venugopalan and Hai, Ling and Li, Wei and Sundberg, Jan and Waters, Rafael and Leijon, Mats, "Lysekil research site, sweden: A status update," in *Proceedings of the 9th European Wave 1 Tidal Energy Conference, Southampton, UK*, 2011.

[58] S. Bellew and T. Stallard, "Linear modelling of wave device arrays with comparison to experimental measurements 1 second order models," in *21st International Workshop on Water Waves 1 Floating Bodies (21st IWWWFB); Harbin, China. 2010.*, 2010.

[59] S. Weller, S. T.J., and P. Stansby, "Experimental measurements of irregular wave interaction factors in closely spaced arrays," *IET Renewable Power Generation*, vol. 4, pp. 628–637, 2010.

[60] E. Tedeschi, M. S. P. Ricci, M. Molinas, and J.L.Villate, "Control strategies for the grid integration of wave energy converters at the biscay marine energy platform," in *Proceedings of the 9th European Wave and Tidal Energy Conferenceand Southamptonand UK*, 2011.

[61] M. Molinas, O.Skjervheim, B. Sorby, P. Andreasen, S. Lundberg, and T. Undeland, "Power smoothing by aggregation of wave energy converters for minimizing electrical energy storage requirements," in *Pro-*

ceedings of the 7th European Wave 1 Tidal Energy Conference, Porto, Portugal., 2007.

[62] D. OSullivan and G. Dalton, "Challenges in the grid connection of wave energy devices," in *Proceedings of the 8th European Wave and Title Energy Conference, Uppsala, Sweden*, 2009.

[63] F. Sharkey, E. Bannon, M. Conlon, and K. Gaughan, "Dynamic electrical ratings and the economics of capacity factor for wave energy converter arrays," in *Proceedings of the 9th European Wave and Tidal Energy Conference, Southampton, UK*, 2011.

[64] P. C. Vicente, A. F. de O. Falcão, and P. A. Justino, "Dynamics of arrays of floating point-absorber wave energy converters with inter-body and bottom slack-mooring connections," *Applied Ocean Research*, vol. 31, pp. 267–281, 2009.

[65] P. Ricci, A. Rico, P. Ruiz-Minguela, F. Boscolo, and J. Villate, "Design, modelling and analysis of an integrated mooring system for wave energy arrays," in *Proceedings of the 4th International Conference on Ocean Energy, 17 October, Dublin*, 2012.

[66] C. Beels, P. Troch, J. P. Kofoed, P. Frigaard, J. V. Kringelum, P. C. Kromann, M. H. Donovan, J. De Rouck, and G. De Backer, "A methodology for production and cost assessment of a farm of wave energy converters," *Renewable Energy*, vol. 36, pp. 3402–3416, 2011.

[67] P. Ricci, M. Alves, A. F. ao, and A. Sarmento, "Optimisation of the geometry of wave energy converters," in *Proceedings of the Int.Conf. on Ocean Energy, Bremerhaven, Germany*, 2006.

[68] H. Wolgamot, P. Taylor, and R. Eatock Taylor, "The interaction factor 1 directionality in wave energy arrays," *Ocean Engineering*, vol. 47, pp. 65–73, 2012.

[69] Child, *On the configuration of arrays of floating wave energy converters.* PhD thesis, The University of Edinburgh, 2011.

[70] J. Cruz, *Ocean Wave Energy.* Green Energy 1 Technology, Springer, 2008.

[71] J.-C. Gilloteaux and J. Ringwood, "Control-informed geometric optimisation of wave energy converters," in *Proc. IFAC Conf. on Control Applications in Marine Systems (CAMS), Rostock*, 2010.

[72] A. A. E. Price, *New Perspectives on Wave Energy Converter Control.* PhD thesis, The University of Edinburgh, 2009.

[73] J. Falnes, "On non-causal impulse response functions related to propagating water waves," *Applied Ocean Research*, vol. 17, pp. 379–389, 1995.

[74] F. Fusco and J. Ringwood, "Short-term wave forecasting for real-time control of wave energy converters," *IEEE Transcations on Sustainable Energy*, vol. 1, pp. 99–106, 2010.

[75] F. Fusco and J. Ringwood, "Quantification of the prediction requirements in reactive control of wave energy converters," in *proceedings of the 18th World Congress of the International Federation of Automatic Control (IFAC), Milan, Italy,*, 2011.

[76] J. Hals, J. Falnes, and M. Torgeir, "A comparison of selected strategies for adaptive control of wave energy converters," *Journal of Offshore Mechanics 1 Arctic Engineering*, vol. 133, pp. 1–31, 2011.

[77] E. Tedeschi and M. Molinas, "Control strategy of wave energy converters optimized under power electronics rating constraints," in *3rd International Conference on Ocean Energy, 6 October, Bilbao, Spain*, 2010.

[78] R. Antonutti and G. E. Hearn, "Optimisation of point-absorber arrays," in *Proceedings of the 9th European Wave and Tidal Energy Conference, Southampton, UK*, 2011.

[79] A. Annuar, D. Macpherson, D. Forehand, , and M. Mueller, "Optimum power control for arrays of direct drive wave energy converters," in *6th IET International Conference on Power Electronics, Machines 1 Drives (PEMD 2012), Bristol, UK*, 2012.

[80] G. Bacelli, J. V. Ringwood, and J.-C. Gilloteaux, "A control system for a self-reacting point absorber wave energy converter subject to constraints," in *IFAC World Congress, Milan, Italy.*, 2011.

[81] J. Newman, *Marine Hydrodynamics.* MIT Press, 1977.

[82] C. C. Mei, M. Stiassnie, and D. K.-P. Yue, *Theory 1 Application of Ocean Surface Waves Part 1: Linear Aspects.* World Scientific Publishing Co. Pte. Ltd., 2005.

[83] The Specialist Committee on Waves, "Final report and recommendations to the 23rd ittc," in *Proceedings of the 23rd ITTC Volume II*, 2002.

[84] Y. Goda, *Random Seas and Design of Maritime Structures (2nd Edition).* ADVANCED SERIES ON OCEAN ENGINEERING, World Scientific, 2000.

[85] W. Cummins, "The impulse response function 1 ship motions.," *Schiffstechnik*, vol. 9, pp. 101–109, 1962.

[86] J. Falnes, *Ocean waves 1 oscillating systems : linear interactions including wave-energy extraction.* Cambridge University Press, 2002.

[87] G. Bacelli, J. Ringwood, and J.-C. Gilloteaux, "Control of a wave energy device for potable water production," in *Proceedings of the 8th European Wave and Title Energy Conference, Uppsala, Sweden*, 2009.

[88] J. Westphalen, G. Bacelli, P. Balitsky, and J. Ringwood, "Control strategies for arrays of wave energy devices.," in *Proceedings of the 9th European Wave and Tidal Energy Conference, Southampton, UK*, 2011.

[89] G. Bacelli, P. Balitsky, and J. V. Ringwood, "Coordinated control of arrays of wave energy devices - benefits over independent control," *IEEE Transactions on Sustainable Energy*, 2013 in press.

[90] S. Thomas, S. Weller, and T. Stallard, "Float response within an array: Numerical and experimental comparison," in *Proceedings of the 2nd International Conference on Ocean Energy (ICOE 2008), 15th 17th October 2008, Brest, France*, 2008.

[91] J. Falnes, "Wave-energy conversion through relative motion between two single-mode oscillating bodies," *Journal of Offshore Mechanics 1 Arctic Engineering*, vol. 121, no. 1, pp. 32–38, 1999.

[92] M. Folley, T. Whittaker, and J. van't Hoff, "The design of small seabed-mounted bottom-hinged wave energy converters," in *Proceedings of the 7th European Wave 1 Tidal Energy Conference,Porto, Portugal.*, 2007.

[93] J. Journée and W. Massie, *Offshore Hydrodynamics*. Delft University of Technology, 2001.

[94] J. F. Douglas, J. Gasiorek, and J. Swaffield, *Fluid Mechanics*. Addison Wesley Longman, 1995.

[95] T. Sarpkaya and M. Isaacson, *Mechanics of wave forces on offshore structures*. Van Nostr1 Reinhold Company, 1981.

[96] J. Morison, M. O'Brien, J. Johnson, and S. Schaaf, "The force exerted by surface wave on piles," *Transactions of the American Institute of Mining 1 Metallurgical Engineers*, vol. 189, pp. 147–164, 1950.

[97] A. Troesch and S. Kim, "Hydrodynamic forces acting on cylinders oscillating at small amplitudes," *Journal of Fluids 1 Structures*, vol. 5, pp. 189–199, 1991.

[98] B. Uzunoglu, M. Tan, and W. G. Price, "Low reynolds number flow around an oscillating circular cylinder using a cell viscous boundary element method," *International Journal for Numerical Methods in Engineering*, vol. 50, pp. 2317–2338, 2001.

[99] A. Otter, "Damping forces on a cylinder oscillating in a viscous fluid," *Applied Ocean Research*, vol. 12, pp. 153–155, 1990.

[100] A. Cobbin, P. Stansby, and P. Duck, "The hydrodynamic damping force on a cylinder in oscillatory, very-high-reynolds-number flows," *Applied Ocean Research*, vol. 17, pp. 291–300, 1995.

[101] C.-Y. Wang, "On high-frequency oscillatory viscous flows," *Journal of Fluid Mechanics*, vol. 32, pp. 58–68, 1968.

[102] B. Molin, *Hydrodynamique des Structures Offshore*. TECNIP, 2002.

[103] G. M. Terra, W. J. van de Berg, and L. R. M. Maas, "Experimental verification of lorentz linearization procedure for quadratic friction," *Fluid Dynamics Research*, vol. 36, pp. 175–188, 1995.

[104] J. Hazewinkel, "Lorentz linearization 1 its application in the study of the closure of the Zuiderzee." Lecture Notes,Physics of Coasts, Universiteit Utrecht, 2004.

[105] J. H. Nath, "Wave force-phase method for vertical cylinders," tech. rep., Oregon State University, Corvallis, Oregon, 1985.

[106] H. Lorentz, "Het in rekening brengen van den weerst1 bij schommelende vloeistofbewegingen," *De Ingenieur (in Dutch)*, p. 695, 1922.

[107] H. Lorentz, "Verslag staatscommissie zuiderzee 19181926," tech. rep., Alg. L1sdrukkerij, Den Haag (in Dutch, report senate committee on Zuiderzee), 1926.

[108] H. Yavuz, T. J. Stallard, A. P. McCabe, and G. A. Aggidis, "Time series analysis-based adaptive tuning techniques for a heaving wave energy converter in irregular seas," *Proceedings of the Institution of Mechanical Engineers, Part A: Journal of Power 1 Energy*, vol. 221, pp. 77–90, 2006.

[109] A. F. d. O. Falcão, "Control techniques for wave energy converters," in *Supergen Marine 7th Doctoral Training Programme Workshop Control of Wave and Tidal Converters*, 2010.

[110] M. Santos, F. Salcedo, E. Tedeschi, E. Robles1, and J. Villate, "Centralized control of a wave energy farm," in *International Conference on Renewable Energies and Power Quality (ICREPQ12),Santiago de Compostela (Spain), 28th to 30th March, 2012*, 2012.

[111] B. Child, J. Cruz, and M. Livingstone, "The development of a tool for optimising of arrays of wave energy converters," in *Proceedings of the 9th European Wave and Tidal Energy Conference, Southampton, UK*, 2011.

[112] A. Babarit, "On the park effect in arrays of oscillating wave energy converters," *Renewable Energy*, vol. 58, pp. 68–78, 2013.